SIGNATURES OF FULLY DEVELOPED TURBULENCE AND THEIR EMERGENCE IN DIRECT NUMERICAL SIMULATIONS

A Dissertation

by

SUALEH KHURSHID

Submitted to the Graduate and Professional School of
Texas A&M University
in partial fulfillment of the requirements for the degree of

DOCTOR OF PHILOSOPHY

Chair of Committee,	Diego A. Donzis
Committee Members,	Katepalli R. Sreenivasan
	Sharath S. Girimaji
	Alexei Poludnenko
Head of Department,	Srinivas Rao Vadali

December 2021

Major Subject: Aerospace Engineering

ABSTRACT

Turbulent flows are ubiquitous in natural and engineering applications. For example, stellar formation rates are an order magnitude larger due to turbulence effects and quarter of all energy expended in transport and commercial applications is used to move fluids or move objects through fluids, which are largely turbulent in nature. Prediction and control of turbulent flows, especially their extreme fluctuations, is an important challenge in diverse practical applications such supersonic and hypersonic flows, both in terms of flight performance and materials needed to build these vehicles. Turbulent flows have thus far been studied in the limit of high-Reynolds numbers ($R_\lambda > 10^3$), largely due to their prevalence in applications. In this regime, turbulence has a wide-range of excited scales, with the largest scales often dictated by non-universal features such as the geometry of the object generating turbulence. Small scales are known to exhibit non-trivial statistics characterized by extreme fluctuations, a phenomenon collectively called intermittency. Higher-order statistics of velocity fluctuations, those describing the extreme events, are however exceedingly challenging to measure and compute. Computations have been carried out with over 16384^3 grid-points to measure them accurately. The observed scaling of extreme event statistics is known to be anomalous i.e. it differs greatly from classical predictions. The prediction of this anomalous behavior from first principles is still an open problem. Furthermore, the parameter range where the scaling behavior must be observed is also not well defined by classical theories. It is therefore important to understand and characterize the fundamental aspects of turbulent flows. In particular how turbulent behavior emerges, what its characteristics are, and how they relate to conditions found in realistic flows. This is the main thrust of this dissertation. This work provides a novel approach to to address these open questions. We use highly resolved direct numerical simulations at low to moderate $R_\lambda \sim O(1-100)$, which are easily realizable on current generation of supercomputers, to measure high-order statistics and establish their scaling. The simulations in this dissertation have the finest small-scale and temporal resolution in literature. Anomalous scaling of high-order moments, assumed to be a high-R_λ feature, is shown to emerge at $R_\lambda \sim O(10)$ and

we directly test its universality with respect to large scale production mechanisms. The observed scaling exponents are compared to recently developed theory. In contrast to classical theories, we also show that most extreme fluctuations develop turbulent character first. Therefore, high-R_λ features can be reliably computed by studying highly resolved low-R_λ turbulent flows. The classical concept of small-scale independence, a widely made assumption in modelling approaches, is also studied using the energy spectrum of turbulent fluctuations. We also extend the new formalism to compressible turbulence and show that the vortical modes behave similar to their incompressible counterpart. Compressible modes are shown to scale differently. Based on our results and a survey of the literature, we speculate that the asymptotic scaling at large parameter values in spatio-temporal chaotic systems can be understood by careful study of transition to this scaling at much lower parameter values. Within computing, this means that well-resolved simulations at low parameter values, X (e.g. $X = R_\lambda$ etc.), which are order magnitudes cheaper than high-X, can reveal important and relevant physics at high-X.

DEDICATION

To Abu and Mummy.

ACKNOWLEDGMENTS

This dissertation and my academic journey has been made possible by the generosity, patience and advice of a lot of people. The most important contribution to this dissertation and my academic career has been that of my advisor Prof. Diego A. Donzis. He has been a great academic and research mentor as well as an important personal influence. He gave me the opportunity to join his group as a sophomore, guided my undergraduate research and supported my academic pursuits through perhaps the toughest stretch of my life. I am quite sure I would not have pursued graduate education without his support and guidance. My research philosophy is also greatly influenced by his never ending curiosity, passion for learning new aspects of the world around us and pursuit of rigor. I have learned a lot about fluid mechanics, computation and science in general from the multiple courses I took with him and the many stimulating discussions with him. I am extremely grateful for his kindness and constant support, especially over the last two years.

I was also provided with opportunities to discuss my work and pursue research directions with eminent scholars in our field. I am extremely grateful to Prof. K.R. Sreenivasan for providing significant insights towards my work and elevating its quality. His deep knowledge of the field, humility and care towards developing new experts in the field are particularly inspirational. From him I have also learnt the important art of making strong and precise claims based on available evidence and providing speculative context when needed. I would also like to thank him for his hospitality during my visits to NYU. I am also grateful to Profs. J. Schumacher and V. Yakhot for their insights regarding my work and many discussions about important questions in turbulence.

I would also like to thank Prof. Sharath Girimaji for his advice, the many times I have sought it. It was his advice to work with Prof. Donzis in 2013. I have also learned a great deal about fluid mechanics from his courses and research from his group, which often provides important perspectives about my own work. I would like to thank Prof. Poludnenko for taking the time to be on my dissertation committee and asking important questions about my work and its implications for applications and simulations in general. I am also thankful to the many graduates students in our

Lab, Drs. Shriram Jagannathan, Agustin Maqui, Konduri Aditya, Chang Hsin-Chen, John P. John, Komal Kumari and Akanksha Baranwal, for their friendship, probing questions during meetings and teaching me about their work through the years. I am particularly grateful to Komal and Rishita Das for sharing the challenging Ph.D. journey with me and their support through qualifying exams and many courses we took together. I am also grateful to graduate students in Prof. Girimaji's lab, Drs. Divya Sri Praturi and Ankita Mittal for their friendship and teaching me more about the applied aspects of fluid turbulence. I am grateful to the many friends that have shared their lives with me and been a constant source of support and enjoyment. I am also grateful to the department staff for skillfully handling the administrative side of things. In particular, I would like to acknowledge Colleen Leatherman for her painstaking work towards managing the financial aspects of our work masterfully and with very little input from me.

My academic journey would not be possible without the love, support and sacrifices of my parents, to whom this dissertation is dedicated, and my younger sister. I am constantly in awe of their strength and will forever be indebted to them. I would also like to thank my wife-to-be Dr. Senin for her friendship, constant support over the years and for simply being a major part of my life. I am extremely happy and grateful to share my life with you.

I would like to thank the Texas A&M University Graduate and Professional School to allow me to construct this LaTeX thesis template.

CONTRIBUTORS AND FUNDING SOURCES

Contributors

This work was supported by a dissertation committee consisting of Professors Diego A. Donzis (advisor), Katepalli R. Sreenivasan of Texas A&M University Department of Aerospace Engineering and New York University, Sharath S. Girimaji of Texas A&M University Department of Ocean Engineering and Alexei Poludnenko of Texas A&M University of Aerospace Engineering and University of Connecticut.

The analysis depicted in Chapter III and IV were published in Journal of Fluid Mechanics (2021) and Physical Review Fluids (2018) respectively in collaboration with Profs. Diego A. Donzis and Katepalli R. Sreenivasan. All other work conducted for the dissertation was completed by the student independently.

Funding Sources

Graduate study was supported by a HEEP Graduate fellowship from Texas A&M University Hagler Institute for Advanced Study, Texas A&M Energy Institute Fellowship and Department of Aerospace Engineering, Texas A&M University. The computing resources were provided by the Extreme Science and Engineering Discovery Environment (XSEDE) supported by NSF and early access programs at TACC.

TABLE OF CONTENTS

Page

LIST OF FIGURES

FIGURE Page

LIST OF TABLES

TABLE Page

1. INTRODUCTION

Turbulence is ubiquitous in natural and engineering applications. It can suppress energy loss in fusion reactors [4] and plays a crucial role in stellar formation [5]. Turbulence has first order effects in processes critically important to society such as mixing of chemicals and pollutants in the atmosphere and oceans [6] and high speed flight [7]. Understanding the structure and dynamics of turbulence is thus of obvious fundamental and engineering importance. Yet, turbulence is a notoriously difficult phenomenon to describe [8]. The problem of turbulence is much different than other complex systems such as in biology and economics where the equations governing their dynamics are unknown. For turbulence, the widely accepted governing equations of fluid motion have been known since the 19^{th} century [9, 10, 11]. These are based on fundamental concepts in mechanics and thermodynamics– the conservation of mass, momentum and energy with the general form

$$\frac{\partial \rho}{\partial t} + \frac{\partial \rho u_i}{\partial x_i} = 0 \tag{1.1}$$

$$\frac{\partial \rho u_i}{\partial t} + \frac{\partial (\rho u_i u_j)}{\partial x_j} = -\frac{\partial p}{\partial x_i} + \frac{\partial \sigma_{ij}}{\partial x_j} + \rho f_i \tag{1.2}$$

$$\frac{\partial (\rho e)}{\partial t} + \frac{\partial (\rho e u_j)}{\partial x_j} = -p\frac{\partial u_i}{\partial x_i} + \frac{\partial}{\partial x_i}\left(\kappa \frac{\partial T}{\partial x_i}\right) + \sigma_{ij} S_{ij} - \Lambda \tag{1.3}$$

where ρ is the density of the fluid, u_i is the velocity in i direction, p is the pressure, T is temperature, κ is thermal diffusivity, e is the internal energy per unit mass, f_i is the force along ith direction and Λ is an energy sink or source. σ_{ij} is the viscous stress tensor and S_{ij} is the strain tensor with the form

$$\sigma_{ij} = \mu\left(\frac{\partial u_i}{\partial x_j} + \frac{\partial u_j}{\partial x_i} - \frac{2}{3}\delta_{ij}\frac{\partial u_k}{\partial x_k}\right) \tag{1.4}$$

$$S_{ij} = \frac{1}{2}\left(\frac{\partial u_i}{\partial x_j} + \frac{\partial u_j}{\partial x_i}\right) \tag{1.5}$$

where μ is the fluid viscosity. Viscosity is the physical mechanism for converting kinetic energy to heat via dissipation $\epsilon = 2\nu S_{ij}S_{ij}$, largely at the smallest scales. The thermodynamic equation of state used to close the above set of equations, in this work, is the ideal gas law i.e. $p = \rho RT$. The complexity of turbulence is an emergent phenomenon of the above mentioned equations which result from a strong coupling across different scales and between mechanics and thermodynamics of the system. The highly non-linear, non-local and chaotic nature of these equations renders them enormously difficult to analyze mathematically and simulate computationally [12].

Within incompressible (constant ρ) fluids with constant transport properties, turbulence is simply a problem in mechanics. This reduced set of incompressible Navier-Stokes equations is, in general, a good approximation for fluids moving much slower than the speed of sound and has the following form

$$\frac{\partial u_i}{\partial t} + u_j \frac{\partial u_i}{\partial x_j} = -\frac{\partial p}{\partial x_i} + \nu \frac{\partial^2 u_i}{\partial x_i^2} + f_i \tag{1.6}$$

where $\rho = 1$ without the loss of generality, f is a body force and the velocity field is subject to the incompressible mass conservation condition $\partial u_i/\partial x_i = 0$. The velocity field is decoupled from the thermodynamic field. The thermodynamic state however is determined by the velocity field. The mathematical complexity of even this reduced set warranted their inclusion in Clay Institute Millennium problems [13]. The still unsolved problem seeks to establish basic properties such as a proof (or lack thereof) of existence and uniqueness of a solution from a given initial conditions. While these equations have allowed us to compute and analyze laminar flows across a wide range of highly simplified problems, under simplifying assumptions, the emergence of turbulence and its properties from these equations is still not well understood.

The transition to turbulence itself was first observed by Reynolds [14] in pipe flows and continues to be a focus of active research even today [15, 16]. The analysis of the turbulent regime presents extreme challenges due to the non-integrability of governing equations and their extreme sensitivity to initial conditions. The problem is further complicated by an increasing number of

excited and non-linearly interacting spatio-temporal scales. Thus far, the stochastic or statistical approach for describing and analyzing turbulent flows has been most successful. Other deterministic and structure based (e.g. coherent structures, wavelet etc.) approaches have found limited success [17, 18]. The statistical approach for analyzing turbulent flows was first introduced by Reynolds where the velocity is decomposed into a statistical mean and random fluctuations around it. Kolmogorov [19] formalized this further by developing a theory of turbulence based on the statistical features of velocity fluctuations.

1.1 Statistical description of turbulence

Kolmogorov first formalized the statistical approach towards a theory of incompressible turbulence (K41), valid at asymptotically high (yet undetermined) Reynolds number ($Re = \rho u L/\mu$) [19]. Re is the only non-dimensional parameter characterizing the incompressible Navier-Stokes equations. The theory describes turbulent velocity field using statistics of its increments ($\delta u(r) = u(x+r) - u(x)$) and is based on two features. First, an experimental observation that the kinetic energy dissipation ε is independent of Re for a large enough Re i.e. a non-vanishing dissipation in the limit of vanishing viscosity. This fact, termed dissipative anomaly, was established a decade earlier by Taylor [20] (see also [21] for other references). Second, small scales are independent of the large scales and are homogeneous and isotropic. Between the largest energy containing scales (L) and smallest dissipative scales (η), exists a so-called inertial range of scales where the energy cascades successively from larger to smaller scales without any dissipative losses. Conservation of energy then prescribes the energy transfer rate across these scales to be equal to dissipation which is the same as the energy input at the largest scales. These range of scales are self-similar and therefore are characterized solely by the energy transfer rate (ε) and scale size r. This was an early attempt of introducing scaling in physical systems, at least a decade before the establishment of critical phenomena in statistical mechanics [22]. The p^{th} order statistics of the velocity increments then have the general form $\langle(\delta u(r))^p\rangle = \langle u((x+r) - u(x))^p\rangle$, where $\langle\ \rangle$ represent an appropriate statistical average. Navier-Stokes then imposes an important constraint on the probability distribution function (PDF) of velocity increments which must satisfy $\langle \delta u(r)^3\rangle = -4/5(r\varepsilon)^{1/3}$ [23]. This

negative skewness is interpreted as the average direction of energy flux being from large to small scales, a phenomenon called turbulent cascade [24]. Dimensional arguments can then be used within these inertial scales for the second order moment having the form $(\langle \delta u(r)^2 \rangle) = C_2(r\varepsilon)^{2/3}$. This is important as the Fourier transform of $\langle \delta u(r)^2 \rangle$ is the energy spectrum of turbulent fluctuations across scales. This was further generalized to speculate pth order moment of the velocity increments then scales with the exponent $p/3$ over distance r with $L > r > \eta$ i.e.

$$\langle (\delta u(r))^p \rangle = C_p(r\varepsilon)^{p/3} \tag{1.7}$$

where C_p may be dependent on large-scale flow features. Beyond the inertial range of scales are the smallest dissipative scales characterized by the viscosity $\nu = \mu/\rho$ and energy transfer rate. Therefore, the smallest scales can be estimated to be $\eta = (\nu^3/\varepsilon)^4$. One can then show that $L/\eta \propto Re^{3/4}$ and therefore a wider inertial range develops in high-Re flows. This initiated a decades long research agenda to measure turbulence properties across various flows at ever increasing Re [21, 25, 26]. Although early experimental results appeared to support this power-law scaling, at least for energy spectrum, careful analysis revealed departures from K41 prediction for all n except $n = 3$ [25]. These departures from predicted scaling were attributed to large deviations of the velocity increments from the mean, which become larger with increasing Re. Even though the predictions from K41 do not agree well with data, it laid the foundations for a statistical theory of turbulence. The theory also did not address, how an initial flow transitions to this asymptotic statistical state. Since the theory itself was only valid at an arbitrarily large value of R_λ, departures from predictions were often attributed to finiteness of Re [27]. However, the persistence of departures across flows and ever increasing range of Re has firmly established the existence of extreme events as a feature of turbulent dynamics that must be accounted for by a successful theory [25, 26].

The high-Re required by K41 can be estimated from the behavior of dissipative anomaly. Dissipative anomaly requires that the normalized dissipation $\beta = \varepsilon L/u^3$, where L and u are some viscosity independent length and velocity scales respectively, approach a constant in the limit of

high-Re [28, 29, 30]. A functional form for $\beta = A(1 + \sqrt{1 + B/Re})$ is proposed by Doering & Foias [31] that satisfies rigirous bounds deduced from Navier-Stokes. A simple fit of the data from our DNS database to the proposed form suggests $A \approx 0.16$ and $B \approx 143$. Similar values have been estimated by others [29, 28, 32]. Therefore in the limit of $Re \to \infty$, $\beta \to 0.32$ and at low-Re, $\beta \propto 1/\sqrt{Re}$. The Re where dissipative anomaly is established can be estimated by extrapolating the low-Re power-law region until it intersects the asymptotic value. Based on our fit, the intersection occurs at $Re \sim 36$. Although, other estimates can been made based on different fits reported in the literature, they are of the same order [29, 33, 28, 32]. Therefore, dissipative anomaly and the underlying assumption in K41 is satisfied at very low-Re.

An implicit consequence of dissipative anomaly in K41 is the energy cascade across scales is local. This means that energy is transfered between scales of similar size (on average from larger to smaller scales), among the wide range of available scales in turbulent flows. This behavior has been widely studied [34, 35, 36, 37, 38, 39, 40] and a broad conclusion is that the interactions can be highly non-local but the integrated effect yields a cascade-like local energy transfer between scales of similar size. However, the low Reynolds number in those studies, due to limitations of computing power at that time, did not allow previous researchers to distinguish the inertial range from the bottleneck region ([41, 42, 43, 44, 45]).

K41 also assumes a global scale invariance which has the consequence that the smallest scales are Re independent when normalized by η. This has thus far been studyied using the energy spectrum in the dissipation range and establishing that the spectra collapse when length scales are normalized by η, i.e. the spectra in dissipation range exhibit complete self-similarity. Other theories use different arguments to make similar predictions. A notable exception is the milti-fractal formalism [46] which replaces the global scale invariance with local scale invariance (detailed in section 4). The theory then predicts that the dissipation range should exhibit Re dependent scaling. The validity of this prediction is yet to be established. Although, a wide range of studies claim (or assume) that the dissipation range is completely self-similar, they do not include a large range of Re, or do not measure scales too far into the dissipation range.

An important feature of turbulent velocity fluctuations, ignored in K41, is the presence of extremely large fluctuations compared to mean quantities. These fluctuations become stronger with increasing Re and decreasing scale size (r) [46]. This phenomenon is referred to as intermittency and subsequent work, from Kolmogorov and others, attempted to include its effect on scaling exponents in the inertial range [47]. Many are cast in the framework of multifractal formalism, with K41 being a degenerate case [48, 49, 46, 25]. The case of K41 is referred to as "trivial" scaling. In fact, any fractional Brownian motion satisfies the K41 scaling exponent relation $\zeta_p = (p/2)\zeta_2$ for even orders [25]. Intermittency is equivalent to a non-linear or anomalous variation of scaling exponents and is attributed to a complex relationship between velocity increment PDFs and scale size. The connection to Navier-Stokes for most models is, however, often missing or inadequate. Therefore, they do not provide insights into the detailed physics of turbulence *a priori*. They simply provide means of calculation, usually of the scaling exponents at asymptotically large-R_λ. Some models fit the data better than others, but none of them are deemed definitive, based on several physical considerations [50]. None of the theories, including K41, or models address the emergence of this predicted scaling and often emphasize the role of very large Reynolds numbers. Turbulence research, therefore, has sought an ever increasing growth in Re and the complexity of the problem has been attributed, partially, to the difficulty of realizing high-Re flows in experiment or computation [51].

Intermittency has also been observed in the dissipative scales and many models have been developed to describe it [25]. The models largely link the statistics of velocity increments in inertial range to those of velocity gradients at small scales, where the inertial and dissipative scales match (e.g. $\delta u(r \to \eta)$). Most models however, again, do not have a clear connection with Navier-Stokes equations. Recent work by Yakhot provides new insights into the problem while keeping its considerations close to the governing equations [52, 53, 54, 55, 56]. An important feature of these models and others (e.g. [57, 2]) is to consider the dissipative scales (η) as a field rather than a unique scale as in K41. A unique feature of Yakhot's model is the presence of a finite critical-Re beyond which turbulent features are present and this state is predictive of IR scaling exponents in

the $Re \to \infty$ limit. This will be discussed next.

1.1.1 An alternate perspective: Yakhot model and critical Reynolds number

Recent work has considered an alternate approach for incompressible turbulence [16, 53, 58, 52, 59, 60, 33] in an infinite domain stirred at the largest scales by a random force. These flows are governed by Eq. (1.6). The force (f_i) is white-in-time Gaussian defined by the correlation

$$\langle f_i(\mathbf{k},\omega) f_j(\mathbf{k'},\omega')\rangle = (2\pi)^{d+1} D_0 d(k) P_{ij}(\mathbf{k})\delta(\omega+\omega')\delta(\mathbf{k}+\mathbf{k'}) \tag{1.8}$$

where D_0 is the forcing amplitude, $(\mathbf{k},\omega)$ is the four vector and $P_{ij}(\mathbf{k} = \delta_{ij}k_ik_j/k^2)$ is the projection operator. The forcing amplitude distribution is described by $d(k)$ which is non-zero in a small interval $|\mathbf{k}| \approx 2\pi/L_0$. This function represents the different mechanisms of energy injection across various turbulent flows. Then, one can write the Fourier transform of Eq. (1.6) as

$$u_l(\mathbf{k},\omega) = G^0 f_l(\mathbf{k}\omega) - \frac{i}{2} G^0 P_{lmn} \int u_m(qi,\Omega) u_n(\mathbf{k\text{-}q},\omega-\Omega) d\mathbf{q} d\Omega \tag{1.9}$$

where $G^0 = (-i\omega + \nu k^2)^{-1}$, $P_{lmn}(\mathbf{k}) = k_n P_{lm}(\mathbf{k}) + k_m P_{ln}(\mathbf{k})$. Introducing the zeroth-order solution $\mathbf{u}_0 = G^0\mathbf{f} \propto \sqrt{D_0}$ such that $\mathbf{u} = G^0\mathbf{f} + \mathbf{v}$ where the perturbation $\mathbf{v}$ is given by

$$\begin{aligned} v_l(\hat{k}) = &-\frac{i}{2} G^0(\hat{k}) P_{lmn}(\mathbf{k}) \int v_m(\hat{q}) v_n(\hat{k}-\hat{q}) d\hat{q} \\ &-\frac{i}{2} G^0(\hat{k}) P_{lmn}(\mathbf{k}) \int \Big(v_m(\hat{q}) G^0(\hat{k}-\hat{q}) f_n(\hat{k}-\hat{q}) + G^0(\hat{q}) f_m(\hat{q}) v_n(\hat{k}-\hat{q}) \Big) d\hat{q} \\ &-\frac{i}{2} G^0(\hat{k}) P_{lmn}(\mathbf{k}) \int G^0(\hat{q}) f_m(\hat{q}) G^0(\hat{k}-\hat{q}) f_n(\hat{k}-\hat{q}) d\hat{q} \end{aligned} \tag{1.10}$$

For the case where Eq. (1.9) and Eq. (1.10) are driven by a regular force, the flow is considered laminar at low Re with $\mathbf{v} = 0$. The zeroth order solution becomes unstable as Re is increased beyond a threshold Re_{inst} and perturbations grow in time. For the case of $Re/Re_{inst} - 1 \gg 1$, the coupling becomes stronger and leads to the state of fully developed turbulence. The growth of such instabilities is often complicated and dependent on flow features, especially near Re_{inst}. For the

case of flow generated by a Gaussian force Yakhot & Sreenivasan [16] argue that the large scales are Gaussian by virtue of Central Limit Theorem and the flow is in "thermodynamic equilibrium". For smaller scales, far away from the forcing scales, the dynamics are out-of-equilibrium as they are populated by non-linear interactions across scales. Yakhot & Donzis [60] argue that even at very low-Re, when the flow is Gaussian, there exist rare events that lead to departure of the PDF from gaussianity. These rare events are responsible for dissipation of large amounts of kinetic energy. At higher-Re, the non-linear dynamics in Eq. (1.10) determines the dynamics entirely leading to velocity fluctuations far from the forcing scale. Therefore, low and high-order moments of the fluctuations may describe entirely different phenomena.

For a random Gaussian field, e.g. the velocity gradients, where the variance depends on Re ($\langle(\partial u/\partial x)^2\rangle \propto Re^{\rho_2}$), all the moments are described by $\langle(\partial u/\partial x)^{2n}\rangle = (2n-1)!!\langle(\partial u/\partial x)^2 \propto Re^{n\rho_2}$. For high-$Re$ however, we know the flow is non-gaussian and the anomalous exponent for a moment $\langle(\partial u/\partial x)^{2n}\rangle \propto Re^{\rho_{2n}}$ with $\rho_{2n} \neq n\rho_2$. In the case of transitional flow (between Gaussian and fully turbulent state), near the transition Reynolds number, the forcing scale is the same order as the dissipative scale. One can then estimate the so-called Taylor Reynolds number

$$R_\lambda = \sqrt{\frac{5}{(3\varepsilon\nu)}}u_{rms}^2 \approx \sqrt{\frac{5L^4}{3\nu\varepsilon}}\langle(\partial_x u_x)^2\rangle \tag{1.11}$$

based on the velocity gradients. Since strong turbulence is described by velocity gradients which cannot be estimated simply by the variance, an infinite number of Reynolds numbers must be introduced

$$R_{\lambda_n} = \sqrt{\frac{5L^4}{(3\varepsilon)\nu}}\langle(\partial_x u_x)^{2n}\rangle^{1/n} \tag{1.12}$$

Yakhot & Donzis [60] consider a low-R_λ flow, forced at the largest scales, where the statistics are Gaussian. Increasing the R_λ eventually leads the flow towards the limit of Gaussianity at a critical Reynolds number ${R_\lambda}^{tr}$. For a similar flow at very high-R_λ, strongly turbulent regime, the low-order statistics are dominated by a huge turbulent viscosity $\nu_T \propto \varepsilon^{1/3}L^{4/3}$ where L is the integral

scale. The effective Reynolds number then is $R_\lambda^+ \propto \sqrt{L^4/(\varepsilon\nu_T)}(\partial_x u_x)^2$. For a smooth transition, indicated by experiments and simulation data, one can write at the transition R_λ

$$R_\lambda{}^{tr}(2) = \sqrt{\frac{5}{3\varepsilon\nu_{tr}}}u_{rms}^2 = \sqrt{\frac{5}{3\varepsilon\nu_T}}u_{rms}^2 \tag{1.13}$$

where the effective turbulent viscosity is given by [59] $\nu_T \approx 0.084K^2/\varepsilon$ and $K = u_{rms}^2/2$ is the kinetic energy of the turbulent fluctuations. Then $R_\lambda{}^{tr}(2) \approx 9$. Further, Eq. (1.11) and Eq. (1.12) can be used to show

$$R_\lambda{}^{tr}(n) \propto (R_{\lambda,n}^{tr})^{n/\rho_{2n}} \tag{1.14}$$

Yakhot & Donzis forced the domain with white-in-time Gaussian force and showed that the velocity gradient statistics are Gaussian at the low-R_λ limit and transition to algebraic scaling beyond a critical R_λ. The transition R_λ for each order moment was consistent with Eq. (1.14). By definition, the order dependent Reynolds will probe increasingly rare events with increase in order of the moment. Each order will transition to algebraic scaling or the strong turbulence regime, when the order dependent Reynolds number exceeds 9. In terms of the global-R_λ, this means higher order moments will transition at a lower-R_λ than low-order moments will. This approach has distinct advantages over K41 and other classical theories. The transition to turbulence occurs at a well defined Reynolds number, which is low-enough to be realized in practice across a wide range of turbulent flows. Further, the scaling exponents of different moments can be calculated by simply matching the Gaussian state with that of algebraic scaling present in the strong turbulence regime at the transition Reynolds number. This is explained in detail in Section 5. Yakhot & Donzis [33] also show that the scaling exponents (ρ_{2n}) derived using this approach and available in flows with $R_\lambda \sim O(10)$ are predictive of the scaling exponents (ζ_p) of velocity increments in the inertial range which only exists for $R_\lambda > 200$. This strong result shows that intermittency itself is not a high-Reynolds number feature and that scaling within turbulent flows emerges much earlier than the emergence of an inertial range. The general validity of this approach beyond Gaussian forcing

is yet to be established. This is particularly important to establish the universality of scaling exponents, both in dissipation and inertial range, which may depend on forcing statistics. The transition proposed by Yakhot & Donzis has only been observed for longitudinal velocity gradients and does not make predictions regarding more complex quantities such as transverse velocity gradients, enstrophy etc. that are relevant to applications and have important consequences for mathematical nature of Navier-Stokes equations [61].

1.2 Intermittency in compressible turbulence

Turbulence theory has largely been driven by exploration of the incompressible regime. However, a wide range of turbulent flows are compressible. For example, stellar formation is a result of shock interactions with turbulent flows in the presence of magnetic and gravitational fields [5, 62, 63, 64]. High-speed aerodynamics and inertial-confinement fusion plasma dynamics are dominated by compressive motions in turbulent flows [65, 66, 4]. A large body of the literature studies compressible turbulence in the context of corrections to incompressible turbulence theory [67, 64]. The corrections are often made to different predictions of K41, which as discussed before, is not an adequate description of incompressible turbulence. Important features of K41 e.g. dissipative anomaly, its relationship to cascade are not at all established in compressible turbulence [68, 69]. Therefore, fundamental questions such as the existence of an inertial range and description of intermittency are not well posed. The complexity of analyzing compressible flows is further increased due to interactions between the velocity field and thermodynamic state. In addition to intrinsic intermittency of turbulence, similar to the incompressible counterpart, compressible flows are comprised of strong gradients due to small shock-like features, termed shocklets [70, 62, 71, 72, 73, 74]. These interactions and their effects on intermittency (or scaling exponents) have yet to be characterized and understood. Measurements of intermittent quantities are further complicated by the increased difficulty of realizing highly compressive flows in simulation and experiment in comparison to their incompressible counterparts [75], especially at high-R_λ. Yakhot's formalism however provides a novel pathway to study intermittency and emergence of scaling in compressible turbulence at low to moderate-Re.

1.3 Objectives of the present work

The general focus of this dissertation is to characterize and understand signatures of fully-developed turbulence and their emergence as the Reynolds number increases. We will systematically assess the assumptions in K41 and contextualize the observed behavior with respect to different theoretical formalisms describing turbulence dynamics. Particular emphasis will be on the universality of small-scales and the scaling of intermittent quantities.

The specific objectives are to

- Build a massive database for incompressible and compressible turbulence simulations which covers a wide range of energy injection mechanisms across a wide range of parameter space. A combination of these mechanisms will allow us to establish universality across different flows and address the effects of forcing on Navier-Stokes dynamics. The simulations presented in this work have the highest spatial and temporal resolution in literature.

- Analyze the dynamic relationship of energy transfer between scales and establish locality (or lack thereof) of energy transfer in inertial, bottleneck and dissipation range. The behavior is analyzed across a range of Reynolds numbers and its dependence on temporal variation in the energy injection at large scales is addressed.

- Establish the behavior of dissipation range in the energy spectrum to enable discrimination between theoretical formalisms based on global and local scale invariance of velocity fluctuations.

- Generalize the Yakhot formalism for flows driven by non-gaussian forces and assess the universality of scaling across different forcing mechanisms and of different intermittent quantities. In particular, establish the scaling of longitudinal and transverse velocity gradients, and dissipation and enstrophy. This will help establish universality across different flows which vary widely in large-scale turbulence production mechanism and other details such as geometry etc.

- Study the emergence of intermittency and scaling within compressible flows. Systematically study the effect of varying levels of compressibility on intermittency and scaling of velocity gradients. The vast majority of flows exhibit varying levels of compressibility. Therefore it is important to study the effect of compressibility on turbulence signatures for incompressible flows.

The remaining parts are organized as follows. In chapter 2, we briefly describe the numerical methods for our direct numerical simulations and establish the resolution criteria for convergence. In chapter 3, we begin our analysis of unsteady inter-scale interactions and their dynamics in spectral space. In chapter 4, we analyze the averaged energy spectrum at small-scales, establish its form in high-R_λ flows and when such a form first emerges. In chapter 5, we complement the spectral perspective of small-scales with their dynamics in physical space. Particular focus again will be to establish the scaling of intermittent quantities in high-R_λ turbulence, at what R_λ they emerge and the universality of these results with different large-scale stirring mechanisms. In chapter 6, we establish the scaling and universality of compressible flows. We separately analyze the solenoidal and dilatational components. Statistics of solenoidal field are compared with incompressible turbulence and those of dilatational field are compared with Burgers turbulence. Chapter 7 summarizes the conclusions and explores future research directions.

2. DIRECT NUMERICAL SIMULATIONS

In this dissertation, we employ direct numerical simulations (DNS) to study fluid turbulence. DNS consists of solving the exact equation of motion, Eq. (1.3) and Eq. (1.6), across all scales at each time instant. We use two separate codes to study incompressible and compressible turbulence. The questions we seek to answer and mention in Section 1 require ensemble averaging in a stationary turbulence. The ensemble statistics for relevant quantities are calculated using snapshots of velocity saved at regular intervals that are sufficiently far apart (of the order of an eddy-turnover time). This approximation is valid due to the ergodic nature of fluid turbulence. Since turbulent flows are dissipative, a statistically stationary state is maintained by forcing at the largest scales.

2.1 Incompressible turbulence simulation: MPI2D

We use MPI2D [76] to simulate homogeneous isotropic incompressible turbulence in a triply periodic domain with zero mean velocity. For this case, the incompressible Navier-Stokes, Eq. (1.6) are solved numerically using Rogallo's method [77]. The Navier-Stokes equation are transformed to Fourier Space and have the form

$$\frac{\partial \hat{u}(\mathbf{k},t)}{\partial t} = -ik_l P_{im}(\mathbf{k}) \int_{\mathbf{k'}} \hat{u}_m(\mathbf{k'},t)\hat{u}_l(\mathbf{k}-\mathbf{k'},t)d\mathbf{k'} - \nu k^2 \hat{u}_i(\mathbf{k},t) + \hat{f}(\mathbf{k},t) \tag{2.1}$$

$$k_i \hat{u}_i(\mathbf{k},t) = 0 \tag{2.2}$$

where $\hat{u}_i(\mathbf{k},t)$is the velocity Fourier coefficient at time t for a wavenumber vector $\mathbf{k}$, $P_{im}(\mathbf{k}) = \delta_{im} - k_i k_m/k^2$ ($|\mathbf{k}| = k$) is the solenoidal projection tensor and $\hat{f}$ is the Fourier coefficient of an external force or forcing. The resulting set of coupled ordinary differential equations is then integrated in time using an explicit second-order Runge-Kutta method. The Eq. (2.1) can be written as

$$\frac{d\mathbf{u}(\hat{\mathbf{k}},t)}{dt} = \hat{\mathbf{g}}(\hat{\mathbf{u}}(\mathbf{k},t)) \tag{2.3}$$

where $\hat{\mathbf{g}}$ is the acceleration given by Eq. (2.1). In order to advance from time t_n to t_{n+1} a first-order predictor approximation is computed as

$$\hat{u}^*(\mathbf{k}) = \hat{u}(\mathbf{k}, t_n) + \Delta t \hat{\mathbf{g}}(\hat{\mathbf{u}}(\mathbf{k}, t_n)) \tag{2.4}$$

The approximation is improved using a corrector step as

$$\hat{u}(\mathbf{k}, t_{n+1}) = \hat{u}(\mathbf{k}, t_n) + \frac{\Delta t}{2} \left(\hat{\mathbf{g}}(\hat{\mathbf{u}}(\mathbf{k}, t_n)) + \hat{\mathbf{g}}(\hat{u}^*(\mathbf{k}))\right) \tag{2.5}$$

The timestep Δt is determined based on numerical stability requirements for explicit schemes and expressed using Courant number (C). The Courant number is conservatively calculated based on the maximum speed i.e.

$$C = \Delta t \; max \left\{ \frac{|u_1(x,t)|}{\Delta x_1}, \frac{|u_2(x,t)|}{\Delta x_2}, \frac{|u_3(x,t)|}{\Delta x_3} \right\} \tag{2.6}$$

where the maximum is computed across the entire domain. Previous test had indicated that $C < 1$ guarantees stability and provides reasonable results. However, recent work has shown that a much smaller value is needed for accurately capturing extreme events. Since we are interested in measuring intermittency and high-order statistics, we have nominally used $C \leq 0.3$ in our database [61]. This temporal resolution is accurately captures the maximum value of the most intermittent quantities, when coupled with a high spatial resolution.

An important challenge for spectral codes is the calculation of convolution terms such as those in Eq. (2.1). A fully spectral method for calculation such a convolution requires N^6 operations as each wavenumber requires an integration with respect to N^3 wavenumbers. Such a cost is computaitonally prohibitive even with the enormous computational power available today. This is mitigated by calculating the non-linear terms in physical space and then transforming them back to Fourier space [78, 79, 80]. This psuedo-spectral scheme reduces the computational cost but introduces aliasing errors. The aliasing errors are controlled by a combination of truncation and

phase shifting techniques based on Rogallos algorithm [77]. The highest wavenumber that can be resolved in the scheme used in this code is $k_{max} = \sqrt{2}N/3$ where N is the number of grid points in each direction. This wavenumber can be compared to turbulence scales by normalizing with the smallest relevant scale, the kolmogorov length scale η where most dissipation occurs. Within literature, a standard of $k_{max}\eta \approx 1.5$ is standard. In this dissertation, we have used a resolution at least twice that and up to an order magnitude larger than this standard to capture scales far smaller than η and accurately capture extreme fluctuations. Since we seek high-R_λ simulations with very high resolutions, the code employs a massive parallel implementation using MPI in FORTRAN. Details regarding the implementation can be found in [76].

2.1.1 Forcing mechanims

In order to maintain a statistically stationary state of turbulence at a given R_λ, we use a large scale forcing mechanism. Since one of the objectives in this dissertation is to establish the universality of various results, we use a range of forcing mechanisms to compare statistics across them. Different sections use a different combination of the below mentioned schemes

1. **Gaussian**: The velocity field is forced numerically at the large scales using a combination of Ornstein-Uhlenbeck processes with Gaussian statistics and finite time correlation. The code is able to force wavenumbers in a sphere i.e. $k \leq k_f$ or within a band $k_{f1} \leq k \leq k_{kf2}$. This mechanism has been widely used in turbulence literature [81] to simulate high-R_λ isotropic flows. It also allows us to force the field with Gaussian white noise when the correlation time is set to zero.

2. **Exponential**: The velocity field is forced in a similar fashion as the Gaussian implementation. However, the random number generator is switched from Gaussian statistics to exponential statistics. This is achieved by generating a random number (r_u) from a uniform distribution between $(0, 1)$ and using the transform $r_e = log(1 - r_u)$. The transformed distribution with r_e is an exponential random distribution.

3. **Deterministic**: This scheme is based on Yeung & Donzis and maintains a constant energy

within each wavenumber in the sphere $k \leq k_f$ [82].

4. **Linear**: This scheme is also widely used in literature for simulation of high-R_λ turbulent flows [83, 30, 84, 85, 86]. In this scheme $\hat{\mathbf{f}}(\mathbf{k}, t) = A\hat{\mathbf{u}}(\mathbf{k}, t)$ where A is a constant. Navier-Stokes with a forcing term of this form is equivalent to a shear-flow with a constant mean velocity gradient of A. It has the desirable property that it sets the dissipation to a set constant proportional to A and is computationally cheaper to implement as no new fields need to be generated for the force term. This scheme can be implemented in a sphere $k \leq k_f$ or a band $k_{f1} \leq k \leq k_{f2}$.

5. **Linear Vorticity**: In this scheme $\hat{\mathbf{f}}(\mathbf{k}, t) = A\hat{\omega}(\mathbf{k}, t)$ where $\omega = \nabla \times \mathbf{u}$. Vorticity in general is known to be more intermittent than the velocity field, so this scheme allows us to compare the effects of large changes in forcing on Navier-Stokes dynamics. Its implemented in a sphere or band, similar to linear velocity forcing.

2.1.2 Convergence and resolution effects

In this dissertation we study small scale statistics in great detail using very high resolution DNS. Within literature a wide range of resolution criteria have been proposed and are used Our spatial resolution is at least twice and up to 10 times better than those reported in the literature at a given R_λ. We have therefore used computational capabilities to improve resolution instead of pushing for higher-R_λ simulations, as is the norm. Recent work has also shown that the standard use of Courant number between 0.6 and 1 is not adequate for accurately capturing extreme events [61]. A more stringent criteria of $C \leq 0.3$ is proposed for capturing extreme events in high-$R_\lambda \sim (\geq 400)$ turbulence. Our simulations satisfy this stringent criteria, even though the R_λ under consideration are smaller and the spatial resolutions are generally higher. In Fig. 2.1, we have plotted the time averaged compensated energy spectrum $\psi(k) = E(k)\langle\epsilon\rangle^{-2/3}k^{5/3}$ for $R_\lambda \approx 50$ at different spatial and temporal resolutions as well as precision. We see that for the case of $N^3 = 512^3$, the three cases overlap up to $k\eta \approx 6$, where the case of single precision departs due to contamination from round-off errors. We have verified this by repeating the simulation in double precision which simply

extends the spectrum to higher wavenumbers without being affected by round-off. Improving the time resolution does not affect the spectrum either. Doubling the spatial resolutions extends the spectrum up to $k\eta \approx 14$, beyond which the round off errors dominate at this precision. Although

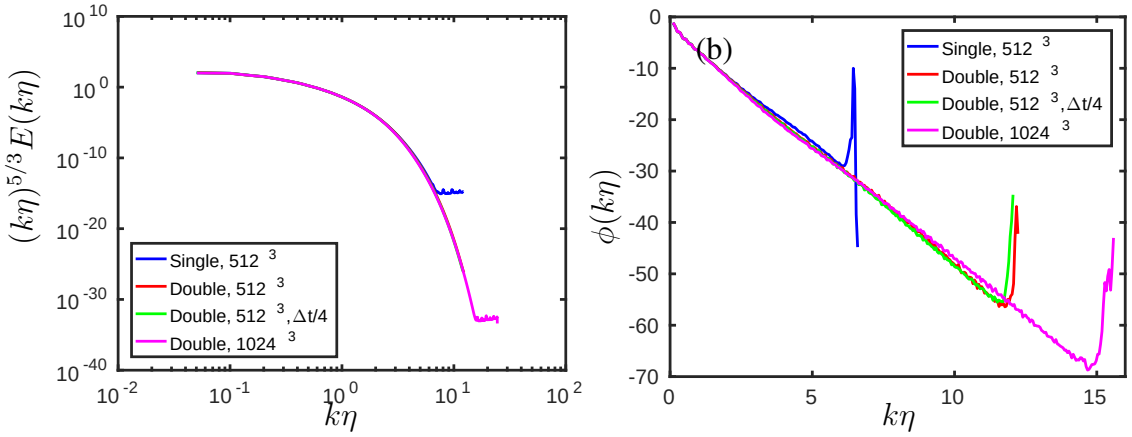

Figure 2.1: Energy spectrum (a) and its log derivative ($\phi(k) = d\log(E(k))/d\log(k)$) (b)for $R_\lambda \sim 50$.

it is clear from Fig. 2.1 that our resolutions are adequate for small-scales, it is important to verify the convergence for higher-order quantities. We therefore plot the moments of transverse velocity gradients ($M_{2n}^{\perp} = \overline{\langle(\partial_y u_x)^{2n}\rangle}/\overline{\langle(\partial_y u_x)^2\rangle})^n$ at higher-orders for $R_\lambda \approx 90$ in Fig. 2.2. Transverse gradients are highly intermittent and are therefore highly sensitive to grid resolution, much more than longitudinal velocity gradients [26, 61, 51, 87]. It is clear that resolutions of $k_{max}\eta \gtrsim 3$ are adequate for capturing moments up to 10th order. We will therefore use this as our minimum resolution criteria.

The simulation details and parameters used for studying various features can be found in each section.

2.2 Compressible turbulence simulation: cDNS

Compressible turbulence simulations are performed using cDNS [75] code. The fully compressible Navier-Stokes equations, Eq. (1.3), are solved using 10^{th} order compact schemes in space

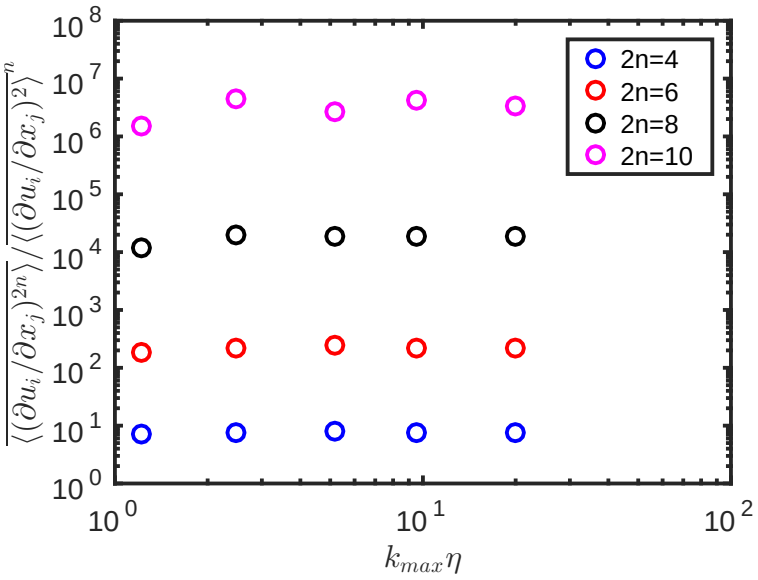

Figure 2.2: Moments of transverse velocity gradients at different grid resolutions.

and are veolved in time using a thrid order Runge-Kutta scheme. Details about the schemes and their implementation can be found in [75, 88, 89]. A statistically stationary state is maintained by forcing at the largest scales and uniformly removing internal energy to maintain constant mean temperature. The code is able to force both the solenoidal and dilatational modes. To accomplish this, the Fourier modes of the forcing vector are projected along the wavenumber k ($\hat{f}_{||}$) and perpendicular to it ($\hat{f}_{\perp}$). These Fourier coefficients follow independent OU processes with a finite time correlation and act only at low wavenumbers inside a shell of radius $k_f \approx 3$. In this dissertation, the forcing is purely solenoidal.

Compressible turbulence is affected by the internal intermittency, similar to incompressible turbulence, as well as shock-like flow structures [70, 74, 64], termed shocklets. These small scale flow features can affect the flow statistics and alter different quantities differently. For example, longitudinal gradients may be affected by a shock-like structure as flow moves perpendicular to it while the transverse gradients will remain unaffected. Therefore, it is important to assess the resolution criteria for both. Within literature, a resolution of $\eta/\Delta x$ ranges from 0.5 to 1 depending on numerical schemes used and the level of compressibility. We know from our experience with

incompressible turbulence that the level of internal intermittency (simply due to mechanics) increases with increase in R_λ. Within compressible flows, the intermittency due to shocklets grows with increase in M_T. Samtaney [70] showed that for moderate compressibility strength, the most probable shocklet thickness is comparable to Kolmogorov length scale. Since we are interested

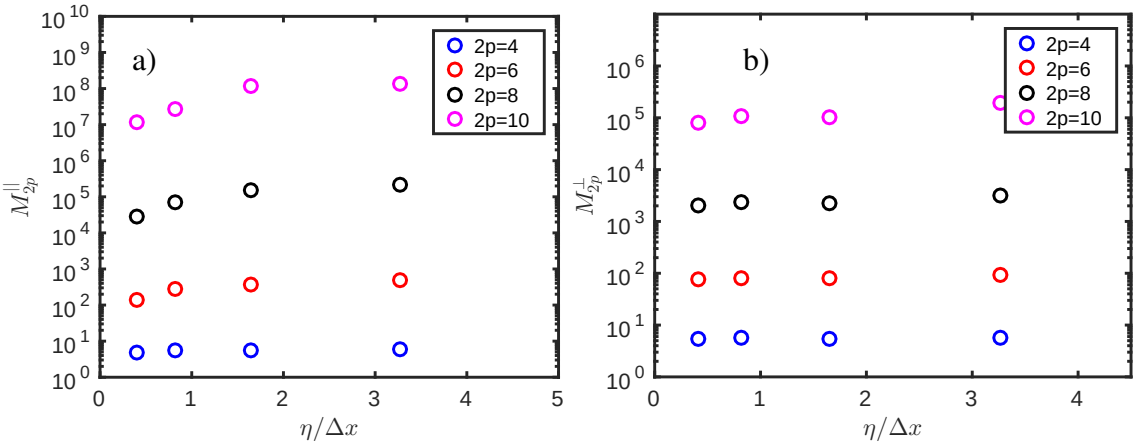

Figure 2.3: Moments of a) longitudinal and b) transverse velocity gradients at $R_\lambda \approx 40$ and $M_T \approx 0.7$.

in velocity gradient moments of high-orders, we perform convergence tests at high R_λ and M_T ($= u_{rms}/c$, c is the speed of sound). In Fig. 2.3, we plot the moments of longitudinal (Fig. 2.3a) and transverse (Fig. 2.3b). It is clear that the resolution criteria are different for longitudinal and transverse. Longitudinal moments converge at a resolution of $\eta/\Delta x \approx 0.8$ while as transverse gradients converge at twice the resolution. This is in contrast with incompressible turbulence where transverse gradients are known to be more intermittent than longitudinal gradients. We therefore use a resolution of $\eta/\Delta x \approx 1.6$. These resolutions are at least two times smaller than those used in previous studies using compact differences and are comparable or better than the ones used along with different numerical methods [88, 89, 68, 74, 73, 70]. The Courant number is kept constant at 0.3.

3. FLUCTUATIONS IN ENERGY AND TRANSFER SPECTRA OF TURBULENCE [†]

3.1 Introduction

Classical phenomenology makes specific predictions for averaged energy and transfer spectra in isotropic turbulence. Although these averaged quantities have been well studied [90, 21, 28, 91, 92, 93, 30, 44, 94] and approximately scale as predicted by [19] scaling, the instantaneous spectra show significant deviation from the averaged ones. The average transfer in particular is assumed to be unidirectional from large to small scales, or in Fourier space, from low to high wavenumbers [95, 23]. The numerous studies addressing non-local interactions in the literature, [34, 35, 36, 37, 38, 96, 39, 40]. have focused mostly on instantaneous or time-averaged snapshots of the flow field at a particular Reynolds number (typically low). In addition, they have largely studied the behavior of so-called individual triads ($T(k|p,q)$, transfers to scale k from non-linear interactions with scales p and q) in order to characterize interactions between similar and disparate scales. A general conclusion that has emerged is that the interactions can be highly non-local but the integrated effect yields a local energy transfer between similarly sized scales [97, 34, 38, 98, 36, 99].

While very useful, all the studies above provide necessarily information at discrete instants of times. This precludes, for example, the study of some of the dynamical aspects of the energy transfer. One can, instead, study the time behavior of spectral components and quantify its statistical behavior through single-time statistics, or two-time statistics to assess correlation between modes. For example, one can study, how high wavenumbers react given a change in a low wavenumber mode. Concepts of cascades can also be investigated. A local cascade, for example, would correspond to strong correlations of neighboring wavenumbers but at a certain time lag, while strong

[†] Figures, tables and portions of text in this chapter reproduced with permission from *S. Khurshid, S., D.A. Donzis, & K.R. Sreenivasan (2021). Slow spectral transfer and energy cascades in isotropic turbulence. Journal of Fluid Mechanics, 908. Copyright 2021 by Khurshid, Donzis & Sreenivasan*

instantaneous correlations between distant wavenumbers could be indicative of short-circuits. A lack of correlation between fluctuations in energy would provide a quantitative measure to assess the independence of scales. Furthermore, this can also be utilized to assess the effect of low-wavenumber forcing at different scales, which would allow one to determine how deep into the inertial or even dissipative scales, specific details of the forcing are imprinted, a question that is intrinsically related to classical justifications behind universal behavior. Thus, understanding the time behavior of fluctuations is of obvious fundamental importance in the physics of energy transfers in turbulence and is the main thrust of the present work. In particular, we are interested in the nature of fluctuations in the three-dimensional energy spectrum and the spectral transfer function as a function of both scale and Reynolds number. The temporal behavior of these spectral functions, thus provide a complementary view of the detailed work based on triadic interactions referenced above.

In this study we use data from direct numerical simulation (DNS) using a pseudo-spectral method with very high spatial resolutions and Taylor Reynolds number ranging from $R_\lambda \sim 3$ to about 400. The resolution is at least $k_{max}\eta \approx 3$ ($k_{max} = \sqrt{2}N/3$ is the highest wavenumber resolvable by the numerical scheme on a N^3 grid, and $\eta = (\nu^3/\langle\epsilon\rangle)^{1/4}$ is the Kolmogorov scale with ν being the viscosity and $\langle\epsilon\rangle$ the average rate of energy dissipation) which is higher than that commonly used in the literature to reach the highest R_λ. The best resolved cases were conducted at $k_{max}\eta \approx 35$. Time stepping is done using a second-order Runge-Kutta method with a time-step size determined by a constant Courant-Friedrichs-Lewy (CFL) number. The highest CFL across the database is kept near 0.3 to accurately resolve extreme events [61]. The flow is forced in Fourier space at non-zero wavenumbers with $|\mathbf{k}| \leq 2$ where $\mathbf{k}$ is the wavenumber vector. To assess the effect of large-scale stirring on all scales we include results from simulations using two different forcing schemes, one stochastic the other deterministic. The former (called SF for short) is based on [100] and have been used extensively in previous studies [101, 102, 94]. The latter (called DF for short) is that introduced in [93] which keeps the energy in the lowest wavenumbers constant. This scheme therefore leads to no time variability in forced modes. In order to ensure convergence

Stochastic Forcing (SF)				Deterministic Forcing (DF)			
R_λ	N	$k_{max}\eta$	T_s/T_E	R_λ	N	$k_{max}\eta$	T_s/T_E
3	128	30.1	15	3	64	15.7	13
7	128	17.4	23	7	128	17.6	19
10	256	27.8	21	10	256	28.3	10
20	512	34.6	21	15	256	20.5	25
50	1024	24.4	34	47	1024	24.1	18
90	2048	21.1	15				
140	1024	5.6	33				
230	1024	2.8	25				
390	2048	2.8	15				

Table 3.1: DNS database: the Taylor microscale Reynolds number is defined as $R_\lambda \equiv u_{rms}\lambda/\nu$, where $u_{rms} = (3/2)\overline{\langle u^2(\boldsymbol{x},t)\rangle}$ (brackets and an over-line correspond to space and temporal averages, respectively), and the Taylor microscale λ is defined using this velocity scale along with its time- and space-average gradient ; N^3 is the grid resolution; T_s is the duration of the stationary state normalized by the eddy-turnover time $T_E \equiv L/u_{rms}$ (L being the longitudinal integral length scale).

of various statistics presented in this section, we have run very long stationary states with at least 10 eddy turnover times. Time averages start when all quantities of interest have reached a stationary state. From careful convergence studies, we found that this is conservatively achieved after eight eddy turnover times from the initial conditions. Simulation details are summarized in Table 3.1.

3.2 Temporal fluctuations of spectral variables

The three-dimensional energy spectrum evolves according to:

$$\frac{\partial E(k)}{\partial t} = T(k) - 2\nu k^2 E(k) + F(k) \tag{3.1}$$

where the intercomponent and interscale energy transfer is represented by the transfer spectrum:

$$T(k) = \frac{1}{2}\Im\left\{[P_{ilm}(k)\hat{u}_i^*(k) + P_{ilm}(k)\hat{u}_i^*(k)]\int \hat{u}_l(p)\hat{u}_m(k-p)dp\right\} \tag{3.2}$$

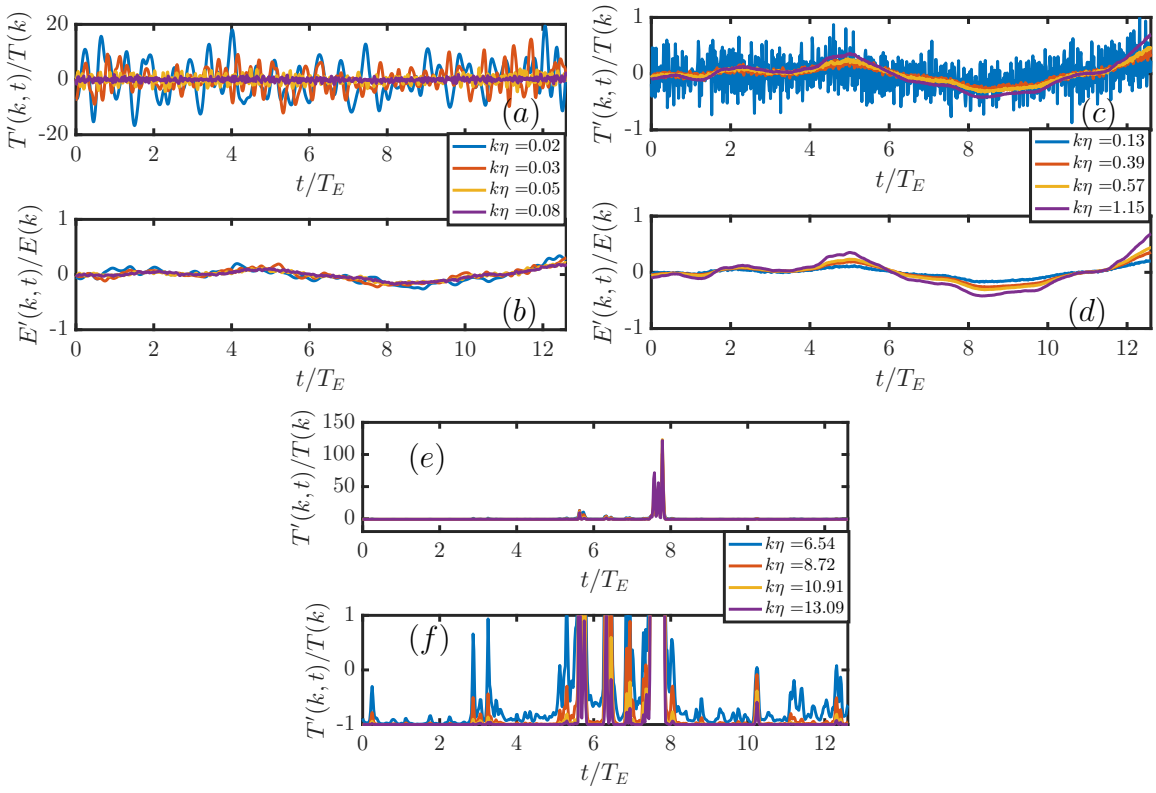

Figure 3.1: Time series of fluctuations in energy and energy transfer in the stationary state; (a-d) $R_\lambda \approx 390$. (a) Temporal change of the energy transfer at wavenumbers in the IR marked in the legend. The time average of the energy transfer has been subtracted, so the quantity presented is the deviation (or the fluctuation) from the average value, divided by the average. Note that the fluctuations are an order of magnitude larger than the average for the transfer. (b) Time series of energy at those same wavenumbers; the fluctuation is of the order of the average. The oscillatory blue line in (c) is the energy transfer in BR, while the others approach NDR; (d) time series for the energy. Figure (e) corresponds to $R_\lambda \approx 90$ and the data are in FDR; (f) highlights the behaviour close to the mean in (e). See text for more details.

and $f(k)$ represents the forcing applied to the lowest wavenumbers ($|k| \leq 2$) as previously described.

It is now convenient to decompose $E(k,t)$ and $T(k,t)$ into a long-time average and fluctuations around it (denoted with a prime). For brevity, we will remove the time argument to denote a time average when no ambiguity is present. Then, we have

$$E(k,t) = E(k) + E'(k,t), \qquad T(k,t) = T(k) + T'(k,t) \tag{3.3}$$

where $E(k) = \overline{E}(k,t) = (1/T_s)\int_0^{T_s} E(k,t)dt$ and T_s is the length of the simulation which is also included in Table 3.1. A similar expression can be written for $T(k)$. Since Eq. (3.1) is linear in $E(k,t)$ and $T(k,t)$, and clearly $\overline{E'(k,t)} = \overline{T'(k,t)} = 0$, one can use Eq. (3.3) in Eq. (3.1) and average to obtain

$$0 = T(k) - 2\nu k^2 E(k) + F(k)\ . \tag{3.4}$$

At low wavenumbers the transfer and forcing terms (first and third term on the right-hand-side of Eq. (3.4)) are expected to be important. For higher wavenumbers, we have $\overline{F}(k) = 0$ since there is no forcing applied at modes with wavenumbers satisfying $k > k_f$. In the inertial range, viscous effects are usually assumed to be negligible and transfer happens without any loss, and thus $T(k) = 0$. The fluctuating components can be easily obtained from Eq. (3.1) with the help of Eq. (3.4). The result is

$$\frac{\partial E'(k,t)}{\partial t} = T'(k,t) - 2\nu k^2 E'(k,t) + F'(k,t). \tag{3.5}$$

which shows that fluctuations in the forcing input would lead fluctuations in energy and thus transfer. Note also that while Eq. (3.5) clearly shows that a change in $T'(k,t)$ will lead (with some delay due to the integral relation between $T'(k,t)$ and $E'(k,t)$) to a change in $E'(k,t)$, the former depends non-linearly on the latter. It is, thus, difficult to understand, a priori, the relation between these fluctuations, the forcing, or even single-time statistics of each term in Eq. (3.5). In

the following two sections, we shed light on these issues.

For convenience (as will be made more clear below), it is convenient to divide the wavenumber space as in [94], that is, the inertial range (IR, $k\eta \lesssim 0.3$), near dissipation range (NDR, $0.3 \lesssim k\eta \lesssim 3$) and far dissipation range (FDR, $k\eta \gtrsim 3$). Typical timeseries of fluctuations in energy and transfer in these ranges are shown in Fig. 3.1. Varying degrees of unsteadiness at all scales are clearly seen from which a few observations can be made. Typical time series in energy ($E'(k,t) \equiv E(k,t) - E(k)$) and energy transfer ($T'(k,t) \equiv T(k,t) - T(k)$) are shown in Fig. 3.1, normalized by their respective averages. T' is an order magnitude larger than the average, leading us to the first observation that *the statistical mechanics of energy transfer is not unidirectional with minor fluctuations in time, but that of a system that fluctuates wildly around a much smaller time average.* The energy itself varies considerably more mildly in IR and BR (an order of magnitude smaller than the average); we will attempt to explain it towards the end of sec. 4. As one approaches NDR, fluctuations in energy transfer are highly correlated at all wavenumbers (Fig. 3.1c). Energy fluctuations in NDR (Fig. 3.1(d)) are small and slow.

Finally, in FDR (Fig. 3.1(e-f)), we see highly intermittent variations in T', much stronger (relative to their averages) than those at lower wavenumbers, as also reported by [94]. The variations are similar in E'. Since the energy content in the dissipation range decays rapidly with increasing k, the energy and local transfer are very small and the signal is dominated by large intermittent fluctuations observed in Fig. 3.1(e,f). This behavior was characterized in [94].

3.3 Single-time statistics

We now show in Fig. 3.2 the standard-deviation ($\sigma(X) \equiv \sqrt{\overline{X'(k,t)^2}}$ with $X = E$ or T) in different wavenumber regions. In IR, the fluctuations in E (Fig. 3.2(a)) are substantially smaller than those in T (Fig. 3.2(b)). All fluctuations become weaker as k increases, reaching a minimum at $k\eta \sim 0.13$ for E, and, much more unambiguously, at $k\eta \sim 0.3$ for T, corresponding to the respective bottleneck peaks in their spectra [41, 42, 44, 45, 85]. Fluctuations in T within IR decay approximately as $k^{-5/3}$ for $R_\lambda \gtrsim 90$. We observe similar features for a given R_λ in the case of DF forcing, as shown in Fig. 3.2c,d. We note that the fluctuations in energy within the forcing sphere

for the case of DF forcing is exactly zero. In Fig. 3.2c,d we still observe fluctuations comparable to the case of SF for wavenumebr outside the forcing sphere. The minimum in the variance of E in BR is consistent with [85], who used a different forcing mechanism from those used here; this suggests that this minimum occurs independent of forcing.

The fluctuations in E were recently studied in the context of non-equilibrium corrections to the spectra by [103], who proposed that the ratio of non-equilibrium and equilibrium parts of the energy spectra scales as $k^{-2/3}$ in IR. This scaling was also proposed by [104]. Using slightly different arguments [105] showed that this scaling is consistent with the transfer fluctuations decaying as $k^{-5/3}$ in IR. This scaling of transfer fluctuations is consistent with the DNS data in Fig. 3.2b. Energy fluctuations, on the other hand, show a weaker decay (approximately $k^{-1/3}$) than predicted by the work referenced above. This apparent discrepancy will be discussed later in this section.

For wavenumbers beyond BR, the relative fluctuations grow almost exponentially with the wavenumber in both the energy and transfer spectra. The presence of large and similar-level fluctuations in T to either side of BR is consistent with our understanding of BR [41, 44]. It is also consistent with conclusions from [106] and [107] where the presence of significant non-local interactions between large and dissipative scales was observed; it is similarly consistent with [34, 35, 38] where it was shown that non-local interactions in T exhibited strong cancellations when averaged over all pertinent triads, weakening their overall effect in the IR.

We do not observe any statistically significant trends with respect to R_λ for fluctuations in the dissipation range but a slight weakening occurs in IR.

A direct application of K41 ideas regarding the independence of small scales on the effect of large scales would suggest that fluctuations at high wavenumbers must become independent of those at low wavenumbers. Obviously, this is expected to be increasingly so as smaller and smaller scales are considered. However, recent work [94] suggests very strong fluctuations in the FDR which are in fact much stronger than those in the NDR. In addition, since classical phenomenology is, in principle, applicable only in the high-Reynolds number limit, it is also important to address trends with R_λ.

In Fig. 3.2, we show the normalized standard deviation of energy and transfer fluctuations for SF(a,b) and DF(c,d) forcings. It is clearly seen that in the IR, the fluctuations in energy (Fig. 3.2(a,c)) are significantly smaller than fluctuations in transfer (Fig. 3.2(b,d)). In fact, the latter are an order magnitude larger than the mean in the IR. These fluctuations become weaker as $k\eta$ increases reaching a minimum at $k\eta \sim 0.1$ for the energy spectrum, and at $k\eta \sim 0.3$ for the transfer spectrum. These wavenumbers correspond approximately to the bottleneck peak in the time-averaged compensated spectra of energy and tranfer respectively [44, 42, 45, 41, 85]. The fluctuations in the transfer spectrum within the inertial range decay approximately as $k^{-5/3}$ for $R_\lambda \gtrsim 90$. The minimum in the variance of $E(k,t)$ around the bottleneck location is also consistent with [85] which used a forcing mechanism different from the ones presented here and appears, thus, as a feature independent of the particulars of forcing.

For wavenumbers beyond the bottleneck peak, fluctuations grow almost exponentially with wavenumber for both energy and transfer spectra. The growth rate is different for near and far dissipation ranges. The presence of large fluctuations in the dissipation range beyond the bottleneck of similar order of magnitude as those in the IR for $T'(k,t)$ with a dip at intermediate wavenumbers, may indicate some level of interaction between the two ranges. This is consistent with conclusions from [106] and [107] where the presence of significant non-local interactions between the largest scales and dissipative scales was observed. The results are also consistent with [34, 35, 38] where they show that the strong non-local interactions observed in transfer spectra tend to exhibit strong cancellations when avereged over all pertinent triads, weakening their overall effect in the IR. Interestingly, they have also observed that the cancellations may be weaker for near dissipation range which again seem to support the large fluctuations observed as one moves deeper into the dissipative range.

We do not observe any statistically significant trends with respect to R_λ for fluctuations in the dissipation range. However a slight weakening of fluctuations with increase in R_λ is observed in the inertial range. Outside of the forcing sphere, we see that fluctuations in energy and transfer spectra are similar at similar R_λ and independent of forcing mechanisms. This is significant as the

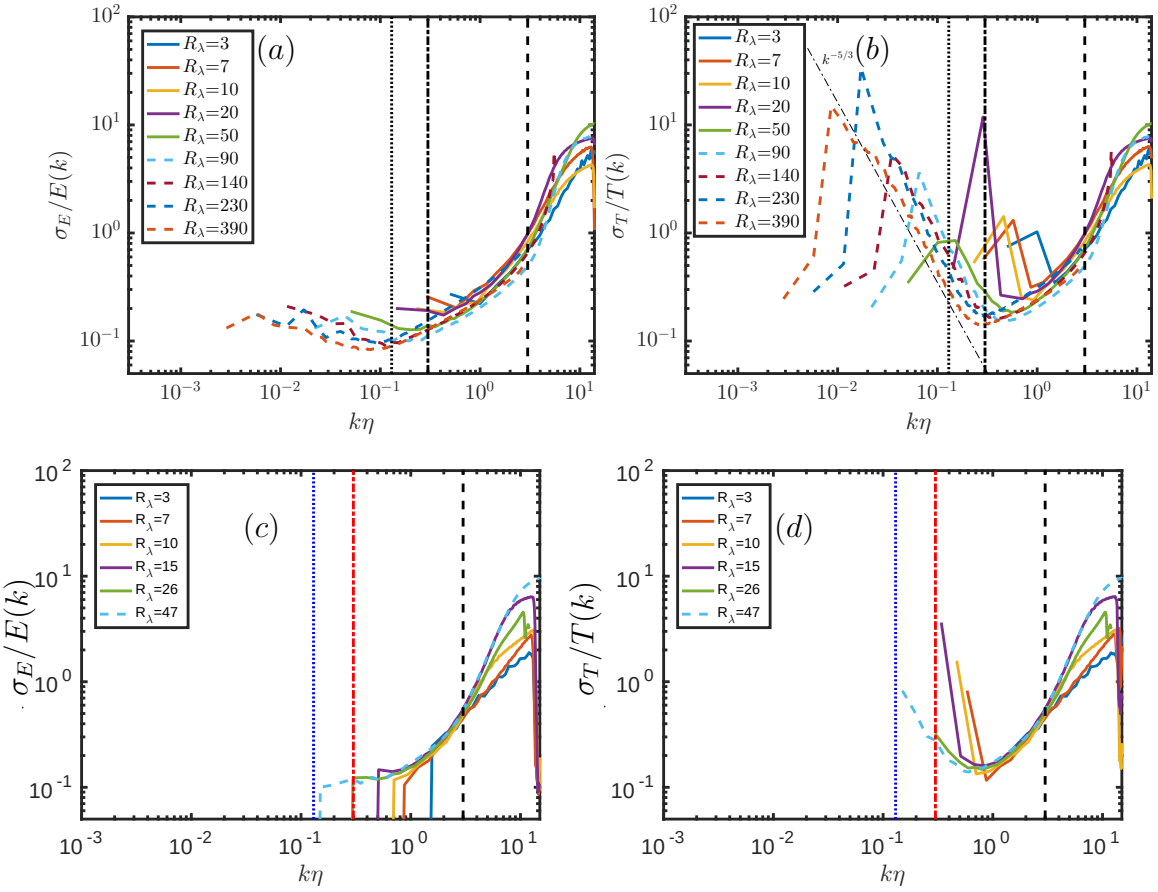

Figure 3.2: Normalized standard deviations $\sigma_E/E(k)$ (left) and $\sigma_T/T(k)$ (right). Figs. (a,b) correspond to SF forcing and (c,d) correspond to DF forcing. The vertical lines correspond to bottleneck peak in energy (blue dotted), and transfer spectrum (red dashed-dotted). The far dissipation range is defined as $k\eta \gtrsim 3$ (black dashed line).

unsteadiness in the forcing sphere for DF was to found to be significantly smaller than SF [93]. This strongly suggests that the temporal fluctuations, while triggered by the forcing mechanism, are dominated by Navier-Stokes dynamics rather than the forcing term. Therefore any non-local interactions, if present, may still lead to universality with respect to different forcings (or potentially flow complexity) at different scales as Navier-Stokes dynamics dominate the forcing effects.

It is clear from Fig. 3.1 that slow fluctuations across scales (e.g. energy in inertial and dissipation range) share correlations with each other. Such correlation is not apparent for fast fluctuations. Furthermore, the slow temporal variations in energy and transfer spectra, also exhibit a degree of correlation with the temporal evolution of the spatially averaged dissipation $\langle \epsilon(t) \rangle$. It is therefore convenient to separate the slow and fast frequencies within these signals and study in which way slow frequencies are in fact correlated with each other, even for transfer in inertial range, which shows large fluctuations at high frequencies We therefore separate both energy and transfer fluctuations at a cut-off frequency ω_c as follows

$$\frac{E'(k,t)}{E(k)} = E_<(t) + E_>(t), \quad \frac{T'(k,t)}{T(k)} = T_<(t) + T_>(t) \tag{3.6}$$

where $E_<(t)$ corresponds to component of singal with $\omega < \omega_c$ and $E_>(t)$ corresponds to components with $\omega > \omega_c$. Transfer signals follow the same convention. We choose ω_c such that the we recover the slow large scale behavior observed in mean dissipation which appears to share this slow frequency. ω_c is chosen such that the correaltion between fluctuations in mean dissipation and its filtered counterpart ($\langle \epsilon_<(t) \rangle$) is more than 99%. In Fig. 3.3a we plot the low-pass filtered fluctuations in transfer for $R_\lambda \sim 389$ with SFforcing. A comparison with Fig. 3.1 reveals that the slow fluctuations are an order magnitude smaller in the inertial range while the dissipation range is largely unaffected. This is clearly shown in Fig. 3.3b, where the standard deviation of the full signal (dashed lines) is much larger than the one observed for the the low-frequency part (dashed) in inertial range. No significant changes are observed in the energy fluctuations strength after filtering as they do not have a significant high frequency content in the inertial and near dissipation

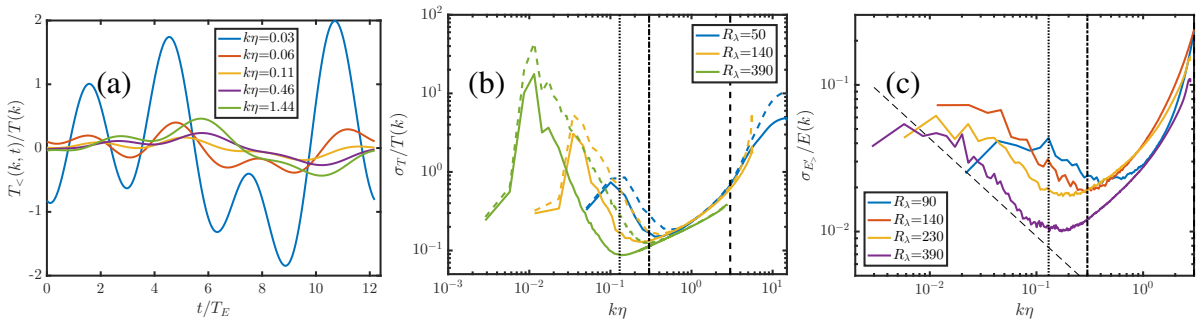

Figure 3.3: (a) Time series of slow component of transfer signals for $R_\lambda \approx 390$. The amplitude of the slow component is much smaller than those observed for the full signal in Fig. 3.1. (b) Normalized standard deviation of slow components (solid line) compared with full transfer signal (dashed line). Slow fluctuations in the inertial range are weaker in comparison to the full signal, while the two are comparable in the dissipation range. (c) The standard deviation of fast fluctuations of energy normalized by the mean energy in the respective wavenumbers. The dashed line corresponds to $k^{-2/3}$. Vertical lines are the same as in Fig. 3.2.

range. This is clearly observed in Fig. 3.1b.

A more complete description of the statistical behavior of $E'(k,t)$ and $T'(k,t)$ is contained in higher order statistics. We therefore compute the skewness of fluctuations in both energy and transfer spectra ($S_E = E'^3/\sigma_E^{3/2}$ and $S_T = T'^3/\sigma_T^{3/2}$, respectively, shown in Fig. 3.4. The skewness is close to zero i.e. fluctuations, both in energy and transfer, are symmetric about the mean for wavenumbers in the inertial and near dissipation range. The skewness and therefore asymmetry of the fluctuations increases rapidly in the far dissipation range. A large positive skewness for both T' and E' in the far dissipation range suggests that it is largely sustained by very large (relative) transfers of energy from elsewhere. Such large transfers can only be the result of non-local interactions with energetic wavenumbers.

A large positive skewness for both transfer and energy fluctuations in far dissipation range suggests that these scales are largely sustained by very large transfers of energy to these scales. As these scales have small energy content, the large transfers are then a result of non-local interactions with low-wavenumbers. The skewness (for energy and transfer fluctuations) in the near dissipation range is comparable to that of inertial range.

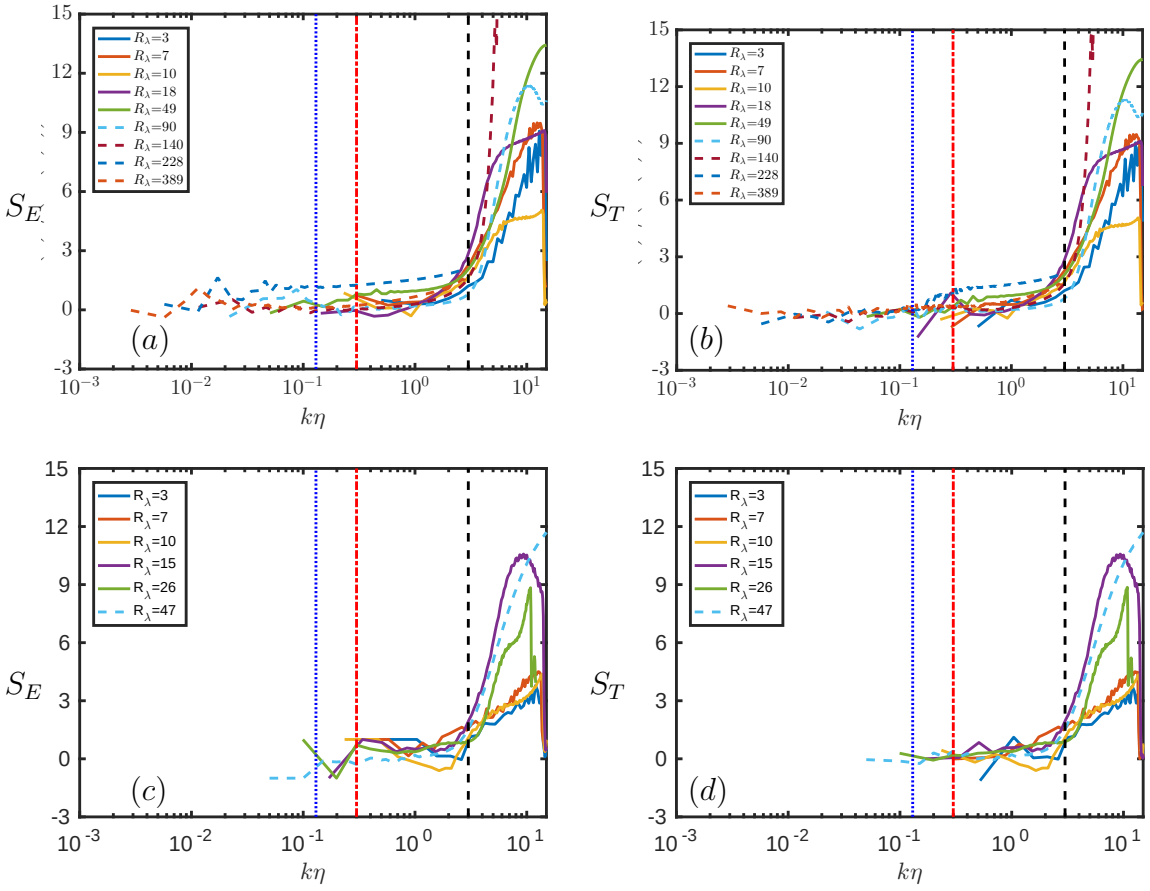

Figure 3.4: Skewness of energy (S_E) and transfer (S_T) fluctuations as a function of $k\eta$ for different R_λ with SF (a-b) and DF (c-d) forcing.

As the behavior discussed in this section is independent of forcing, we will discuss results from SFforcing in the remaining section in order to avoid repetition. We have however verified that all results presented show the same behavior for both forcings.

3.4 Time-delay statistics

We study the relationships between fluctuations in two wavenumber ranges using a time delay between them. The time-delay correlations for energy will be denoted by $\rho(E'(k_1,t), E'(k_2,t+\tau))$ and those for transfer fluctuations by $\rho(T'(k_1,t), T'(k_2,t+\tau))$. Obviously, if a peak in the correlation ($\rho(X(t)', Y(t+\tau)')$) occurs at some $\tau < 0$, it implies that the changes in $X(t)$ are correlated with changes in $Y(t)$ after that time lag τ. Each of the quantities is normalized by its standard deviation so that the correlation coefficient ρ ranges between -1 and 1.

Contours of the correlation coefficient for energy and transfer fluctuations between a selected wavenumber ($k_1\eta \approx 0.02$) in the inertial range and another wavenumber (k_2) with varying time lags (τ) are shown in Fig. 3.5(a-d), for the highest R_λ. Consistent with observations in Fig. 3.1, fluctuations in energy of k_1 for the full signal are well correlated with those at all wavenumbers in Fig. 3.5(a), and are so with no discernible time lag; this strong correlation is present even in BR and NDR. This feature suggests that the energy across wavenumbers is synchronized. We do not observe in Fig. 3.5(a) any significant improvement in correlations with increasing time lag in IR.

One possible explanation for the observed synchronicity is the following. The fluctuations of the kinetic energy around their mean value are related to higher order spectra, associated with 4-th order correlations, etc. Such quantities have been investigated multiple times in the past [108, 109, 110]. The relevant observation for us is that, $E_{uu}(k)$, the spectrum of fluctuations of the kinetic energy around their mean value also scales as $E_{uu}(k) \sim u_{rms}^2 E(k)$. This corresponds to a sweeping-dominated scaling [111]. Such sweeping implies that the typical temporal behavior of the spectrum will follow the fluctuations of the velocity, a point we will explore in the last section.

This result is contrary to the expectation based on the traditional cascade scenario in which the best correlation would occur with a finite time lag that increases with the wavenumber. On the other hand, the contours shown in Fig. 3.5(c) suggest that slower wavenumbers are better correlated

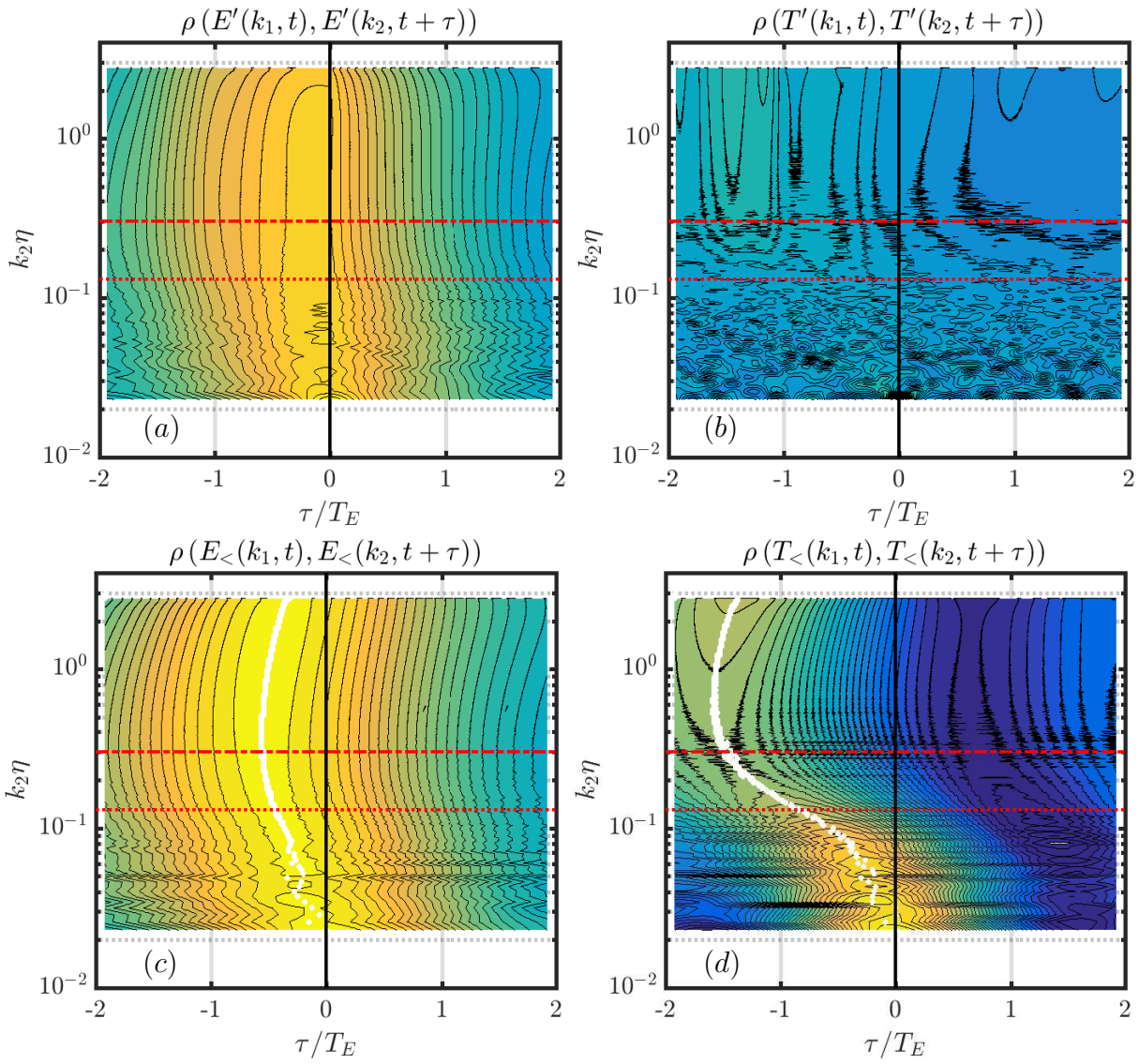

Figure 3.5: Contours of correlations at different time lags τ for E and T at a typical low wavenumber ($k_1\eta \approx 0.02$) with fluctuations at other wavenumbers k_2 for $R_\lambda \sim 390$. Correlations for the full signals are shown in top panels and those for their slow components in the bottom panels. The horizontal lines are same as vertical lines in Fig. 3.2, the vertical solid line marks zero lag. The contour levels range from -0.6 to 1 with a constant difference of 0.04.

with increasing time separation, τ. The maximum correlation is indicated using white dots. Slow fluctuations in E at one value of k in IR are best correlated with slow fluctuations in another value of k in E when the lag time τ increases; this suggests, for slow fluctuations, a picture that is consistent with the Kolmogorov-Richardson cascade with finite speed.

This synchronous feature is even stronger for energy transfer, shown in Fig. 3.5(b,d), with an interesting behaviour of the peak correlation as one moves to smaller scales. In IR, the peak correlation of transfer fluctuations with those at large scales is significantly enhanced compared to the full signal. Further, the peak correlation is observed at later times for higher k_2. In BR, the peak correlation is weaker but the increase in lag is more dramatic than in the inertial range, up to $k_2\eta \approx 0.3$ beyond which the peak occurs at a constant lag time of about 1.5 eddy-turnover time. This suggests that the slow modes adhere most to a cascade scenario in the IR followed by a seemingly synchronized response of the dissipative ranges. One may speculate that fast fluctuations may well be the result of incomplete cancellation of averages over individual triads in wavenumber shells and correspond to instantaneous transfer. This may be important in models that attempt to capture temporal dynamics assuming only a local scale by scale transfer. In the near dissipation range, the peak correlation is independent of the scale.

To address the R_λ trend of the features observed above, we plot the maximum correlation (ρ_{max}) for the full signals and the slow frequency components of T in Fig. 3.6(a,b) for three R_λ and a fixed $k_1\eta$. The left panel contains correlations from full signals and the right from slow fluctuations only. We show the correlations between fluctuations at all $k_2 \geq k_1$ for two different k_1, one in IR (dashed lines) and another in BR (solid lines). In these figures, a high correlation between disparate wavenumbers does not necessarily mean a non-local interaction as the peak correlation may occur with a lag.

It is immediately evident that stronger correlations occur at higher R_λ for a given pair of k_1 and k_2, but the figures reveal other features worth discussing. For the full signal, Fig. 3.6(a) shows that the fluctuations in T at all k_2 are largely uncorrelated with fluctuations when k_1 is in IR. In fact, the correlation drops steeply from a ρ_{max} of 1 when $k_1 \neq k_2$. For k_1 in the bottleneck region,

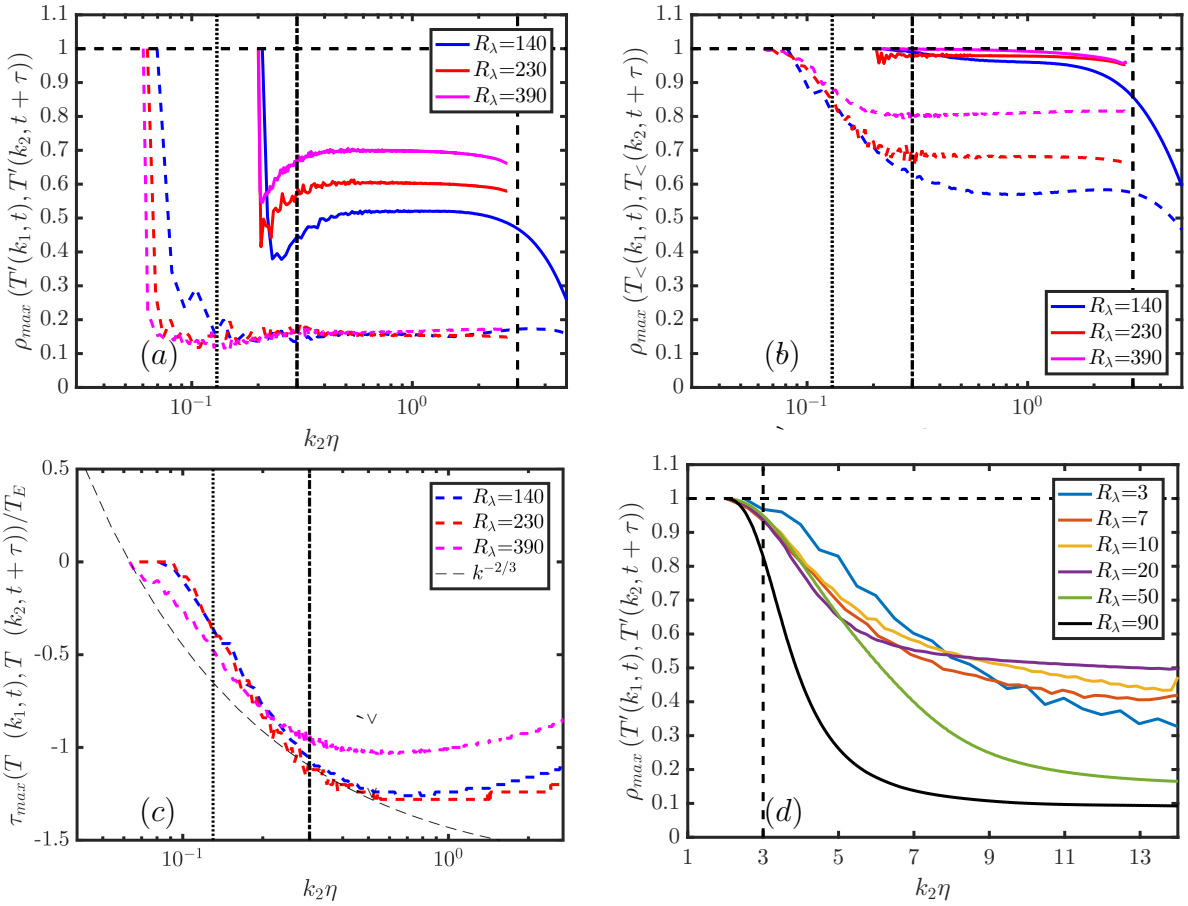

Figure 3.6: These figures show the maximum correlation coefficient (ρ_{max}) between (a) full and (b) slow modes of energy transfer functions. Dashed lines correspond to $k_1\eta \approx 0.06$ and solid lines for $k_1\eta \approx 0.2$. (c) Time lag corresponding to ρ_{max} in panel (b). (d) ρ_{max} for $k_1\eta \approx 2$. Vertical lines same as Fig. 3.2.

stronger correlations are observed at all k_2. For $k_2\eta > 0.3$, the peak correlation is independent of the wavenumber. Together with earlier observations, the fact that the peak correlation time in this range is also independent of k_2 shows that fluctuations in these scales are synchronized across wavenumbers.

The corresponding correlations for slow transfer fluctuations are shown in Fig. 3.6(b). These correspond to white dots in Fig. 3.5 and they confirm the R_λ trend seen in Fig. 3.6(a). A comparison of figures 5(a) and 5(b) shows that slow fluctuations are correlated much more strongly than the full signals. The effect of fast fluctuations is thus to reduce the correlation between signals. This reduction effect is stronger at lower R_λ.

For k_1 in IR, the reduction in correlation with k_2 ($k_2 \neq k_1$) is weaker for the slow part than for the full signal. The correlation decays up to $k_2\eta \approx 0.3$, beyond which it remains constant. The constant value is significantly larger than that for the full signal correlations. This feature again highlights that correlations between slow fluctuations are stronger for slow signals, particularly in the transfer. Wavenumbers in BR are almost perfectly correlated in slow modes.

A similar analysis for fluctuations in E confirms that fluctuations are highly correlated across all wavenumbers with no significant R_λ trends. We have therefore not shown those data here.

Returning to Fig. 3.5, especially panel (d) for slow fluctuations, we saw that changes in E and T at large scales are highly correlated with changes at smaller scales, up to NDR, with a time lag. This time lag increases with the distance between the scales being considered. As noted earlier, this is qualitatively consistent with classical cascade concepts. Note that the slope of the white markers in Fig. 3.5(c),(d) can be interpreted as the “speed" of the transfer across scales. This information can be used to further our comparison to the classical cascade more quantitatively. The time scale associated with a scale $1/k$ can be estimated by knowing that its energy content is $E(k)k$. Dimensional analysis would then yield $T_c \propto 1/\sqrt{E(k)k^3}$ where T_c is the local time scale associated with $1/k$. In classical phenomenology, this is also the time associated with the transfer of energy to neighboring smaller scales. In the inertial range, if $E(k) = C_k\langle\epsilon\rangle^{2/3}k^{-5/3}$, we obtain $T_c \approx C_k^{-1/2}\langle\epsilon\rangle^{-1/3}k^{-2/3}$ where $C_k \approx 1.6 - 1.7$ [21, 44]. Finally, the total time taken

by a perturbation in k_1 to reach k_2 would be the sum of all time intervals to cross the wavenumber interval. If wavenumbers are binned in octaves, for example, the total time is a sum of T_c across different bins [112, 113]. If one considers a continuum spectrum instead, one obtains

$$\tau_{k1\to k_2} = \int_{k_1}^{k_2} |dT_c/dk|dk = C_k^{-1/2}\langle\epsilon\rangle^{-1/3}k_1^{-2/3}\left(1-(k_1/k_2)^{2/3}\right) \tag{3.7}$$

This can be normalized by the local cascade time scale $T_c(k_1) \approx C_1 T_E$ where C_1 is a proportionality constant of order unity relating T_E and T_c when k_1 is near the large scales. Then

$$\frac{\tau_{k_1\to k_2}}{T_E} \;=\; C_1\left(1-(k_1/k_2)^{2/3}\right) \tag{3.8}$$

This expression (also derived by [114]) is compared against τ_{max} in Fig. 3.6(c), where the transfer fluctuations peak at later times with increase in k_2 within IR. The measured lag times agree reasonably well with the expression Eq. (3.8) for $C_1 = 1.7$, shown as a dashed black line. Such a behavior is in contrast to the full signal for which there is no readily identifiable time lag, as discussed earlier. This observation further supports the conclusion that the classical cascade occurs only for the slow signals. As noted earlier, for $k_2\eta > 0.3$—that is, beyond BR—in the energy transfer spectrum, we have a different behavior in which the peak correlation is independent of wavenumber. These results are consistent with the results reported in [115] and [116] where the authors studied the correlation between the subgrid-scale stress tensor for velocity fields filtered at different spatial subgrid scales.

The peak correlations for FDR with a wavenumber in NDR, shown in Fig. 3.6(d), lose the correlation rapidly in both energy and transfer fluctuations. The concept of cascade is not expected to be valid here as the scales are dominated by dissipation. These scales also show large fluctuations that oscillate rapidly. In addition, they are fully correlated with each other as confirmed in Fig. 3.1 by the constant correlation in Fig. 3.5 and Fig. 3.6d for $R_\lambda > 10$ and $k_2\eta \geq 6$. We note that the loss of correlation with increase in k_2 for all wavenumbers is only observed for $R_\lambda < 10$. This again emphasizes that the loss of correlation may be a low-R_λ feature. At higher R_λ, the correlation

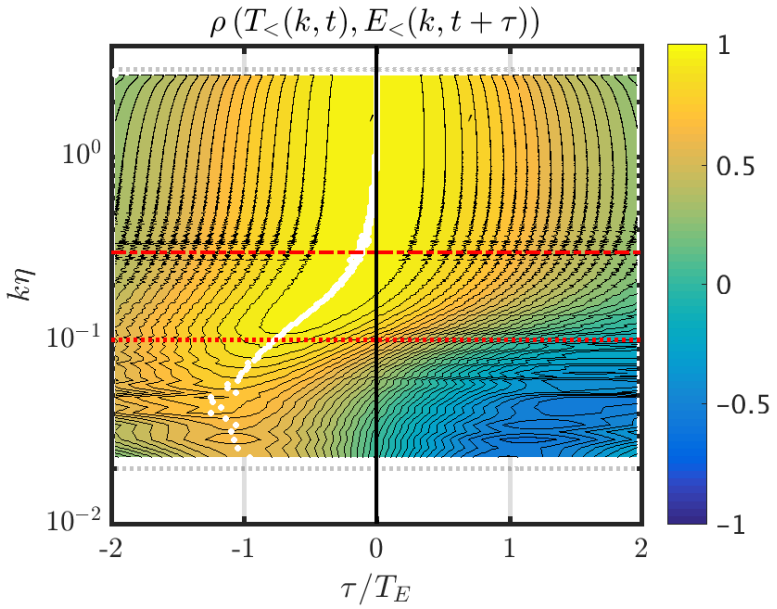

Figure 3.7: Contours of correlation at different time lags for slow modes of transfer and energy at the same scale ($k_1 = k_2 = k$) for $R_\lambda \approx 390$. Horizontal lines are the same as the vertical lines in Fig. 3.2. Solid black line is zero lag.

becomes approximately independent of k_2 in FDR.

Finally, we comment on the relation between transfer and energy fluctuations at the same wavenumber. Because of the differential relation between E and T (Eq. (3.1)), temporal changes in $T(k,t)$ will lead to temporal changes in $E(k,t)$ only after some delay. As a complement to the analysis above, one can look at the peak correlation between $T(k_1,t)$ and $E(k_1,t+\tau)$, now at the same wavenumber $k_1 = k_2 = k$. When k is the dissipative region, Fig. 3.7 shows that the peak occurs with zero delay but the delay increases in magnitude across IR (marked by white dots). In other words, when the slow component of energy is transferred to a wavenumber in IR, it takes longer and longer for that change to be observed in the energy at that same wavenumber. Over that period other energy exchanges to/from that wavenumber can take place, which may explain why signatures of a classical cascade are much clearer for T than for E. These to-and-fro exchanges may also explain why the oscillations around the average value are significantly damped out in the energy signals. Needless to say, no such behavior is observed in IR for the full signal.

3.5 Discussion and conclusions

When we force a flow at low wave numbers, whether steadily or randomly, the resulting turbulent fluctuations develop significant temporal fluctuations. It is important to understand how these fluctuations are transmitted across the wavenumber space. Here, we studied single-time and time-delay statistics of energy and energy transfer spectra using well-resolved isotropic DNS for a range of Reynolds numbers, with two different forcing mechanisms (although results were presented for only the SF forcing). We found that the fluctuations in energy transfer in the inertial range and the far-dissipation range are much larger than their time average. In the inertial range, the amplitude of the fluctuations at a given wavenumber decreases with increasing R_λ while in FDR the fluctuations are in the form of (skewed) large intermittent bursts.

One main lesson is that the local cascade scenario is observed only for slow modes of energy transfer. Large-amplitude fast time variations are present across the inertial range and tend to mask the inter-scale correlations observed for slow fluctuations. Rapid fluctuations cannot be transmitted through the large and inertial ranges, since the reaction time of these scales is too long. Indeed, there is some non-equilibrium basis for understanding the statistics of fast fluctuations in the inertial range [103, 104].

The second main lesson is that the energy transfer in the inertial range for the full signal is more like a slight imbalance between two opposing fluxes, oscillating up and down in time at any given k. We speculate that the fast modes, which are instantaneously felt across all wavenumbers, are signatures of significant non-local interactions in energy transfer at a given scale in the inertial range. The effect of the rapidly oscillating part is similar to decreasing R_λ, where a clear separation between largest and smallest scales is absent. Fluctuations in the far-dissipation range are uncorrelated with the inertial range and become increasingly so at high R_λ. For $R_\lambda > 10$, we found that the fluctuations at all wavenumbers in the far-dissipation range synchronize with each other (still uncorrelated from large scales). Similar synchronization was observed for fluctuations in both energy and energy transfer at wavenumbers $k\eta > 0.3$ which include bottleneck region and the near dissipation range.

4. ENERGY SPECTRUM IN THE DISSIPATION RANGE[†]

In the previous section we established that a cascade type scenario is only valid for slow fluctuations. An important consequence of the local cascade in turbulence phenomenology is the complete self-similarity (independent of R_λ) of dissipation scales in energy spectra. We however observed that the total transfer across scales is dominated by non-local interactions which are transmitted across all the wavenumbers instantaneously. The far dissipation range was dominated by large fluctuations in energy which indicate non-local energy transfers from scales much larger in size. We now asses the behavior of energy spectrum in turbulent flows, for which different forms are predicted based on local and non-local energy transfer mechanisms.

4.1 Introduction

The energy spectrum of turbulent fluctuations has been the subject of considerable attention since Kolmogorov's seminal work (K41) [19] on the structure of homogeneous, isotropic turbulence. A large body of literature has been devoted to understand, characterize and predict the actual form of the spectrum, distinguish between universal and non-universal aspects, and use the information to understand energy distributions, energy transfers, locality, among others (see [30] for an exhaustive list). K41 predicted, at asymptotically large Reynolds numbers (R_λ), a universal three-dimensional energy spectrum, determined solely by the mean dissipation rate ($\langle\epsilon\rangle$) and viscosity (ν):

$$E(k) = C_k \langle\epsilon\rangle^{2/3} k^{-5/3} F(k\eta) \tag{4.1}$$

where k is the wavenumber and $\eta = (\nu^3/\epsilon)^{1/4}$ is the Kolmogorov length scale. In the so-called inertial range ($1/L \ll k \ll 1/\eta$, where L is the integral length scale) the dynamics become independent of dissipative mechanisms and thus of ν and $F(k\eta) \to 1$. This form has been the subject of sustained numerical and experimental investigations since. Significant departures from Eq. (4.1)

[†]Figures, tables and portions of text in this chapter reproduced with permission from *S. Khurshid, D.A. Donzis & K.R. Sreenivasan. "Energy spectrum in the dissipation range." Physical Review Fluids 3.8 (2018): 082601. Copyright 2018 American Physical Society*

have been observed [85, 117, 45, 1] and a general conclusion is that the spectrum exhibits a R_λ dependent behavior in inertial range and the bottleneck region. The form of $F(k\eta)$ has now been well established, both numerically and experimentally, for the so-called inertial range but remains a topic of investigation for far dissipation range ($k\eta \gg 1$). Most experiments are limited to a range of $k\eta \leq 1$. Smaller scales are prohibitively difficult to measure due to interference from experimental noise which is of a similar scale in terms of energy content, especially at large R_λ. Well resolved direct numerical simulations (DNS), augmented by massive increase in computational power over the last two decades, have allowed the investigation of these small scales at increasingly large R_λ [30, 1, 85]. The increase in R_λ in DNS, however, is in direct competition with increased resolution for a given amount of computational time. Highly resolved simulations, for $k\eta \gg 1$, are therefore limited to small $R_\lambda \sim O(10^2)$ [118, 119].

The nature of dissipation range of the energy spectrum is of particular interest in theory of turbulence as well as engineering problems that exploit small scale dynamics. K41 assumes this range to be universal as mentioned before. The observed collapse of the normalized energy spectrum ($E(k\eta) \equiv E(k)/(u_\eta^2 \eta)$) in the dissipative range using Kolmogorov variables, has been reported in multiple experiments and numerical simulations [2, 120, 1] providing evidence for universality of scales within this range. The dissipative range has also received considerable theoretical attention. Several researchers have proposed analytical forms for this range with the widely accepted general form being

$$E(k\eta) \sim (k\eta)^\alpha e^{-\beta(k\eta)^\gamma} \tag{4.2}$$

though the numerical values of the coefficients are still inconsistent throughout the literature. The power law in Eq. (4.2) has been derived in some cases [121, 122] and justified in others to agree with empirical evidence [123]. Kraichnan [121], under the assumptions of his direct approximation interaction (DIA), argued that the spectrum must have a faster-than-algebraic roll and derived an exponential form for the spectrum with $\gamma = 1$ and $\alpha = 2$. Foias *et al.* [124] also derived an exponential roll-off using Stokes eigenfunctions but without the preceding power law. Sirovich *et al.* [122] derived a form for the dissipation range using the third order structure function which

depends on skewness of velocity gradients, assumed to be independent of R_λ [25]. Their function has two modified Bessel functions which, in the high-k range, can be expanded into an exponential preceded by the sum of two power laws. She and Jackson [123] proposed a similar empirical form. Several values have also been proposed for α, β, and γ experimentally. Smith and Reynolds [125] used the constraint $\epsilon = 2\nu \int_0^\infty k^2 E(k) dk$ and Eq. (4.2) to show that $\gamma = 2$ provides a better agreement with skewness of velocity gradients. Manley [126] changed the upper limit on that integral to $1/\eta$ to show that $\gamma = 1$ is a better fit. A survey of other values for γ including $4/3$ and 2 is given in [124]. Sreenivasan [127] suggested that different exponentials fit different ranges of the near dissipation region. Numerical simulations have supplemented these investigations by providing well resolved near and far dissipation ranges. A major assumption in these studies (described below) is that $\gamma = 1$ which leaves only two coefficients to be fit. Under this assumption, Chen *et al.* [128] found that $\alpha \sim 3.3$ and $\beta \sim 7.1$ for $R_\lambda \sim 15$ within the range $5 < k\eta < 10$. Martinez *et al.* [3] improved on their work by studying a range of R_λ. They locally fit the log-derivative of Eq. (4.2), which has the form

$$\frac{d\log(E(k\eta))}{d\log(k\eta)} = \alpha - \beta\,\gamma\,(k\eta)^\gamma \tag{4.3}$$

with $\gamma = 1$. They used their highest resolved simulation to suggest that the observed values of α and β point to two scaling ranges below and above $k\eta \sim 4$. They further noted that a simple exponential may not be an appropriate guess for the near dissipation range. Ishihara *et al.* [129] fit the near dissipation region for Eq. (4.2), again with fixed $\gamma = 1$, but for R_λ higher than those of [3]. Both show a R_λ dependence for α and β. Schumacher [119] performed a similar analysis as [3] using higher resolution data and reported that no systematic trend can be observed for either α or β with respect to the wavenumber. They did note, however, a saturation in the values of these coefficients around $R_\lambda \sim 100$.

The goal of this section is two fold. First, we investigate the degree of collapse for the energy spectrum in the dissipation range using Kolmogorov variables and how this presumed universality

Table 4.1: Summary of DNS runs. N is the number of grid points in each direction. ΔT_E is number of eddy turnover times in stationary state. The upper limit on far dissipation range is determined by the smaller number between $k_{max}\eta$ and $k\eta$ near round-off limit.

R_λ	N	$k_{max}\eta$	ΔT_E	NDR	FDR
1	128	53.7	9.06	2.5-6	6-14
3	128	30.5	13.6	2-6	6-12.5
7	128	17.8	15.9	2-6	6-11
9	256	28.1	11.8	1.5-4.5	8-11.5
10	512	55.6	10.2	2-4	8-11.5
14	256	20.7	7.38	2-4	8-12
19	512	34.7	9.93	2-4	8-11
25	256	12.3	19.6	2-4	8-11.1
47	1024	24.8	19.2	2-4	8-12.5
55	1024	19.9	18.4	1.5-3	8-11.7
68	1024	14.9	19.3	1.5-3	8-12.9
89	2048	21.2	24.2	1.5-3	8-13.7

emerges with R_λ. Second, we investigate whether the proposed functional form Eq. (4.2) is indeed appropriate for the dissipation range. The work here addresses and explains the inconsistencies between the different results reported in the literature.

4.2 DNS details

We perform DNS with very fine resolution, as detailed in Table 4.1, for R_λ ranging from 1 to about 100. The code is pseudo-spectral and uses RK2 for time integration. The time step is $3 - 80$ times smaller than the Kolmogorov timescale in the stationary state (CFL range: $0.1 - 0.7$). The flow is forced in Fourier space with integrated Ornstein-Uhlenbeck processes [81] (EP) with finite-time correlation at the largest scales within the sphere $k < 2.01$. Reynolds number is changed by changing the viscosity. In all cases, the highest resolvable wavenumber $k_{max} = \sqrt{2}N/3$ (N being the number of grid point in each direction) is at least an order of magnitude larger than Kolmogorov scale. The stationary state averaging is started at least 6 eddy turnover times from initial conditions. We have tested for potential numerical artifacts caused by finite-arithmetic precision or truncation (Section 2), aliasing errors and numerical differentiation schemes, and have shown that these effects do not influence the results.

4.3 Reynolds dependence of energy spectrum

In Fig. 4.1(a) we collect spectra for a range of Reynolds numbers. From a quick look, the data show approximate collapse at all Reynolds numbers, as expected from classical phenomenology; interestingly, this rough collapse seems to cover even very low Reynolds numbers of $\sim O(1)$. A more careful inspection of the spectra, however, reveals two important departures from the self-similarity implied in K41. First, spectral collapse is not strictly achieved at the low end of the dissipation range, say, $k\eta \sim 0.1 - 1$, as seen better on the linear scale of the inset (Fig. 4.1(a)). As pointed out in [1], there is a clear systematic decrease of this so-called bottleneck effect (the spectral bump that precedes the dissipative region at $k\eta = 0.13$) with the Reynolds number; this can also be observed in the data of Ref. [120]. Second, and this is the focus of the present work, one can also see persistent systematic trends with the Reynolds number even at higher wavenumbers; see Fig. 4.1(b). Several previous simulations did not observe or emphasize this aspect. The observed behavior cannot be fitted by an exponential over the entire range and, indeed, the non-monotonic shape of the data precludes the applicability of spectral formulas such as Eq. (4.2).

Nevertheless, it appears useful to consider the spectral shape to consist of two exponentials with an extended crossover, the near-dissipation range (NDR), $k\eta \lesssim 3$, and the far-dissipation range (FDR), $k\eta \gtrsim 6$, for each of which one may be able to fit Eq. (4.2), but with different set of constants. This approach is in contrast to virtually all theoretical models which predict, for $k\eta \gg 1$, the general form Eq. (4.2), sometimes with a sum of more than one power-law in the prefactor [130, 131]. Although no rigorous argument has been put forth for multiple exponentials, there have been some efforts to use Eq. (4.2) with different coefficients in different ranges—for example, [3] though their simulations did not resolve far enough into the FDR to reliably obtain the coefficients and their fits used $\gamma = 1$, which does not apply. There has also been some recent theoretical work on chaotic system which may justify the appearance of multiple exponentials [132].

To compute the coefficients we first plot the log derivative of the normalized energy spectrum,

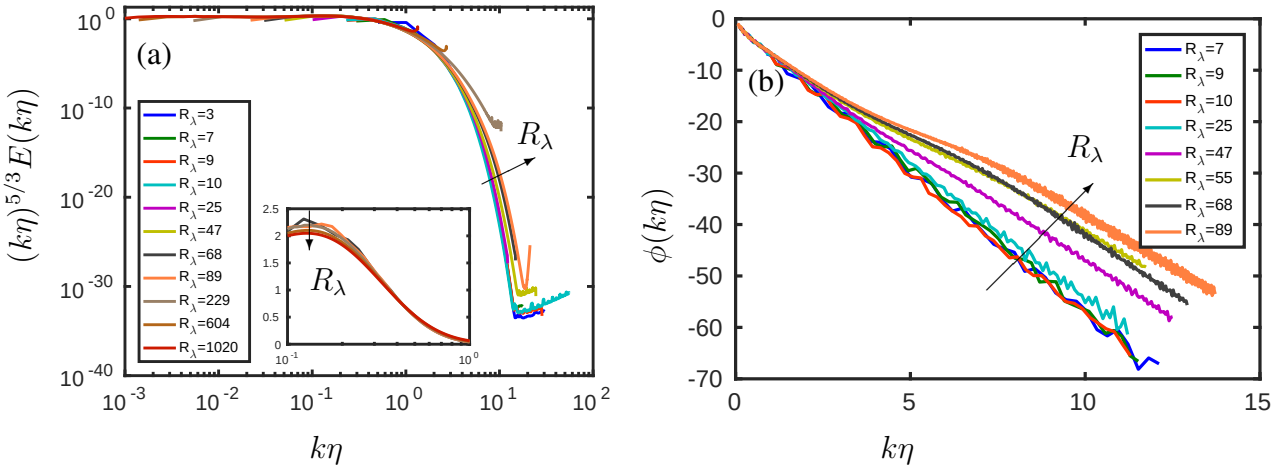

Figure 4.1: (a) Energy spectrum for all R_λ in the database. Inset: detail of $(k\eta)^{5/3}E(k\eta)$ for $R_\lambda \gtrsim 50$. Data for $R_\lambda > 89$ are taken from [1]. (b) The log-derivative $\phi(k\eta)$ for very well resolved simulations shows two ranges. Selected R_λ are shown to reduce clutter and illustrate the trend.

compensated with $\gamma(k\eta)^\gamma$, such that Eq. (4.3) yields

$$\frac{\phi(k\eta)}{\gamma\,(k\eta)^\gamma} = \frac{\alpha}{\gamma\,(k\eta)^\gamma} - \beta. \tag{4.4}$$

If $\alpha = 0$, for instance, even for a limited range of $k\eta$, a constant β would result and γ can be determined by searching for the value that results in the widest plateau of the left-hand-side of Eq. (4.4).

For R_λ up to about 10 (perhaps even 25), Fig. 4.1(b) shows that $\gamma = 1$ approximates the data well which in this figure would be seen as a straight line; we then obtain $\beta = 6.7$, similar to [3, 118]. A few remarks are in order for determining the constants for larger R_λ. First, past efforts have generally used a fixed value of γ and used a finite non-zero value of α. But fixing γ at a predetermined value can only lead to incorrect values for the coefficients, as seen clearly in Fig. 1b. Second, the optimization procedure that can be used to find the best fit coefficients by minimizing the error between DNS and Eq. (4.2) leads to a number of challenges to find the global minimum in the error, because of the strongly nonlinear nature of the procedure. Standard techniques typically

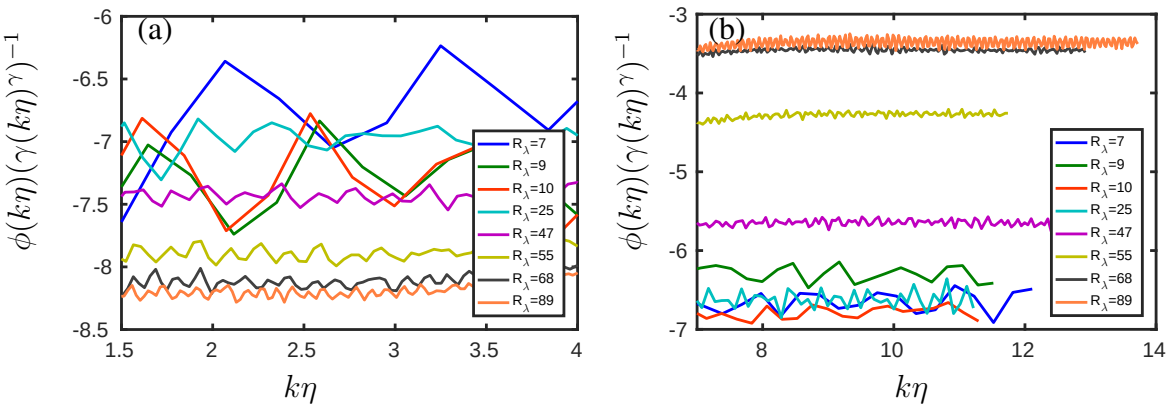

Figure 4.2: The compensated log derivative for (a) NDR and (b) FDR of the energy spectrum.

find local minima strongly dependent on the initial seeds. In any case, such efforts in NDR and FDR generally give values of α that are relatively small, fluctuating inconsistently around zero, from which one can justify setting $\alpha \approx 0$ without any loss of accuracy of fits. This conclusion is reinforced from typical compensated log-derivatives shown separately in Fig. 4.2 for NDR and FDR, whose extent (by visual inspection) is summarized in Table 4.1: One can see clear plateaus in Fig. 4.2, rather than an asymptotic approach to plateaus at high $k\eta$ as would be the case if $\alpha/[\gamma(k\eta)^\gamma]$ is not negligible. This plateau effect can be due either because $\alpha \approx 0$ or because $k\eta$ is high enough to make that term negligible. In both cases, the conclusion is that the value of α is largely inconsequential in both the NDR and FDR (see also appendix). This is consistent with the extreme sensitivity in determining α from fits including only $k\eta \gtrsim O(1)$ using standard minimization tools.

A phenomenological argument for including the power-law term with non-zero α is essentially that the exponential roll-off in the dissipation range must transition smoothly to a power law in the inertial range with an exponent of $-5/3$ [19]. However, it is now well-established that the dissipation and inertial ranges are separated by a spectral bump due to the bottleneck effect [41, 1]. This realization has led to the use of varying power laws as prefactors [130, 133]. However, as argued above, a simple sensitivity analysis of the fitting parameters reveals that changes in α do not significantly affect β. We thus put $\alpha = 0$ in NDR and FDR but accept two different γ values

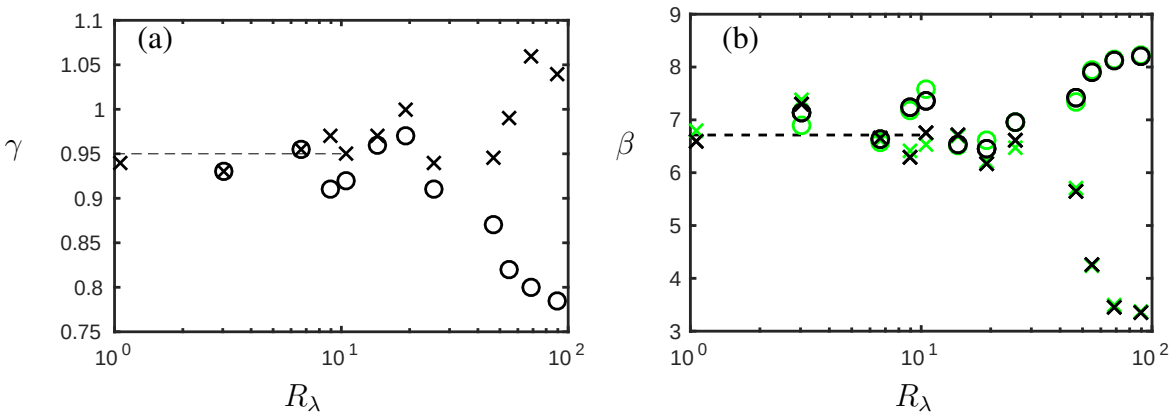

Figure 4.3: (a) Values of γ as a function of R_λ found from the compensated log-derivative form as described in the text. NDR values are represented by O and FDR by $\times$. (b) The constant β after fitting Eq. (3) for appropriate γ as a function of R_λ. Symbols O and $\times$ are from NDR and FDR fits respectively. Black symbols correspond to fits with $\alpha = 0$ and green for fits with α as a fit parameter. The 2-norm of relative error between DNS data and the fit (not shown) is less than 4% and decreases with increasing R_λ. No significant improvements in relative error are observed with inclusion of α in the fit.

in each of the regions.

Still, if one insists on using a finite, non-zero α, the present data indicate that the effect is relatively small because the clear plateau observed in the compensated log-derivative seen in Fig. 4.2, which implies that the first term in Eq. (4.4) is indeed small. The observed plateaus can be used to estimate bounds on α. Requiring that the second term be much larger (needed for a plateau), say, an order of magnitude larger than the first requires (using the fact that $\beta\gamma \approx 6.4$, see the paragraph immediately below) that $\alpha \ll 0.1\beta\gamma(k\eta)^\gamma \approx 0.64$ in the NDR and $\alpha \ll 2.4$ in the FDR; the observed plateaus actually suggest that α is much smaller.

Once γ is known, it is straightforward to determine α and β (or only β) using standard minimization tools. The values of γ found using the compensation method detailed above which led to the plateaus observed in Fig. 4.2 are collected in Fig. 4.3(a). At low R_λ, γ is slightly smaller than 1 for both NDR and FDR, but it is hard to assign any deep significance to the observed difference from unity. At higher Reynolds number, however, we see the emergence of the two ranges. In the NDR, γ decreases with increasing R_λ and remains below 1. With these values of γ we performed least squares fits to determine β. The results are shown in Fig. 4.3(b). Here too, we observe dif-

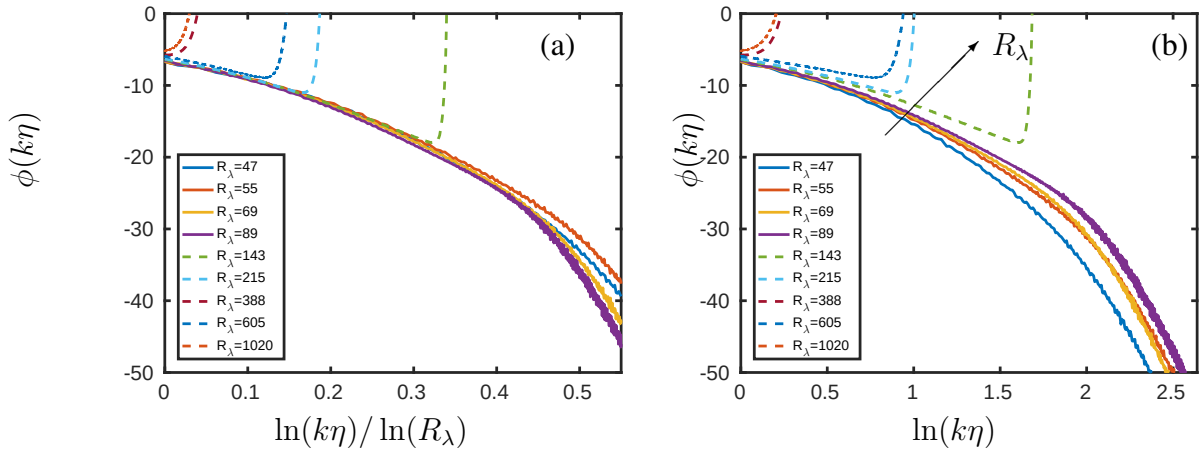

Figure 4.4: Log-derivative of the energy spectrum according to the (a) multifractal formalism (see [2]) and (b) K41 scaling. The range $0 < \ln(k\eta)/\ln(R_\lambda) < 0.4$ corresponds to the so-called intermediate dissipative range [2]. Data for $R_\lambda > 89$ (dashed lines), taken from [1], correspond to simulations with limited resolution to assess FDR scaling as well-known aliasing errors (seen as a strong uptick in the present normalization) are apparent in the figure.

ferent behaviors for for the two ranges of the spectrum when $R_\lambda \geq 10$. The parameter β increases with increasing R_λ for the NDR but decreases for FDR. An interesting result in the NDR is that $\beta\gamma$ is fairly constant around 6.4 for all R_λ studied here.

In contrast to K41, multiple dissipation ranges are predicted by the multifractal formalism [2], which assumes a local scale invariance rather than the global scale invariance of K41. This manifests as a scaling of velocity increments with a Hölder exponent h within an interval (h_{min}, h_{max}); for each h, a fractal set with dimension $D(h)$ can be determined [2]. Scaling exponents are turned off successively as viscosity becomes increasingly important at higher k. In doing so, a new similarity parameter $\theta = \ln(k\eta)/\ln(R_\lambda)$ is derived such that $\ln(E(k\eta))/\ln(R_\lambda) \equiv f(\theta)$. In Fig. 4.4, we show the log derivative of energy spectrum in the new variables which has a more compelling case of collapse than K41. The collapse of the spectrum is robust for the data presented here ($R_\lambda > 50$) in the range $0 < \ln(k\eta)/\ln(R_\lambda) < 0.4$ (loosely covering NDR) but it is also clear that the multifractal description has limited success in the FDR, broadly speaking.

In an attempt to physically understand how the pure exponential of low R_λ assumes a multi-exponential form at higher R_λ, we note that the pure exponential simply represents the case when

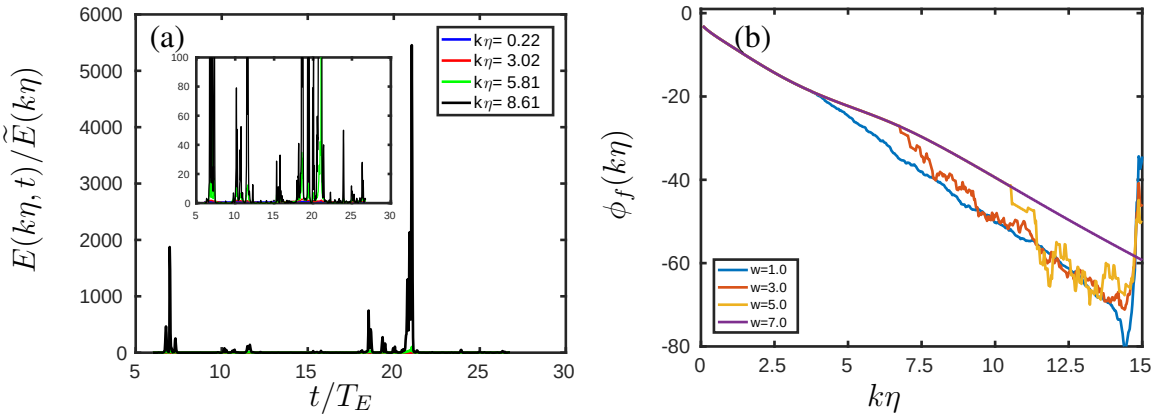

Figure 4.5: (a) Time series of energy spectrum $E(k\eta, t)$ normalized by the median value of the time series $\widetilde{E}(k\eta)$ for a subset of wavenumbers at $R_\lambda \approx 90$. Inset shows the same data on an expanded scale. (b) Log-derivative of the filtered time average for energy spectrum, $\phi_f(k\eta)$ for different values of the threshold cut-off w. Data with $w = 7$ was found to correspond to the unfiltered time series.

the energy dissipation is proportional to the energy at each of the wavenumbers. As the Reynolds number increases, however, there is an intermittent transfer of energy to small scales, potentially from larger scales. This effect becomes increasingly important at increasing wavenumbers (though at some truly large wavenumber, the effects will presumably vanish). This is seen in Fig. 4.5(a) which shows a time series of the energy spectrum $E(k\eta, t)$, normalized by the median value of the time series $\widetilde{E}(k\eta)$. Large bursts in energy are observed intermittently for high wavenumbers. It is thus natural to assess the effect of these intermittent events on the time-averaged energy spectrum. To do so, we remove large bursts by filtering out spectra at time instants where $E(k, t)$ exceeds a chosen threshold; that is, we retain $10^{-w} < E(k, t)/\widetilde{E}(k) < 10^{w}$ in the average. With this so obtained filtered time-averaged spectrum ($E_f(k\eta)$) one can compute the filtered log-derivative $\phi_f(k\eta)$, shown in Fig. 4.5(b) for different values of w. The data show that as we remove more of the intermittent events, we essentially recover the low-R_λ exponential, and the difference between NDR and FDR vanishes. This is a clear demonstration that the deviation from the exponential form occurs essentially from busts of energy transfers. Based on the elementary argument given by Kraichnan [134], it can be argued that extreme fluctuations at high wavenumbers are due to large-scale activity. Regardless of their specific origin (a topic by itself warranting further re-

search), extreme energy fluctuations at high wavenumbers and high R_λ, appear to alter the single exponential representation in the entire dissipative range $k\eta \gtrsim 1$.

4.4 Conclusions

In summary, we have used highly resolved DNS data of isotropic turbulence to investigate the dissipative wavenumber part of the energy spectrum for a range of R_λ. We have shown that the collapse of the Kolmogorov-scaled spectrum reported in the literature (between $0.13 \lesssim k\eta \lesssim 1$) is an artifact of limited resolution and Reynolds number range. The results presented here (see also [129, 85, 1]) demonstrate a systematic R_λ dependence (up to $R_\lambda \sim 2300$) of all resolved scales in the energy spectrum. While we have observed an exponential roll-off for the spectrum of the form Eq. (4.2) at low R_λ, a systematic analysis of the coefficients involved shows two distinct scaling ranges. A general expression that captures these two regimes can be written as $E(k\eta) \sim e^{\beta_1(k\eta)^{\gamma_1}} + Ae^{\beta_2(k\eta)^{\gamma_2}}$ where $\gamma_2 \sim 1,\ A \ll 1$. This form is not found in traditional formalisms. The second exponential $(\gamma_2 \sim 1)$ has been predicted using different approaches but, as we have shown, it is realized at much higher wavenumbers than previously considered. The multifractal scaling seems to provide a better representation in the intermediate dissipation range (around NDR), but not at very high wavenumbers in the FDR. We have made a connection between the second exponential and intermittent energy transfer. By removing these intense fluctuations (argued to be due to activity in the larger scales by Kraichnan), the spectrum reverts to the single low-R_λ exponential. It is also interesting to note that the two-exponential behavior is observed for $R_\lambda \gtrsim 20$. This Reynolds number is not far from the critical value recently put forth by Yakhot & Donzis [60, 33] beyond which moments of velocity gradients and dissipation transition from the Gaussian state to fully anomalous state characterized by intermittency. Finally, this work suggests two more conclusions. First, fitting a single exponential to high-R_λ data may lead to conflicting results as the numerical values of the parameters depend strongly on the range over which the fit is performed as it may cover NDR, FDR or both. Second, the very large bursts of energy that are observed in FDR present difficulties in time averaging as strong and localized events can be missed or skew the mean. Thus, very long records with very high time resolution (both perhaps beyond

current practices) are needed for converged averages especially in the FDR.

4.5 Appendix: Determination of fitting parameters

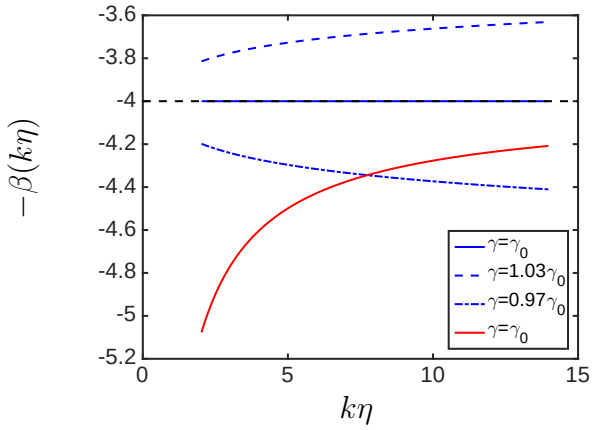

Figure 4.6: Compensated curves with over and underpredicted value for γ. Blue lines are for a pure exponential and red line is for an exponential prefixed with a power law ($\alpha_0 = -5/3$). Both have $\beta = 4$ (dashed black line) and $\gamma_0 = 0.85$.

Here we show further tests for the compensation method used to determine the coefficients. As explained in the text, the method is based on obtaining γ as the value that results in the widest plateau for $\phi(x)/(\gamma x^\gamma)$. To test the accuracy of the method, we use a known function $(k\eta)^{\alpha_0}\exp(\beta_0(k\eta)^{\gamma_0})$ with given α_0, β_0, and γ_0 and use our technique based on Eq. (4.4) to compare the obtained coefficients. In Fig. 4.6 we show typical results for $(\alpha_0, \beta_0, \gamma_0) = (0, 4, 0.85)$ (blue lines) and $(\alpha_0, \beta_0, \gamma_0) = (-5/3, 4, 0.85)$ (red line). It is clear from Eq. (4.4) that a wide plateau, with the correct β is, in theory, only observed for the case with no power law ($\alpha_0 = 0$). We look at that case first. In the figure we plot results for γ which is deliberately selected to be 3% below and above the exact value (γ_0). In both cases no plateau is observed and no β could thus be identified. This example shows how the compensation method is found to be able to visually account for a few percentage points errors in the determination of γ. For the case with a power law ($\alpha_0 \neq 0$), the approach to the right value of β is seen to occur only asymptotically at very large $k\eta$ when the correct γ is used (red line): no plateau is observed in this case. Thus, the plateau

observed in DNS data (Fig. 4.2) is indicative of both an appropriate value of γ and a negligible α, as argued in the text.

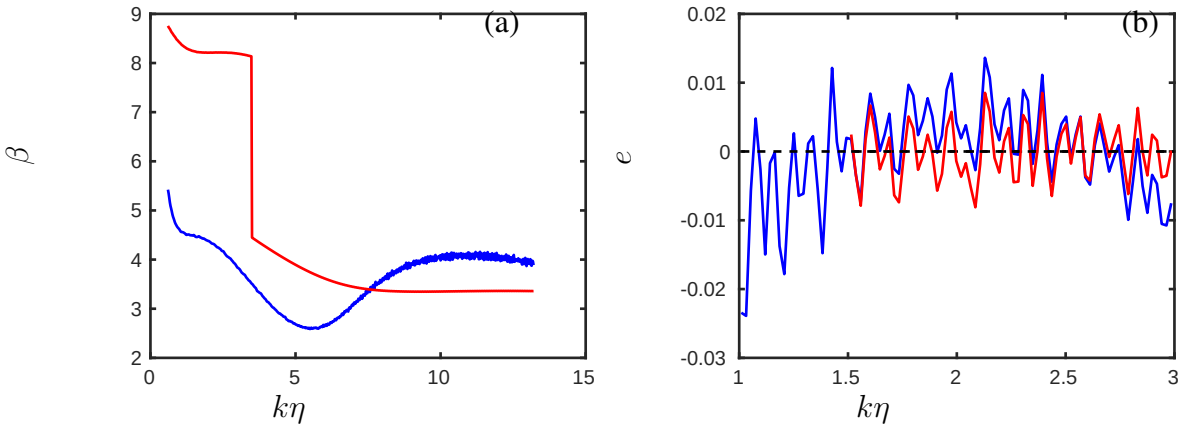

Figure 4.7: $a)$ Value of β when fit locally for $R_\lambda \sim 90$. $b)$ Relative error between DNS data and Eq. (4.2) using parameters obtained with the present method (red) and that of [3] (blue).

We also compare our local fitting procedure with that of [3, 119]. Both studies assumed $\gamma = 1$ and fit locally both α and β. Schumacher [119] concluded that no visible asymptotic behavior was observed for his data and that α appears to change sign. Martinez *et al.* [3] used their highest resolved simulation to show that β approaches a constant. However, they could only resolve up to $k\eta \approx 11$. In Fig. 4.7(a) (blue line) we show a case in our DNS database using their method. What we observe is that β does not approach a constant but instead a local maximum around $k\eta \approx 10$ which may be mistakenly taken as an asymptote if no data at higher wavenumbers are available. If instead we use the present method on the same data we find clear asymptotic behavior in both NDR and FDR (red line). A constant value of β is now observed as the proper value of γ is used and α is not a fitting parameter. We also see that our method results in smoother curves especially at high $k\eta$. The relative error between DNS and Eq. (4.2) with parameters obtained by these two methods is shown in Fig. 4.7(b). An important observation in the figure is that the procedure in [3] leads to errors with non-random structure: negative error at low and high k and positive error

at intermediate k. This is indicative of an inappropriate fitting function, or, in this case, γ values. The method proposed here, instead, leads to a randomly distributed error and with overall smaller error.

5. SCALING IN INCOMPRESSIBLE TURBULENCE

Thus far we have addressed the spectral properties of turbulence including the energy spectrum, which is a second order statistical measurement. We found that the smallest scales have a prominent R_λ dependence, even at the energy spectrum level (a second order statistic). We also established that global scale invariance is not valid for the energy spectrum in the dissipation range. In this section, we complement the spectral perspective by studying higher order statistics of velocity fluctuations in physical space. Increasing the order of statistics is equivalent to exploring more extreme fluctuations or at smaller scales.

5.1 Introduction

Turbulence is characterized by a wide range of fluctuating spatial and temporal scales. These range from the energy containing large scales (L) to the energy dissipating small scales (η). Within turbulence phenomenology, it is largely expected that large scales depend on the generation mechanism while as the small scales are increasingly universal as the separation between the two grows [19, 23, 135, 136, 46]. A sense of the scale separation in turbulent flows is given by the Reynolds' number $R_\lambda = \sqrt{5/(3\varepsilon\nu)}u_{rms}^2$ where ε is the ensamble averaged kinetic energy dissipation, u is the fluctuating velocity field and ν is the fluid viscosity. The universality of small scales, at high R_λ in some quantitative sense, is an enduring notion in turbulence theory and forms the bedrock of most modelling approaches [19, 23, 137, 25]. This view was formalized in Kolomogorov's seminal work (K41) which predicted a statistical behavior for fluctuations at different scales, in particular a R_λ independent asymptotic state in the so called inertial range $(L \geq r > \eta)$ and dissipative range $(r \leq \eta)$ [19, 136]. A universal behavior, according to K41,for small scales is then expected for very large R_λ flows and this has been the motivation for studying turbulence at ever increasing R_λ, largely seeking the asymptotic state described by K41 [30, 85]. The theory itself does not provide and there is no empirical consensus on a quantitative measure of *high enough* R_λ. An important feature of K41 is the presence of a R_λ independent self-similar scaling in the

so-called inertial range scales. This is observed for $R_\lambda \sim O(10^2)$ [25, 138, 139, 140, 26, 117, 30]. Recently, however, it was shown that moments of a key fluctuating quantity, kinetic energy dissipation $\epsilon = 2\nu s_{ij}s_{ij}$, a small-scale quantity, obeys algebraic scaling with R_λ across different flows at much lower-R_λ than expected from K41 [141]. Here s_{ij} is the rate of strain given by $(\partial_i u_j + \partial_j u_i)/2$ using Einstein summation. Dissipation is the mechanism that converts kinetic energy to heat through molecular viscosity, at the smallest ($\sim O(\nu^{3/4}\epsilon^{-1/4})$) scales of motion. For the case of initially Gaussian fluctuations stirred by Gaussian white noise at large scales, it was also shown that this algebraic scaling emerges from a phase transition from a Gaussian state at at very low Reynolds number (R_λ) [60, 33]. Yakhot & Donzis [60] showed that even order moments of longitudinal velocity gradients

$$M_{2n}^{||} = \overline{\langle(\partial_\alpha u_\alpha)^{2n}\rangle}/\overline{\langle(\partial_\alpha u_\alpha)^2\rangle}^n \tag{5.1}$$

exhibit asymptotic behavior below a critical $R_{\lambda,tr}(n)$. Beyond the transition R_λ for a given order moment, algebraic scaling is observed i.e. $M_{2n}^{||} \propto R_\lambda^{2d_n}$. This is sketched in Fig. 5.1. The low-R_λ asymptote is shown to have Gaussian statistics for a flow forced with Gaussian random force at the large scales and an order dependent transition Reynolds number ($\hat{R}_{\lambda,tr}(n) \equiv L\overline{\langle(\partial_\alpha u_\alpha)^n\rangle}^{\frac{1}{n}}/\nu$) is derived to be approximately 8.91. The global transition-R_λ for each order moment then decreases with increase in order of the moment ($R_{\lambda,tr}(n) \propto \hat{R}_{\lambda,tr}^{\frac{2nd_n}{2d_n+3}}$) [33]. This means higher-order moments (extreme events) transition to turbulent scaling at a lower-R_λ than low-order moments. This is sketched in Fig. 5.1. If one assumes the low-R_λ statistics are known (denoted by P_{2n}) and the transition-R_λ is known, then the algebraic scaling can simply be derived by matching the power-law with the asymptotic value at the transition Reynolds number. Then d_n has the form

$$\begin{aligned} d_n = &-\frac{2n\log(\hat{R}_{\lambda,tr}) - 3n\log(C) + 2\log(P_{2n})}{4\log(C)} + \\ &\frac{\sqrt{(2n\log(\hat{R}_{\lambda,tr}) + 3n\log(C) - 2\log(P_{2n}))^2 + 24n\log(C)\log(P_{2n})}}{4\log(C)} \end{aligned} \tag{5.2}$$

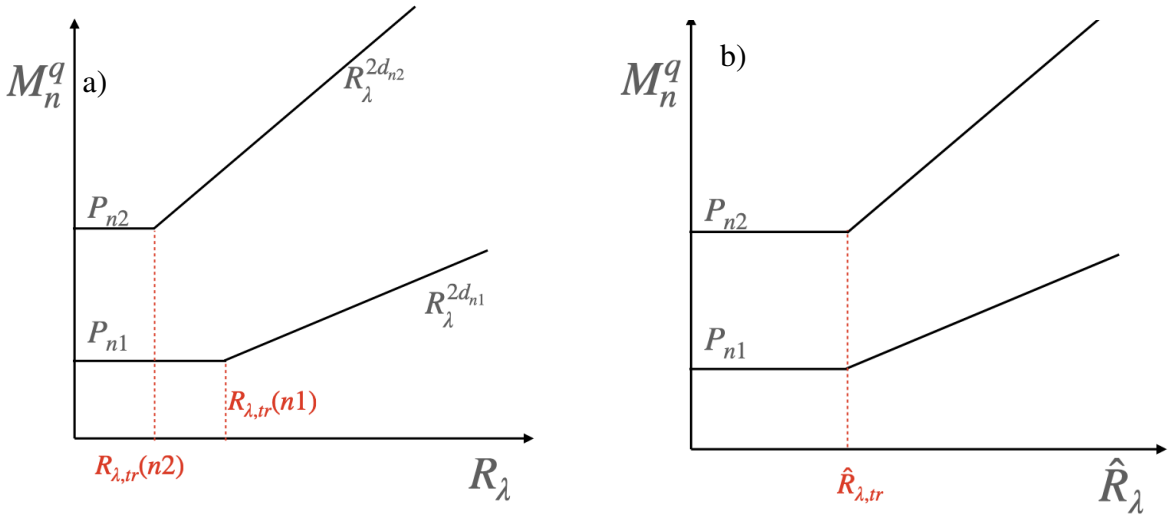

Figure 5.1: Sketch depicting the transition from low-R_λ asymptote to algebraic scaling for moments of two different orders $(n_2 > n_1)$ with respect to a) global Reynolds number b) order-dependent Reynolds number

The scaling predicted at these low and moderate R_λ allow for calculating the universal properties of inertial range range turbulence which is observed at much higher R_λ than the ones considered [33]. This means that high-R_λ properties are already present even at very modest R_λ.

Given the ubiquity of turbulent flows in natural and engineering applications, it is extremely important to establish the general validity of this new formalism and its extension to more complex flows. Therefore, in this section, we test the universality of the transition of velocity gradients and their scaling under different large scale stirring mechanisms. A universal transition and scaling (or lack thereof) can also provide important evidence for establishing the universality class for transition to turbulence and its anomalous scaling exponents. In addition to longitudinal gradients, we also consider transverse velocity gradients $(\partial u_\alpha/\partial x_\beta)$ and more complex quantities dependent on velocity gradients. One such quantity is instantaneous enstrophy $(\Omega = \omega_i\omega_i)$ which is a measure of vorticity $(\vec{\omega} = \nabla \times \vec{u})$. Enstrophy has a complicated relationship with dissipation in general but the mean dissipation is equal to entrophy times viscosity. The scaling of enstrophy is also important for understanding the finite time blow-up and uniqueness problem in Navier-Stokes equations [142, 8]. The scaling of enstrophy moments has not been studied yet and therefore we

present those and refer readers to other sources for dissipation [143, 52, 141, 144].

5.2 Direct Numerical Simulations

In particular we study forced homogeneous, isotropic turbulence in a triply periodic domain governed by the Navier-Stokes equations,

$$\frac{\partial u_i}{\partial x_i} = 0 \tag{5.3}$$

$$\frac{\partial u_i}{\partial t} + u_j \frac{\partial u_i}{\partial x_j} = -\frac{1}{\rho}\frac{\partial p}{\partial x_i} + \nu \frac{\partial^2 u_i}{\partial x_i^2} + f_i \tag{5.4}$$

where u_i is the velocity component in x_i direction, p is the pressure and ν is the viscosity. The forcing term f_i adds energy into the system to balance dissipation and achieve a statistically stationary state. The details of different forcing mechanisms are summarized in Table 5.1. We use stochastic forcing where the velocity increments are derived from white in time gaussian and exponential random distributions These are applied at large scales or low wavenumbers. These forcings have been widely used in literature [81, 129, 60, 145]. The random number generator is changed, from Gaussian to exponential, to study the effect of forcing statistics on the universality of the low-R_λ Gaussian asymptote and the subsequent transition to anomalous scaling. In order to generalize the results for more complex flow types, we also use a linear forcing where the velocity field is forced by itself. Such a forcing is equivalent to generating turbulence through shear. This type of forcing has been applied at low wavenumbers, as has been done previously for studying high-R_λ turbulence. The forcing has also been shown to exhibit more complex dynamical states which are similar to those observed in shear flows [146, 29, 147, 148]. We also implemented a modification of this linear forcing where we force the velocity field with vorticity to study the effect of statistics of forcing term on universality of low-R_λ features and transition. Vorticity in general has been shown to have more extreme fluctuations than velocity. All the simulations are initialized with the same initial velocity field. We use a standard psuedospectral method to solve the equations with small scale resolution $k_{max}\eta \gtrsim 3$. The time step is evolved using a Runge-Kutta 2 algorithm with a constant time step such that the Courant-Friedrichs-Lewy condition ($CFL = |u_{max}|\Delta t/\Delta x$) remains

Table 5.1: Forcing details. Gauss and Exponential are stochastic forcings where the forcing term (r_i) is derived from white in time gaussian and exponential random distributions. A is a constant. The last column lists the maximum and minimum small scale resolution across simulations for each forcing.

Type	Forcing band	f_i	Resolution
Gauss	$0 < k \leq 2$	(r_1,r_2,r_3)	60,3
Exponential	$0 < k \leq 2$	(r_1,r_2,r_3)	60,3
$u(k)$	$5 \leq k \leq 6$	(Au_1,Au_2,Au_3)	60,3
$\omega(k)$	$5 \leq k \leq 6$	($A\omega_1$,$A\omega_2$,$A\omega_3$)	60,3

below 0.3. These high resolutions allow us to reliably measure higher order moments of velocity gradients [61, 149]. In order to guarantee convergence, we record at least 50 large scale eddy turnover times in the stationary state. The moments are computed using at least 100 snapshots separated by about half an eddy turnover time. We have verified that the skewness in the scaling range is -0.5, the ratio of longitudinal and transverse integral length scales is 2 and the kinematic constraint on isotropic fields $g(r) = (f(r) + 0.5rf'(r))/g(r)$, where $f(r) = \overline{u_\alpha(x_\alpha)u_\alpha(x_\alpha + r)}/\overline{u_\alpha^2}$, $g(r) = \overline{u_\beta(x_\alpha)u_\beta(x_\alpha + r)}/\overline{u_\beta^2}$, is satisfied [135].

5.3 Asymptotic States and scaling

We are interested in the moments of a quantity *q* in the form $M_n^q = \overline{\langle q^n \rangle}/\overline{\langle \tilde{q} \rangle}^n$ where $\langle q \rangle$ denotes volume averages, $\overline{q}$ denotes time averages, $\tilde{q}$ is a non-zero moment of q and n is the order of the moment. The ensemble averaged moments of longitudinal $(||)$ and transverse $(\perp)$ velocity gradients from simulations with different forcing mechanisms are shown in Fig. 5.2a. It is clear that the moments of velocity gradients are independent of forcing, with small differences near the transition region. Such a universal behavior is expected at much higher R_λ than the ones reported here. The moments of the longitudinal and transverse velocity gradients exhibit Gaussian statistics (dashed horizontal lines) and transition to an algebraic scaling beyond a transition-R_λ, independent of the forcing statistics. The transition Reynolds numbers is qualitatively lower for transverse gradient statistics as the moments transition to algebraic scaling seemingly at a lower-re in comparison to their longitudinal counterparts. The algebraic scaling for longitudinal gradients is the same as

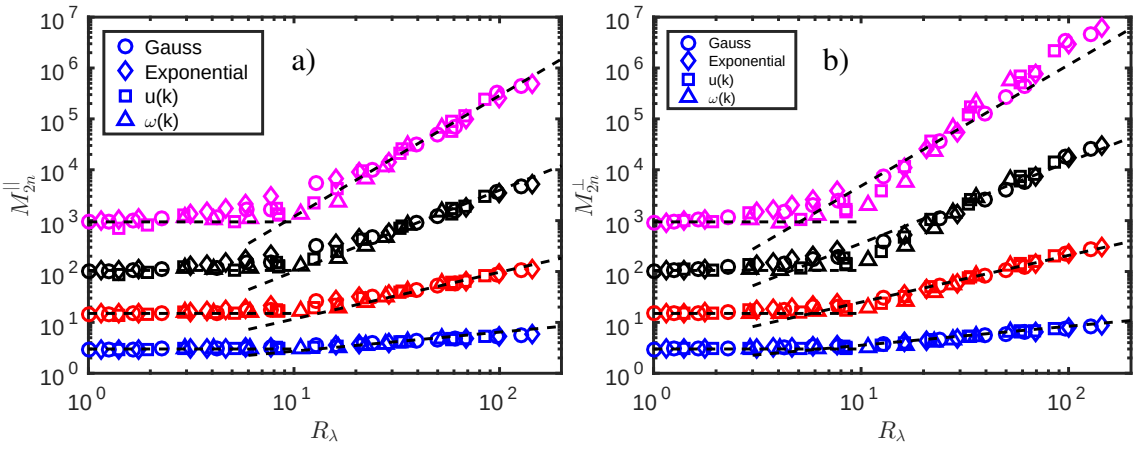

Figure 5.2: Moments of a) longitudinal and b) transverse velocity gradients for $2n = 4$ (blue),6 (red), 8 (black), 10 (magenta). The horizontal dashed lines are Gaussian moments and power-laws correspond to $R_\lambda^{2d_n}$ where d_n is given by Eq.Eq. (5.2) with $\hat{R}_{\lambda,tr} = 9.89$.

derived analytically (dashed power-laws) assuming the low-R_λ moments are Gaussian (Eq. (5.2)). In Fig. 5.2b, we have plotted the moments of transverse velocity gradients (symbols) along with the scaling predicted for longitudinal gradients (dashed power-laws). Comparing Fig. 5.2 a and b, it is clear that the moments of transverse gradients grow faster than longitudinal gradient moments and increasingly so with increasing order of the moment. Therefore transverse gradients exhibit a larger degree of intermittency than longitudinal gradients. This was recently shown using velocity differences at very large-R_λ [26] . In the past this result has been questioned based on symmetry arguments [150, 151, 139] . Longitudinal gradients are constrained by the incompressibility condition while as transverse gradients have no such constraint. Therefore in general transverse velocity gradients are expected to be more intermittent. This means the scaling predicted in Eq. (5.2) is different for different quantities, albeit universal for a given quantity across different forcings. The theory allows for this possibility if different quantities transition at a different R_λ. Then Eq. (5.2) needs to be modified to $d_n^q = f(\hat{R}_{\lambda,tr}^q, C, 2n)$ rather than $d_n^q = f(\hat{R}_{\lambda,tr}, C, 2n)$ for different $q = ||, \perp$ etc.

We quantitatively compare the transition and scaling of different quantities using a fitting procedure. A simple power-law fit only within the scaling range is highly sensitive to bounds of the

fitting range. Instead, we attempt to fit the entire data-series with a single expression that captures the low-R_λ asymptotic behavior as well as the algebraic scaling range. Such a procedure has been shown to be more reliable in measuring the scaling parameters within inertial range [152]. In order to construct such a function, we note that for a $2n$ order moment of quantity q and $R_\lambda/R_{\lambda,tr} \ll 1$, the statistics are constant ($M^q_{2n} = C^q_{2n}$). For $R_\lambda/R_{\lambda,tr} \gg 1$, $M^q_{2n} \propto R_\lambda^{\beta^q_{2n}}$. The power-law must be Gaussian at the transition-Re [33]. Since the details are transition are not well understood, we empirically propose the below function form that fits the data and satisfies previously mentioned properties.

$$M^q_{2n} = C^q_{2n} + \alpha^q_{2n} C^q_{2n} \left(\frac{R_\lambda}{R_{\lambda,tr}(2n)} \right)^{\beta^q_{2n}} \tag{5.5}$$

where $\alpha^q_{2n} < 1$ and we have four fitting parameters. However, we are only able to measure $\alpha^q_{2n}/(R_{\lambda,tr})^{\beta^q_{2n}}$ accurately as the two cannot be fit independently. Further, the fit is highly non-linear and susceptible to intital seeds. We therefore perform a fit with an equivalent function

$$M^q_{2n} = C^{2n}_q \left(1 + \left(\frac{R_\lambda}{b^{2n}_q} \right)^{\beta^q_{2n}} \right) \tag{5.6}$$

where $b^q_{2n} = R_{\lambda,tr}(2n)/(\alpha^q_{2n})^{1/\beta^q_{2n}}$ for a given quantity q and order $2n$. Although other functions with the same properties are possible, this form is favorable as the fit parameters are independent of initial seeds and fitting range. We have checked the convergence of the fit by varying the largest-R_λ considered and conclude (convervatively) that a $R_\lambda \sim 90$ is needed for converged fit parameters. This is satisfied by data from Gaussian, Exponential and Linear forcing simulations only. In order to provide statistical bounds of fit parameters for a given order $2n$, we generate synthetic data from a normal distribution with the same mean and standard deviation as the $2n$ moment at a given R_λ from DNS data. This is repeated 50 times for each datapoint in Fig. 5.2 which provides us 50 independent datasets for fitting with Eq. (5.6). This allows us to generate a distribution for each fit parameter and determine their respective confidence intervals. The fit parameters and their 95% confidence intervals are shown in Figs. 5.3, 5.4, 5.5 for three different forcings.

The asymptotic value at low-R_λ (C_{2n}) is plotted in Fig. 5.3 along with the moments for a Gaussian distribution (dashed line). It is clear that the low-R_λ asymptotic value is Gaussian for longitudinal and transverse moments of velocity gradients across all forcings, consitent with observation in Fig. 5.2. The parameter b_{2n}^q which is proportional to transition R_λ is shown to decrease with increase in order of the moment as expected from theory. We note that the large values of b_{2n}^q are not representative of large transition-R_λ. For example, for $b_4^{||} = 100$ and $\alpha_4^{||} = 0.5$, $R_{\lambda,tr}(4) \approx 13$, close to the expected value of $O(10)$. We also observe that for a given forcing, the transition-R_λ is lower for transverse gradients (blue symbols) in comparison with longitudinal gradients (red symbols). Although small differences are observed for b_q at a given n for different forcing, these are within our statistical bounds on fit parameters. In Fig. 5.4d, we plot the average of b_{2n}^q across the three forcings. A difference in b_q is clear for transverse and longitudinal gradients, indicating that the scaling of the two is different. The algebraic scaling exponent, $\beta_{2n}^q = 2d_n^q$ is plotted in Fig. 5.5f for the 3 different forcings. We again observe that the scaling exponents are larger for transverse gradients, consistent with earlier observations. Scaling exponents for the longitudinal gradients are consistent with earlier measurements made in HIT, channel and Rayleigh-Bernard convection [153, 154, 141, 144]. The dashed lines are Eq. (5.2) with $\hat{R}_{\lambda,tr} = 11$ (red) and $\hat{R}_{\lambda,tr} = 2$ (blue), which indicate that longitudinal velocity gradients transition at a higher value of $\hat{R}_{\lambda,tr}$ and are more intermittent in comparison to transverse velocity gradients. Based on Eq. (5.2), the scaling exponents of transverse structure functions in the inertial range will then be different (smaller) from longitudinal structure functions. This has recently been reported in [26] using data from $R_\lambda \gtrsim 650$, much larger than the ones reported here. Although Yakhot & Donzis [33] allows for different exponents, the physical reasoning for this difference is not clear. Recent work from Sreenivasan & Yakhot [16, 26] allows us to speculate on this. Sreenivasan & Yakhot argue that high-order moments of longitudinal differences are less susceptible to pressure effects and therefore can form strong departures from mean. The reduced pressure effect with increase in order of the moment leads to strong fluctuations and transition to turbulence at a lower-R_λ for high-order moments, consistent with our observation. We speculate that similar effects lead to

differences in transition of longitudinal and transverse gradient to algebraic scaling. Transverse gradients are not constrained by the incompressible condition and therefore are far less affected by pressure. Therefore, reduced pressure effects lead to a lower transition-R_λ for transverse gradients.

It is also important to study the moments of other small scale quantities which are comprised of multiple velocity gradients. Of particular interest in turbulence theory are dissipation and enstrophy ($\Omega_i = |\omega|^2$) moments. In previous work, the moments of dissipation were shown to follow algebraic scaling given by $d_n^{||}$, at moderate R_λ. In Fig. 5.6, we plot the moments of enstrophy (symbols) at different R_λ and forcings. For $R_\lambda \lesssim 10$, the asymptotic values correspond to moments of χ^2 distribution with 3 degrees of freedom. This is expected as enstrophy is composed of sum of squares of 3 trasnsverse gradients each of which are Gaussian in this range. Similarly dissipation will exhibit statistics of χ^2 distribution with 5 degrees of freedom as the incomrpessibility condition imposes that only 5 gradients are independent. We do observe this in our data as well, although have not shown it here. The moments transition to an algebraic scaling regime which is the same for all forcings. We compare the moments (symbols) with the predicted scaling for dissipation moments (dashed power-laws). It is clear that enstrophy moments grow faster than dissipation and increasingly so at higher orders. This is more evidence supporting that the most extreme events in enstrophy are more probable than the most extreme events in dissipation. This question has been studied previously with data at much larger R_λ [61, 87, 150, 155].

5.4 Conclusions

In this section, we have shown that scaling is established for velocity gradients and enstrophy at $R_\lambda \sim O(10)$, much lower than expected before. For a given quantity, universal scaling is observed across different forcings reinforcing the idea of universality in turbulent flows. However, the notion of universality is modified as different quantities exhibit different scaling exponents, within the same data. We have shown this by comparing the scaling exponents of longitudinal and transverse velocity gradient moments as well as those of dissipation and enstrophy. We have shown that the scaling exponents are larger for transverse gradients which are representative of higher level of intermittency. The scaling exponents can be predicted by Yakhot & Donzis theory after a

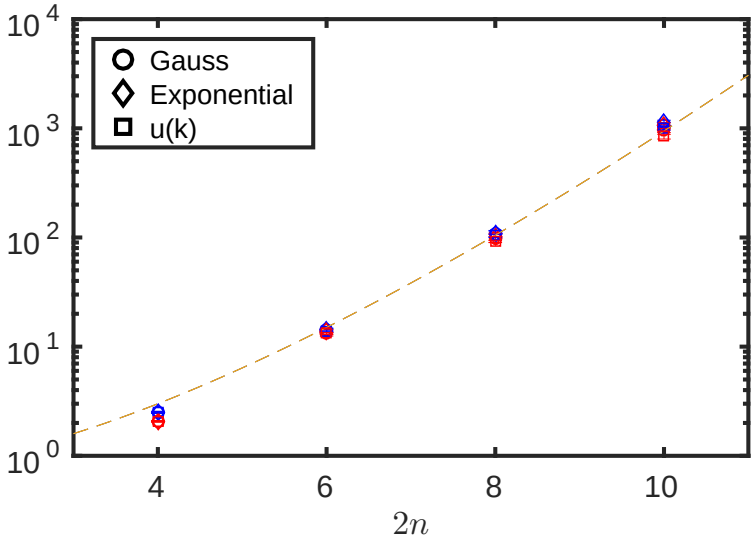

Figure 5.3: Fitting parameter C_{2n} in Eq. (5.6) for different forcings. All the constants are independent of forcing and agree well with the expected Gaussian value (dashed line) for each moment. Red and blue symbols represent fit parameters from longitudinal and transverse gradients respectively.

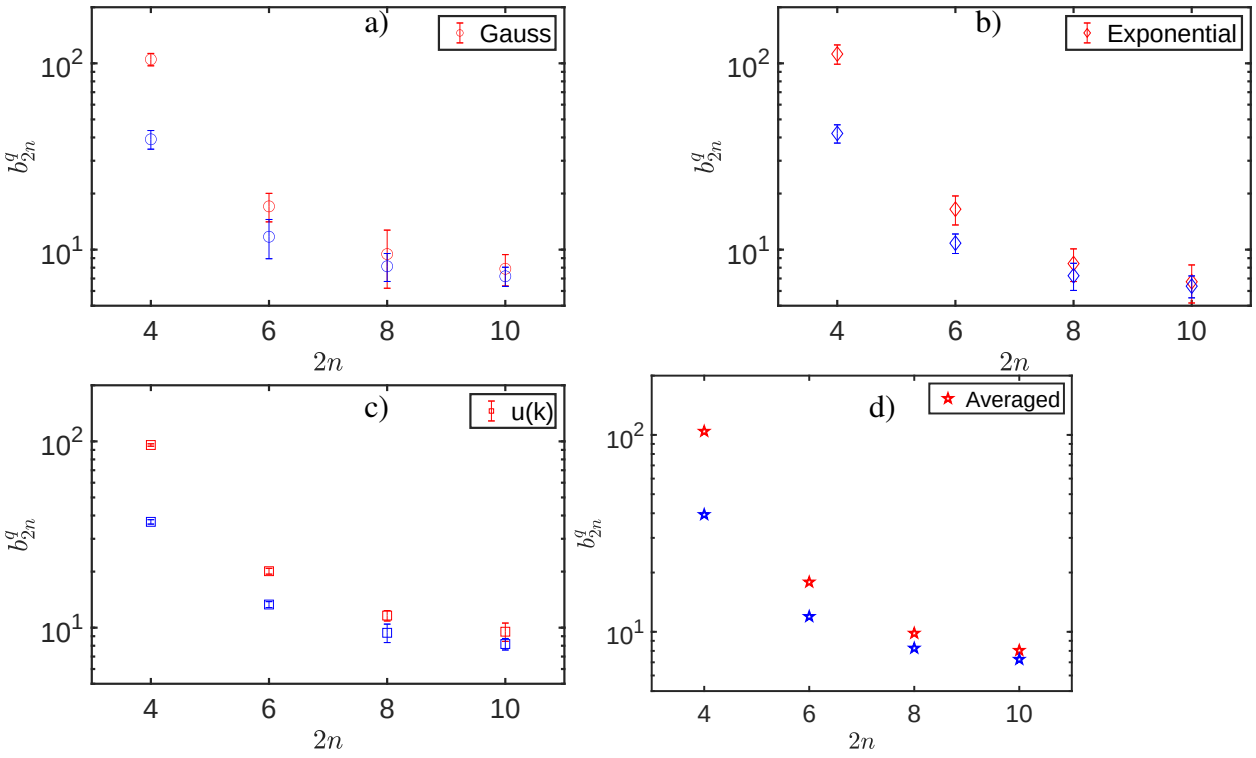

Figure 5.4: The constant $b \propto R^{tr}_{\lambda}(n)$ in Eq. (5.6) for a) Gauss b) Exponential c) u(k) forcings. d) The mean b^q_{2n} across three forcings. f) Scaling exponents for different forcings. Red and blue symbolds are for longitudinal and transverse gradients respectively.

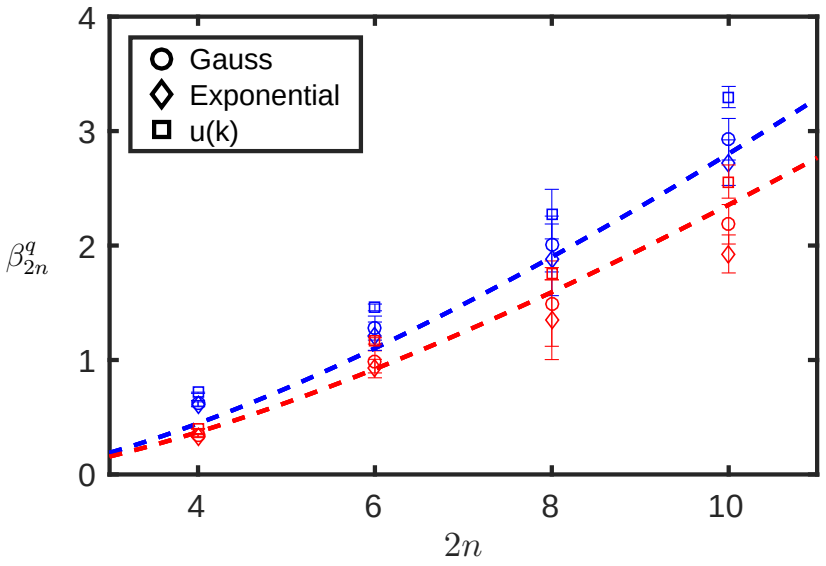

Figure 5.5: Power-law scaling exponent β^q_{2n} for the fit in Eq. (5.6). The red and blue lines are with $R^{tr}_\lambda = 11$ & 2 respectively in Eq. (5.2).

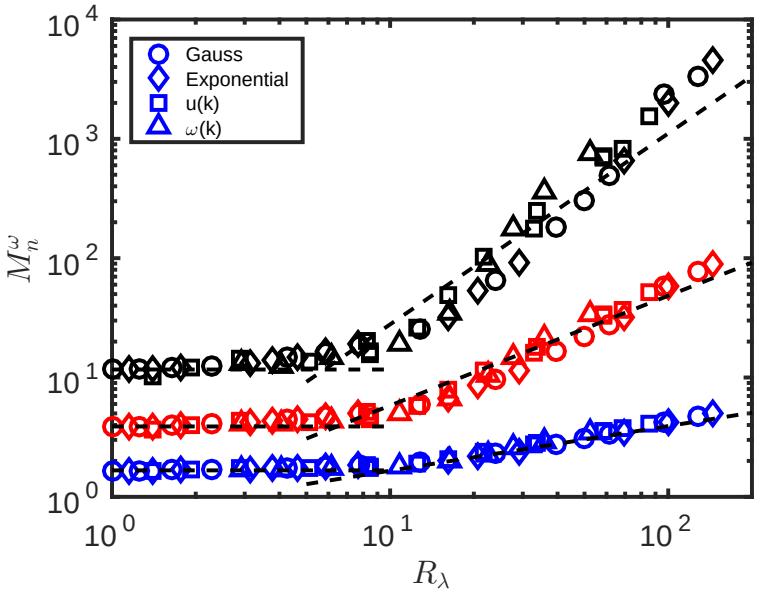

Figure 5.6: Moments of enstrophy for $n = 2$ (blue), 3 (red), 4 (black). Horizontal lines correspond to moments of χ^2 distribution with 3 degrees of freedom. The power-laws corresponds to $\langle \epsilon^n \rangle / \langle \epsilon \rangle^n \propto R_\lambda^{d_n}$.

quantity specific transition R_λ is accounted for. The more intermittent traverse gradient transition at a lower-R_λ (~ 2) compared to longitudinal gradient moments which transition around $R_\lambda \sim 11$. The scaling is studied for at $1 \lesssim R_\lambda \lesssim 100$, much before an inertial range is established. The scaling exponents are predictive of scaling in the inertial range. Therefore high Reynolds features can be studied using data from well resolved DNS at low to moderate R_λ, instead of chasing the goal of ever increasing values. We note that this procedure of predicting features of non-linear systems at asymptotic parameter values (R_λ in this case) using information about a transition from a low-order state may be a general feature of non-linear spatio-temporal chaotic systems. We have found early evidence to support this in passive scalar advection [156], scaling exponents in compressible turbulence (Chapter 6) and Burgers equation [157]. These results will be reported elsewhere in future communications.

6. SCALING IN COMPRESSIBLE TURBULENCE

6.1 Introduction

In previous sections, we have explored different aspects of incompressible turbulence. A wide range of flows in natural and engineering applications have significant changes in density and (or) are high-enthalpy flows where incompressibility assumptions breakdown. Fundamental understanding of the structure of compressible turbulence and characterization of its statistics is therefore important in a wide range of fields e.g. design of hypersonic aircraft, combustion applications, stellar formation and inertial fusion problems. Compared to incompressible turbulence, fewer studies have explored fundamental aspects of compressible turbulence and most work has been recent [74, 69, 68, 71, 73, 71, 70, 63]. This is in part due to added complexity in compressible turbulence due to the strongly non-linear coupling between velocity field and thermodynamics. For computational approaches, the computing cost is much higher in compressible flows in comparison to their incompressible counterparts due to an increase in the degrees of freedom [75].

In this section, we will systematically explore intermittency, its scaling and its emergence in compressible turbulence using gradients of velocity. Our focus will be to extend the Yakhot formalism to compressible turbulence and study the emergence of scaling at low to moderate parameter values. In the literature, similar to incompressible turbulence, the focus thus far has been on exploring the high Reynolds number (R_λ) and high turbulent Mach number $M_t = u_{rms}/\langle c \rangle$, where c is the speed of sound. Further, all the studies thus far have studied intermittency within the inertial range using structure functions [62, 63, 64, 71, 72]. Benzi *et al.* [62] studied scaling in the inertial range for inviscid weakly compressible flows and showed that the scaling for longitudinal and transverse structure functions of velocity is similar to incompressible flows. They did however note the presence of front like structures in the density field which led to saturation of scaling exponents for density at high orders. Transverse structure functions of velocity were also studied by [63, 64] in inviscid isothermal highly compressible turbulence. They noted significant

departures of scaling exponents compared to incompressible turbulence and a dependence on large scale forcing mechanism. However, a reformulation of the structure functions in terms of density-weighted velocity ($\rho^{1/3}u$) showed scaling that was independent of forcing and consistent with Burgers scaling. Recent work from Wang *et al.* [72] studied the compressible and solenoidal velocity fields separately in a simulation at $R_\lambda \approx 250$ and $M_t \approx 1$. The velocity field is decomposed into solenoidal ($\mathbf{u}^s$) and compressible ($\mathbf{u}^d$) components based on Helmholtz decomposition where $\nabla \cdot \mathbf{u}^s = 0$ and $\nabla \times \mathbf{u}^d = 0$. They show that the scaling of longitudinal structure functions of the solenoidal component is the same as incompressible turbulence. The longitudinal structure functions of compressible velocity component however saturated at high orders consistent with Burgers turbulence scaling. The saturation of scaling exponents in Burgers turbulence is a consequence of high dissipation events dominated by shocks connected by smooth ramps.

6.2 DNS details

We perform direct numerical simulations of compressible turbulent flows in a triply periodic domain as described in Section 2. A 2π domain is discretized into $N = 128, 256, 512$ grid points in each direction where the resolution $(\eta/\Delta x)$across simulations varies between 0.96 and 10. The Courant number is kept constant at 0.3. The highest-R_λ in the database is approximately 60 with an $M_t \approx 0.7$. We note that the highest-R_λ considered in this study is comparable to the lowest-R_λ studied in the literature with the higher-end being an order magnitude larger.

6.3 Scaling of total velocity field

We are again interested in moments of velocity gradients of the form

$$M^q_{2n} = \frac{\overline{\langle(\partial_\alpha u_\beta)^{2n}\rangle}}{\overline{\langle(\partial_\alpha u_\beta)^2\rangle}^n} \tag{6.1}$$

where $\alpha = \beta$ corresponds to longitudinal gradients and $\alpha \neq \beta$ corresponds to transverse gradients. In this case, q can be full velocity field, solenoidal (s) component or the compressible component (d). In Fig. 6.1, we plot the transverse gradients of the full velocity field for our entire database. It is clear from Fig. 6.1, that the transverse gradients of the full velocity field are independent of M_t

or compressibility levels. At very low-R_λ, we observe Gaussian statistics for the gradients, similar to incompressible counterpart. The gradients transition at a $R_\lambda \sim O(10)$ to algebraic scaling. The power-laws plotted are scaling laws for transverse gradients in incompressible flows as discussed in the previous chapter. We again observe that high-order moments transition earlier than low-order moments do and that scaling emerges at very low-R_λ. This is consistent with results of Benzi *et al.* [62], although the M_t in their paper is 0.3 and the flow is inviscid. This means that transverse gradients are unaffected by level of compressibility or by the randomly scattered shock structures in the flow field. In Fig. 6.2a, we plot the longitudinal velocity gradients for simulations with M_t up to 0.35. We again observe Gaussian statistics at low-R_λ and a transition to algebraic scaling at $R_\lambda \sim O(10)$. We have plotted two power-laws for each moment order. The black ones represent the scaling for longitudinal gradients in incompressible turbulence as reported in the previous chapter. In this case, the transition region is much wider and a power-law scaling consistent with this case is only observed for $R_\lambda > 30$, in comparison to incompressible flows. The colored power-laws correspond to incompressible scaling as predicted by Eq. (5.2) with the transition $R_\lambda = 20$. Although, this case fits the data better, it is not clear why transition-R_λ should change for the case of full velocity. Literature on transition to turbulence does however support the view that compressibility delays transition. Within this range of M_t, however compressibility effects are considered to be weak and the solenoidal component dictates scaling of the full velocity field [88, 89, 69, 73]. For $M_t > 0.35$, we observe that the longitudinal gradients scaling exponents are much larger than at lower-M_t. The scaling exponents are comparable to those of Burgers turbulence (power-laws in Fig. 6.2b) [157]for $R_\lambda > 30$. The dissipation in this case is dominated by shock structures that are randomly scattered in the domain and vary in strength. Samtaney [70] have shown that shocklet strength does increase with increase in M_t. A burgers scaling in this case, if verified, will be consistent

6.4 Scaling of solenoidal velocity field

Compressible turbulent velocity fields can be decomposed into vortical or solenoidal ($\mathbf{u}^s$) and compressible or dilatational ($\mathbf{u}^d$) components using the Helmholtz decomposition. This decom-

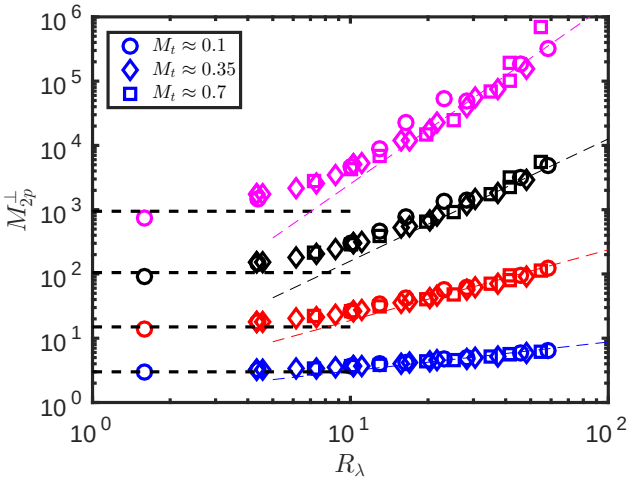

Figure 6.1: Moments of transverse velocity gradient for the full velocity field. Moment orders are $2p = 4$(blue), $2p = 6$(red), $2p = 8$ (black) and $2p = 10$ (magenta). The power-laws correspond transverse velocity gradient scaling for incompressible flows in Section 5.

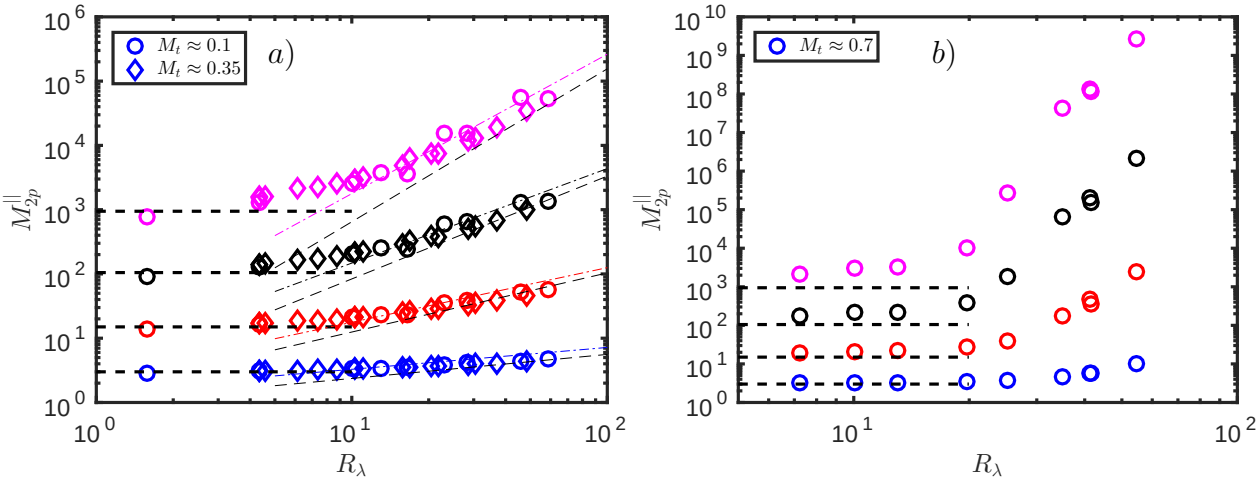

Figure 6.2: Moments of longitudinal velocity gradients for the full velocity field. Moment orders are $2p = 4$(blue), $2p = 6$(red), $2p = 8$ (black) and $2p = 10$ (magenta). a) The colored power-laws correspond Eq. (5.2) with $\hat{R}_\lambda^{tr} = 20$ and the black power-laws correspond to scaling of longitudinal gradients in incompressible turbulence in Section 5. b) Longitudinal velocity gradient moments at $M_t \approx 0.7$. There are no predictions for scaling in this regime that are consistent with data. The approximate power-laws are $M_4 \propto R_\lambda^2$, $M_6 \propto R_\lambda^4$,$M_8 \propto R_\lambda^{8.4}$, $M_{10} \propto R_\lambda^{12}$ for a fit between $R_\lambda \approx$ 10 and 60.

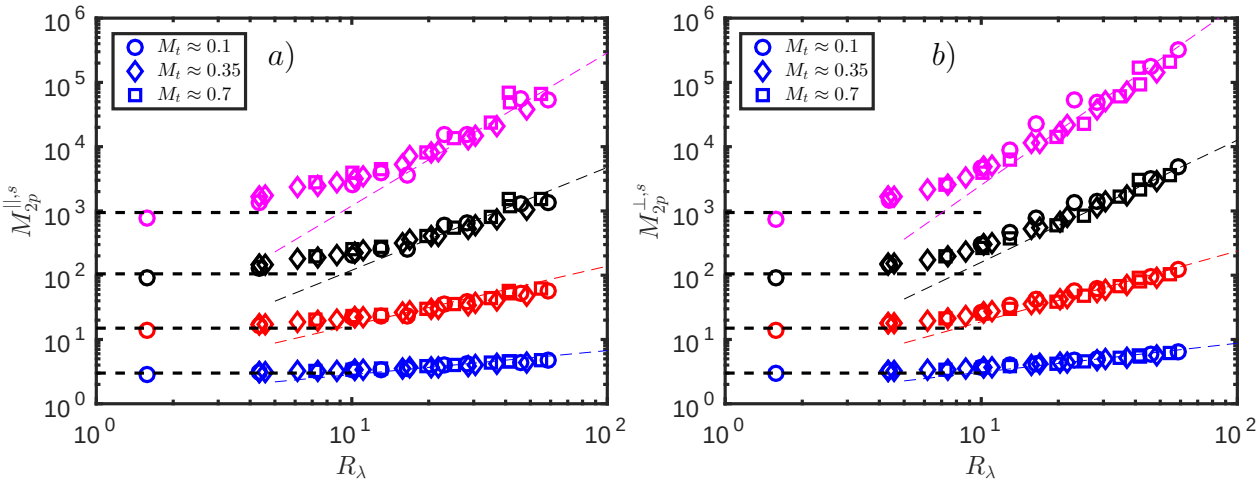

Figure 6.3: Moments of solenoidal velocity gradients. a) Longitudinal gradients for $2p$ =4 (blue), 6 (red),8 (black), 10 (magenta). b) Transverse gradients for same orders as a. The power-laws correspond to respective velocity gradient scaling in incompressible turbulence.

position has been widely used in the literature in order to compare the solenoidal components to incompressible turbulence [89, 88, 69, 68, 69, 71, 72]. In Fig. 6.3, we plot the moments of longitudinal and transverse velocity gradients for the solenoidal velocity only. The solenoidal field is comparable to incompressible turbulence at all orders for both longitudinal and transverse gradients for all M_t. This is consistent with high-M_t results of [71]. Similar to incompressible turbulence, the low-R_λ statistics are Gaussian and transition to scaling beyond $R_\lambda \sim 10$. The scaling exponents are the same as those in incompressible turbulence reported in Section 5. Transverse gradients are again more intermittent than longitudinal gradients. Since the solenoidal field behaves similar to incompressible turbulence, this means it is insensitive to presence of shocks, consistent with recent results [69, 158]. Comparing the point at which the power-laws intersect the Gaussian values, it is also clear that higher order moments transition to scaling at a lower-R_λ than higher order moments do.

6.5 Scaling of dilatational field at high M_t

In the previous sections, we observed that compressibility does not affect the total velocity field for cases with $M_t \leq 0.35$. We've also seen that the solenoidal modes are unaffected by shock

structures at all compressibility levels. Therefore, in our dataset, cases with $M_t \approx 0.7$ have significant dilatational components and they clearly affect the scaling of the total velocity. Therefore, we plot the moments of velocity gradients for the compressible component in Fig. 6.4. Moments for dilatational component are much higher than the solenoidal component. Therefore, intermittency levels are clearly higher for the dilatational field. In the algebraic scaling regime, both longitudinal and transverse moments appear to scale as predicted for Burgers turbulence using the multifractal formalism [157]. The scaling is more robust for $R_\lambda > 20$. In contrast to incompressible turbulence or the solenoidal component in compressible turbulence, both the longitudinal and transverse moments appear to scale similarly. This suggests that scaling is prescribed entirely by shock structures. We also do not observe clear transition from Gaussian state to algebraic scaling in this component. Due to lack of any theoretical guidance, it is not clear whether the low-R_λ asymptote truly is non-Gaussian, as suggested by data in Fig. 6.4, or whether the transition occurs at much lower-R_λ. Within purely Burgers turbulence, a low-R_λ Gaussian asymptote is reported in [157] which is followed by a transition to algebraic scaling. The transition however occurs at R_λ approximately 0.3, much lower than the ones reported here. They also show that the transition range extends up to about $R_\lambda \approx 3$, beyond which algebraic scaling is observed. We are however unable to determine this conclusively in our simulations.

6.6 Conclusions

In this section we have shown that scaling emerges within compressible turbulence at $R_\lambda \sim O(10)$, similar to incompressible flows. We have also shown that the statistics of velocity gradients are largely unaffected by compressibility up to $M_t \approx 0.35$. The scaling of the moments of velocity gradients is comparable to incompressible turbulence. Beyond $M_t \approx 0.35$, a change in scaling of velocity gradients in observed for longitudinal gradients of the total velocity. We decomposed the velocity field into solenoidal and compressible components using Helmholtz decomposition. We showed that the solenoidal field behaves as the incompressible counterpart and is largely unaffected by shock structures, consistent with other studies in literature. We showed that the solenoidal field undergoes a transition from Gaussian statistics at low-R_λ to algebraic scaling beyond $R_\lambda \approx 10$.

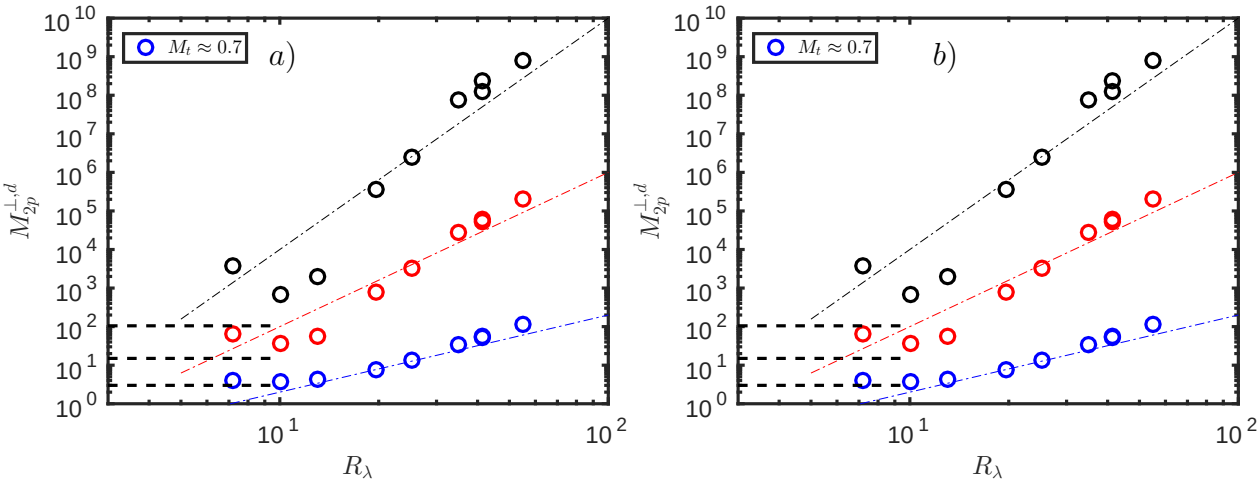

Figure 6.4: Moments of compressible velocity gradients. a) Longitudinal gradients for $2p$ =4 (blue), 6 (red),8 (black). b) Transverse gradients for same orders as a. The power-laws correspond scaling for Burgers turbulence as predicted by multifractal formalism.

Higher order moments transition at a lower-R_λ than low order moments do. This is comparable to the situation in incompressible turbulence. For the dilatational field, we showed that the scaling is largely prescribed by shock structures at high compressibility levels, which are consistent with scaling predicted for Burgers turbulence. Our results show that scaling emerges in compressible turbulence at much lower-R_λ than previously assumed. The scaling is however only evinced in small-scale quantities such as moments of velocity gradients, dissipation or enstrophy. The scaling behavior shown here is consistent with other studies in literature that were achieved at much higher-R_λ and computational effort. The highest-R_λ achieved in our study is comparable to the lowest one reported in literature which attempt to show scaling using structure functions in the inertial range. Our approach has clear advantages. The increase in scaling range is directly proportional to an increase in R_λ and therefore scaling exponents can be measured with improved accuracy at higher-R_λ. This is in clear contrast to the approach of studying scaling in structure functions, where the scaling range is small and increases very slowly with increase in R_λ.

7. CONCLUSIONS AND FUTURE WORK

In this dissertation we studied the statistics of small-scales and extreme events in incompressible and compressible turbulent flows using direct numerical simulations (DNS). Particular focus was on identifying signatures of fully developed turbulence i.e. the features that persist with increasing Reynolds number (R_λ) and the parameter range where they first emerge. The incompressible simulations were performed at box sizes of up to 4096^3 with Taylor Reynolds (R_λ) up to 400. Different large-scale forcing mechanisms were used to establish a statistically stationary state and analyze the effect of forcing statistics on various measurements. The small-scale resolution in the simulations ranges from $k_{max}\eta \approx 3$ (at high-R_λ) up to 60 (at low-R_λ). Simulations with Gaussian forcing had small-scale resolutions an order magnitude larger than the state-of-the art in literature. Compressible turbulence simulations were performed at box sizes of up to 512^3 spanning R_λ between 1 and 60 and turbulent Mach number M_t between 0.1 and 0.75. The resolution in the compressible dataset is at least twice that in the literature, $\eta/\Delta x > 0.8$. The high-resolutions employed in this dissertation provide details about extreme events and small-scales that were not available before. These allowed us to assess the validity of various assumptions and predictions of classical theories and recent theoretical advances.

7.1 Principal Findings

In terms of computational advances for turbulence simulations, we established, for the first time, the resolution criteria for measuring statistics of order up to 10 in compressible turbulence simulations using compact finite differences. We showed that longitudinal gradients require at least twice the resolution $(\eta/\Delta x \approx 1.6)$ than is required for transverse gradients $(\eta/\Delta x \approx 0.8)$ of the velocity field. Higher resolution is required for longitudinal velocity gradients as they are highly affected by non-linear interactions with shock structures in the domain, in addition to intermittency of the velocity field, which is also observed in incompressible turbulent flows. The resolution criteria $\eta/\Delta x \approx 0.5$, used widely in previous studies, can only be used to compute statistical

moments of fluctuating quantities up to order 4. The temporal resolution in our simulations was bound by a Courant number of 0.3. We found this to be an important requirement for improving convergence at a given spatial resolution. However, the high resolution requirement prescribed here may be relaxed by using other schemes such as WENO where shock structures and extreme dissipation events are handled differently. This may however affect the nature and statistics of small scales and must be verified.

In section 3, we analyzed the temporal behavior of spectral transfer and energy in incompressible homogeneous isotropic turbulence that result from low-wavenumber forcing for $R_\lambda \approx 1$ to 400. We found that fluctuations in the spectral quantities were qualitatively independent of fluctuations in energy input at large-scales Single time statistics showed that fluctuations in energy spectra are an order magnitude smaller in the inertial range but grow rapidly for small scales $(k\eta > 0.3)$. The fluctuations in the transfer spectra were found to be an order magnitude larger than the mean in inertial range and become smaller with increase in wavenumber. We also showed that the energy transfer in inertial range is an imbalance between oscillating fluxes that vary in time at a given wavenumber. The fast modes, that are instantaneously felt across all wavenumbers, are signatures of significant non-local interactions in the energy transfer at a given scale in the inertial range. Their effect is similar to reducing the R_λ, where a separation between scales is absent. They appear to completely hide the local transfers which are only revealed in the slow modes at $R_\lambda \geq 90$. The scaling of fast fluctuations was shown to be consistent with recently proposed non-equilibrium corrections to spectral quantities in turbulent flows. Fluctuations in the far dissipation range $(k\eta > 3)$ were independent of the inertial range and become increasingly so with increase in R_λ. We found that the fast fluctuations emerged for $R_\lambda > 10$ and were completely synchronized in time across all wavenumbers in far dissipation range, albeit still uncorrelated with large scales. These results are important in modelling the dynamic interactions across scales, which are often assumed to be highly local, in low-fidelity simulation and modelling approaches. For example, equilbrium Smagorinsky models in large eddy simulations (LES) are unable to capture the non-equilbrium fluctuations discussed in this section and often no time-lag is assumed for energy input

at large-scales and dissipation at small scales which may lead to grossly incorrect prediction of small-scale behavior such as subgrid scale stresses.

In section 4, we studied the time-averaged spectra of energy across scales up to $R_\lambda \approx 1000$. In the earlier section we showed that disparate scales can dynamically interact in incompressible turbulence and therefore affect small scales. An important consequence of the widely assumed cascade scenario is the complete similarity (meaning R_λ independent) of dissipation scales in the energy spectrum. In this section we showed this conclusion is an artifact of limited resolution and Reynolds number range. We demonstrate a systematic R_λ dependence of all resolved scales in the energy spectrum up to $R_\lambda \sim 100$. This has since been verified in experiments and simulations at much higher-R_λ [159]. We showed that the predicted exponential roll-off in the dissipation range of the spectrum is not unique across all wavenumbers. Near dissipation range ($0.13 \leq k\eta \leq 3$) had different coefficients than far dissipation range ($\eta > 6$). The proposed form is not predicted by any classical theories. The second exponential has been proposed but we showed that it was realized at much higher wavenumbers than assumed. The multifractal scaling, which relaxes global invariance in favor of local invariance, accounted for a better collapse in the near dissipation range. However, it too does not collapse the spectra in far dissipation range. We note that the complicated spectrum shape emerges for $R_\lambda > 20$ and persists at all R_λ measured in this dissertation and studies from other groups with R_λ up to an order magnitude larger than the ones considered here. Therefore, the bi-exponential behavior is a feature of high-R_λ turbulence and it is first observed at $R_\lambda \sim O(10)$.

In section 5, we complement the spectral view of turbulence with measurements in physical space. This allowed us to properly quantify the statistics of extreme fluctuations in fluid turbulence. We did so by systematically studying the moments of velocity gradients up to order 10 with different large scale forcing mechanisms. We showed that for a given quantity, e.g. moments of longitudinal velocity gradients, the scaling exponents are independent of large scale forcing. We also showed that scaling is established at $R_\lambda \sim O(10)$, in contrast with classical theories which require the establishment of a wide inertial-range. The R_λ considered in this study are not large enough to have any indication of the existence of an inertial range. We also showed that at low-R_λ,

the statistics are Gaussian regardless of the forcing statistics. This allowed us to verify the general applicability of the recently proposed theory by Yakhot & Donzis [60, 33] which predicts a phase transition from Gaussian statistics to algebraic scaling, like the one observed here. We also showed that the scaling exponents are different for different quantities e.g. longitudinal and transverse gradients scale differently. We proposed that the transition-R_λ predicted by Yakhot & Donzis be different for different quantities and in-fact verified that this modification is able to predict scaling of transverse gradients as well. We also verified an important feature of the theory that high-order moments of velocity gradients transition to algebraic scaling observed in fully developed turbulence at a lower-R_λ than low-order statistics do. This means that turbulence is fully developed in the most extreme fluctuations first, a result with important implications for developing low-order turbulence models. An important consequence of these results is that high-R_λ features can be studied using data from well resolved low to moderate R_λ which are computationally several order magnitudes cheaper.

In section 6, we studied the transition from Gaussian to algebraic scaling as proposed by Yakhot & Donzis within homogeneous and isotropic compressible turbulence. We showed that the statistics of velocity gradients up to order 10 transition from a universal Gaussian state at low-R_λ to an algebraic scaling beyond $R_\lambda \approx 10$. We showed that the scaling of longitudinal velocity gradients is affected by shock-like structures distributed in the domain and therefore the scaling exponents are dependent on M_t for flows with $M_t > 0.35$. This is consistent with previous literature which established that compressibility effects become much stronger beyond $M_t \approx 0.3-0.4$. Below this limit, the compressible flow component is largely determined by solenoidal motions. We also showed that the scaling of transverse velocity gradients is independent of compressibility level and also exhibit a transition to this scaling from a low-R_λ Gaussian state. We also studied the scaling of the solenoidal and compressible components of the velocity field separately using Helmholtz decomposition. We showed that the solenoidal field transitions and exhibits scaling which is consistent with incompressible turbulence regardless of M_t. The solenoidal field is therefore insensitive to the presence of shocks. The dilatational motions at high M_t were shown to scale similar to Burgers

turbulence therefore the scaling of velocity increments of compressible component of velocity in the inertial range should exhibit saturation of scaling exponents. This has been observed in recent work from other groups [71, 72]. We have however shown that similar to incompressible turbulence, scaling emerges at very low-R_λ in compressible turbulence as well. In fact, the highest-R_λ considered in this study is comparable to the lowest-R_λ in previous studies and is an order magnitude smaller than the highest-R_λ considered in other studies.

7.2 Summary

In summary, we have used highly resolved direct numerical simulations to recognize features of high-R_λ fully developed turbulence and characterize the R_λ at which they emerge. We showed that the classical Richardson-Kolmogorov cascade scenario is only exhibited by slow fluctuations in energy transfer across scales. An important consequence of the classical cascade picture is that energy transfers are local in scale. We, however, observed that the total transfer is dominated by fast components which are instantaneously felt across all scales. We speculated that these modes are signatures of non-local interactions. The fast modes emerge for flows with $R_\lambda \geq 10$ and are fully synchronized with each other in the dissipation range. An important consequence of a local cascade is the complete self-similarity of small scales characterized using a global scale invariance. In the past, this had been supported by the collapse of energy spectrum of turbulent velocity fluctuations in dissipation range when the wavenumbers are normalized by the Kolmogorov scale η. We have however shown that this conclusion is not valid. The energy spectrum in the dissipation range exhibits a R_λ dependent behavior which is predicted by multifractal formalism by replacing the global scale invariance with a local scale invariance. Therefore, a multiscale behavior was observed even at the level of energy spectrum, a second order statistical moment of turbulent fluctuations. Non-local interactions have also been proposed as an explanation for so-called anomalous scaling of high-order statistics in fluid turbulence [160, 161]. Laval *et al.* demonstrated that the presence of non-local interactions enhances the spectrum at small scales, in comparison to purely local interactions, and lead to increased probability of extreme fluctuations in the system. Our results, for energy spectrum and higher-order statistics, are qualitatively consistent with their results.

In order to characterize extreme events and high-order statistics of velocity field in fluid turbulence, we studied statistical moments of turbulent velocity fluctuations in physical space. Previous evidence of anomalous scaling in incompressible turbulence was found in scaling of structure functions in the inertial range, a feature of high-R_λ turbulence. Intermittency was therefore attributed to high-R_λ only. Here we have shown that this view is misplaced and is a consequence of the use of structure functions. In this work, we demonstrated that small scale intermittency emerges at $R_\lambda \sim O(10)$ in velocity gradients. The scaling of velocity gradients at these low-R_λ has also been shown to predict the scaling exponents in the inertial range, which exists only at much higher-R_λ [33, 16]. Therefore we have shown that intermittency emerges at R_λ more than an order magnitude smaller than those required to observe an inertial range.

The accuracy of the measurements of scaling exponents critically depend on the width of the scaling regime. Therefore, it is advisable to use statistics of velocity gradients (or dissipation, enstrophy) to measure them as the scaling width increases linearly with increase in R_λ. This is unlike measurements made using structure functions where the scaling range is small and the increase in width of scaling regime is extremely slow with increase in R_λ [26]. We have also shown that at $R_\lambda \ll 10$, the velocity gradients exhibit Gaussian statistics independent of large-scale forcing in periodic domains. There is some early evidence from Rayleigh-Bernard turbulence that the low-R_λ Gaussian asymptote may not fully generalize to flows with boundaries [144]. However, the scaling exponents measured in Rayleigh-Bernard turbulence beyond the transition-R_λ are consistent with those measured in period domains. More complex quantities dependent on velocity gradients, e.g. dissipation and enstrophy, exhibit statistics dependent on the Gaussian state in the low-R_λ regime. We also showed that similar conclusions are valid in compressible turbulence. Intermittency in the gradients of solenoidal velocity field, up to order 10, of compressible turbulence is fully described by incompressible turbulence. At high-M_t, statistics of the gradients of dilatational velocity field exhibit scaling consistent with Burgers turbulence, which is dominated by randomly distributed shock structures. Others have also shown that similar transitions from a low parameter Gaussian state to algebraic scaling is exhibited by Burgers turbulence [157] and passive scalar mixing [156].

We conclude by noting that when all the results in this thesis are taken together and in perspective, a new path towards understanding and modelling complex systems emerges. We speculate that the transition to algebraic scaling from a Gaussian regime may be a general feature of spatio-temporal chaotic systems that exhibit intermittent statistics at very high parameter values X with $X = R_\lambda, Pe$ etc. dependent on the dissipative mechanism in the system. This has important implications for modelling extreme events in low-order models of turbulence. Thus far, most low-order models would seek accurate scaling in low-order statistics only. Our results show that it must be possible to develop models for very high-order statistics and their proper rescaling should provide accurate results at low-orders. This of course is a novel direction in turbulence modelling and is yet to be explored.

7.3 Future Directions

The scaling of intermittency is an active field of research in turbulence. Our work and that of others has helped establish transition to scaling, scaling exponents of various quantities and their agreement with different theories. However, multiple theories often make similar predictions up to a given order. For example, scaling exponents of moments of velocity gradients predicted by Yakhot & Donzis are measurably the same as that predicted by multifractal formalism up to order 14. Simply increasing the resolution of simulations is not enough to reliably measure exponents at these high-orders. New statisitcal measurement methods that appreciate the large variance in high-order moments need to be developed. These will allow us to to discriminate and assess the accuracy of different theories. This is especially important now as the physics and underlying dynamics of turbulence are vastly different in Yakhot's theory and that of multifractal formalism.

Yakhot & Donzis predict that the transition-R_λ and scaling exponents are universal. We have verified this but with important caveats. First, the transition-R_λ was measured with an unknown multiplicative factor, which may depend on order of the moment and forcing, although the scaling exponents across forcings are within statistical bounds. A direct measurement of the transition-R_λ will alleviate this ambiguity and provide more confidence in the theory. Second, the universal scaling and transition-R_λ are specific to a quantity. If different quantities scale differently and a

clear relationship between the two is not available, one needs to address the notion of universality itself and perhaps introduce the concept of universality classes in turbulence. We have empirically identified the transition-R_λ for transverse gradients and shown that its use allows the calculation of accurate scaling exponents as well. It is however not clear why a difference between longitudinal and transverse fields must exist, although we have proposed a possible explanation based on pressure effects. This has of course been discussed before, but needs to be reassessed in view of the new theory. The theory also assumes stirring at the large scales. Energy input in real world flows is however not limited to the largest scales. The effect of broadband forcing and forcing at small scales on intermittency, scaling and universality must be addressed in the future. This is important for guiding the development of low-order models for realistic flows and enabling the application of this theory to flows with multi-physics effects such as chemical reactions at small-scales, multi-scale heat release and atmospheric turbulence.

This dissertation and recent work has largely focussed on questions of scaling and their measurement in turbulent flows. The new direction explored in this dissertation and proposed by Yakhot & Donzis opens new questions about the transition to turbulence, beyond the traditional method of analyzing the growth of specific flow instabilities. The details and the physics of the transition from Gaussian to algebraic scaling were not analyzed in this work and remain unknown at this stage. This phase of the flow needs to studied in further detail. It can potentially answer important questions about the origins of intermittency. A parallel line of research has actively been studying the transition to turbulence in pipe flows and places the transition within directed percolation class [147, 15] in non-equilibrium statistical mechanics. Although qualitatively, and in lay language, the transition in Yakhot & Donzis and this class of flows is similar and perhaps describing the same physics. A connection, or lack thereof, between the two lines of research is an important problem to pursue. If a connection exists, it may reveal the physics of transition within velocity gradients.

Within compressible flows, we have only explored the emergence of scaling in solenoidally forced turbulent flows. Real world flows can however have significant dilatational components

in turbulent production. It is therefore important to characterize the effects of mixed solenoidal-dilatational forcing on the universality and emergence of scaling in compressible turbulence. Extreme events in turbulent flows can have significant effects on multi-physics processes such as bubble breakup, clustering of particles, rates of chemical reactions etc. Quantifying the effects of intermittency on these processes is an interesting and important topic for future research.

This dissertation and a significant amount of literature on intermittency and extreme events has focussed on its statistical nature. Applications however also need important information about how the dynamics evolve from state to state. The temporal dynamics of extreme events in turbulence is therefore an important problem that remains unexplored. DNS will be of particular help with this direction.

We conclude this work with a positive note regarding immediate and long-term prospects in computational approaches and their utility in understanding turbulence physics. Significant advances have occurred in computing within the past few decades and we are less than a year away from exascale computing. Therefore, a dearth of computational power is available. The new direction of low-parameter simulations in this work provides an excellent opportunity to study asymptotic regimes in turbulence and complex systems. The current generation of computing itself provides enough resources to improve resolution for flows such as the ones described here and also those with complicated geometry and physics (such as internal flows, combustion, magnetic fields etc.). These simulations may be enough to characterize the physics and allow us to understand the physics at realistic conditions. Recent advances in data-driven computing and its application to parameterization of extreme events in complex systems may allow us to use the high-resolution simulations to further reduce and (or) characterize uncertainty in simulation outputs furthering their wide-spread adoption.

REFERENCES

[1] D.A. Donzis and K.R. Sreenivasan. The bottleneck effect and the kolmogorov constant in isotropic turbulence. *Journal of Fluid Mechanics*, 657:171–188, 2010.

[2] U. Frisch. *Turbulence: the legacy of AN Kolmogorov*. Cambridge university press, 1995.

[3] D.O. Martinez, S. Chen, G.D. Doolen, R.H. Kraichnan, L-P. Wang, and Y. Zhou. Energy spectrum in the dissipation range of fluid turbulence. *Journal of Plasma Physics*, 57(1):195–201, 1997.

[4] B.A. Grierson, W.X. Wang, S. Ethier, G.M. Staebler, D.J. Battaglia, J.A. Boedo, J.S. DeGrassie, and W.M. Solomon. Main-ion intrinsic toroidal rotation profile driven by residual stress torque from ion temperature gradient turbulence in the diii-d tokamak. *Physical Review Letters*, 118(1):015002, 2017.

[5] M. M-M. Low and R.S. Klessen. Control of star formation by supersonic turbulence. *Reviews of Modern Physics*, 76(1):125, 2004.

[6] C.A. Clayson and L. Kantha. On turbulence and mixing in the free atmosphere inferred from high-resolution soundings. *Journal of Atmospheric and Oceanic Technology*, 25(6):833–852, 2008.

[7] S. Khurshid and D.A. Donzis. Decaying compressible turbulence with thermal nonequilibrium. *Physics of Fluids*, 31(1):015103, 2019.

[8] M. Nelkin. In what sense is turbulence an unsolved problem. *Science*, 255:566–570, 1992.

[9] L. Euler. Principes généraux du mouvement des fluides. *Mémoires de l'Académie des Sciences de Berlin*, pages 274–315, 1757.

[10] C.L.M.H. Navier. Mémoire sur les lois du mouvement des fluides. *Mémoires de l'Académie Royale des Sciences de l'Institut de France*, 6(1823):389–440, 1823.

[11] G.G. Stokes. On the effect of the internal friction of fluids on the motion of pendulums. 1851.

[12] P. Constantin and C. Foias. *Navier-Stokes equations*. University of Chicago Press, 1988.

[13] C.L. Fefferman. Existence and smoothness of the navier-stokes equation. *The Millennium Prize Problems*, 2006.

[14] O. Reynolds. Iv. on the dynamical theory of incompressible viscous fluids and the determination of the criterion. *Philosophical Transactions of the Royal Society of London.(a.)*, (186):123–164, 1895.

[15] N. Goldenfeld and H-Y. Shih. Turbulence as a problem in non-equilibrium statistical mechanics. *Journal of Statistical Physics*, 167(3-4):575–594, 2017.

[16] K.R. Sreenivasan and V. Yakhot. Dynamics of three-dimensional turbulence from navier-stokes equations. *arXiv preprint arXiv:2106.01293*, 2021.

[17] M. Farge. Wavelet transforms and their applications to turbulence. *Annual Review of Fluid Mechanics*, 24(1):395–458, 1992.

[18] P. Holmes, J.L. Lumley, G. Berkooz, and C.W. Rowley. *Turbulence, coherent structures, dynamical systems and symmetry*. Cambridge University Press, 2012.

[19] A. N. Kolmogorov. Local structure of turbulence in an incompressible fluid for very large reynolds numbers. *Doklady Akademiia Nauk SSSR*, 30:299–303, 1941.

[20] G.I. Taylor. Statistical theory of turbulenc. *Proceedings of the Royal Society of London. Series A-Mathematical and Physical Sciences*, 151(873):421–444, 1935.

[21] K. R. Sreenivasan. On the universality of the kolmogorov constant. *Physics of Fluids*, 7(11):2778–2784, 1995.

[22] C. Domb. *Phase transitions and critical phenomena*. Elsevier, 2000.

[23] A. S. Monin and A. M. Yaglom. *Statistical Fluid Mechanics*, volume 2. MIT Press, 1975.

[24] R.M. Kerr. Higher-order derivative correlations and the alignment of small-scale structures in isotropic numerical turbulence. *Journal of Fluid Mechanics*, 153:31–58, 1985.

[25] K.R. Sreenivasan and R.A. Antonia. The phenomenology of small-scale turbulence. *Annual Review of Fluid Mechanics*, 29:435–472, 1997.

[26] K.P. Iyer, K.R. Sreenivasan, and P.K. Yeung. Scaling exponents saturate in three-dimensional isotropic turbulence. *Physical Review Fluids*, 5(5):054605, 2020.

[27] R.A. Antonia, S.L. Tang, L. Djenidi, and Y. Zhou. Finite reynolds number effect and the 4/5 law. *Physical Review Fluids*, 4(8):084602, 2019.

[28] D. A. Donzis, K. R. Sreenivasan, and P. K. Yeung. Scalar dissipation rate and dissipative anomaly in isotropic turbulence. *Journal of Fluid Mechanics*, 532:199–216, 2005.

[29] W.D. Mccomb, A. Berera, S.R. Yoffe, and M.F. Linkmann. Energy transfer and dissipation in forced isotropic turbulence. *Physical Review E*, 91(043013), 2015.

[30] T. Ishihara, T. Gotoh, and Y. Kaneda. Study of high-Reynolds number isotropic turbulence by direct numerical simulation. *Annual Review of Fluid Mechanics*, 41:165–180, 2009.

[31] C.R. Doering and C. Foias. Energy dissipation in body-forced turbulence. *Journal of Fluid Mechanics*, 467:289–306, 2002.

[32] K.R. Sreenivasan. An update on the energy dissipation rate in isotropic turbulence. *Physics of Fluids*, 10:528–529, 1998.

[33] V. Yakhot and D.A. Donzis. Anomalous exponents in strong turbulence. *Physica D*, 2018.

[34] J.A. Domaradzki. Analysis of energy-transfer in direct numerical simulations of isotropic turbulence. *Physics of Fluids*, 31:2747–2749, 1988.

[35] J.A. Domaradzki and R.S. Rogallo. Local energy-transfer and nonlocal interactions in homogeneous, isotropic turbulence. *Physics of Fluids*, 2:413–426, 1990.

[36] P.K. Yeung and J.G. Brasseur. The response of isotropic turbulence to isotropic and anisotropic forcing at the large scales. *Physics of Fluids*, 3:884–897, 1991.

[37] K. Ohkitani and S. Kida. Triad interactions in a forced turbulence. *Physics of Fluids*, 4:794–802, 1992.

[38] J.A. Domaradzki and D. Carati. An analysis of the energy transfer and the locality of nonlinear interactions in turbulence. *Physics of Fluids*, 19, 2007.

[39] M. Kholmyansky and A. Tsinober. Kolmogorov 4/5 law, nonlocality, and sweeping decorrelation hypothesis. *Physics of Fluids*, 20(4):041704, 2008.

[40] J.A. Domaradzki, B. Teaca, and D. Carati. Locality properties of the energy flux in turbulence. *Physics of Fluids*, 21, 2009.

[41] G. Falkovich. Bottleneck phenomenon in developed turbulence. *Physics of Fluids*, 6:1411–1414, 1994.

[42] M.K. Verma and D.A. Donzis. Energy transfer and bottleneck effect in turbulence. *Journal of Physics A*, 40(16):4401–4412, 2007.

[43] P.D. Mininni, A. Alexakis, and A. Pouquet. Nonlocal interactions in hydrodynamic turbulence at high Reynolds numbers: The slow emergence of scaling laws. *Physical Review E*, 77:036306, 2008.

[44] D.A. Donzis and K.R. Sreenivasan. The bottleneck effect and the Kolmogorov constant in isotropic turbulence. *Journal of Fluid Mechanics*, 657:171–188, 2010.

[45] C. Küchler, G. Bewley, and E. Bodenschatz. Experimental study of the bottleneck in fully developed turbulence. *Journal of Statistical Physics*, 2019.

[46] U. Frisch. *Turbulence*. Cambridge University Press, 1995.

[47] A.N. Kolmogorov. A refinement of previous hypotheses concerning the local structure of turbulence in a viscous incompressible fluid at high reynolds number. *Journal of Fluid Mechanics*, 13(1):82–85, 1962.

[48] E. Leveque and Z-S. She. Viscous effects on inertial range scalings in a dynamical model of turbulence. *Physical Review Letters*, 75(14):2690, 1995.

[49] C. Meneveau and K.R. Sreenivasan. Simple multifractal cascade model for fully developed turbulence. *Physical Review Letters*, 59(13):1424, 1987.

[50] M.S. Borgas. A comparison of intermittency models in turbulence. *Physics of Fluids A: Fluid Dynamics*, 4(9):2055–2061, 1992.

[51] P.K. Yeung and K. Ravikumar. Advancing understanding of turbulence through extreme-scale computation: Intermittency and simulations at large problem sizes. *Physical Review Fluids*, 5(11):110517, 2020.

[52] J. Schumacher, K.R. Sreenivasan, and V. Yakhot. Asymptotic exponents from low-Reynolds-number flows. *New Journal of Physics*, 9:89, 2007.

[53] V. Yakhot. Mean-field approximation and a small parameter in turbulence theory. *Physical Review E*, 63, 2001.

[54] V. Yakhot. Dissipation-scale fluctuations and mixing transition in turbulent flows. *Journal of Fluid Mechanics*, 606:325–337, 2008.

[55] V. Yakhot. Probability densities in strong turbulence. *Physica D*, 215:166–174, 2006.

[56] V Yakhot and K.R. Sreenivasan. Towards a dynamical theory of multifractals in turbulence. *Physica A*, 343:147–155, 2004.

[57] M. Nelkin. Multifractal scaling of velocity derivatives in turbulence. *Physical Review A*, 42:7226–7229, 1990.

[58] V. Yakhot and K.R. Sreenivasan. Anomalous scaling of structure functions and dynamic constraints on turbulence simulations. *Journal of Statistical Physics*, 121(5):823–841, 2005.

[59] V. Yakhot. Reynolds number of transition and self-organized criticality of strong turbulence. *Physical Review E*, 90(4):043019, 2014.

[60] V. Yakhot and D.A. Donzis. Emergence of multiscaling in a random-force stirred fluid. *Physical Review Letters*, 119(4):044501, 2017.

[61] P.K. Yeung, K.R. Sreenivasan, and S.B. Pope. Effects of finite spatial and temporal resolution in direct numerical simulations of incompressible isotropic turbulence. *Physical Review Fluids*, 3(6):064603, 2018.

[62] R. Benzi, L. Biferale, R.T. Fisher, L.P. Kadanoff, D.Q. Lamb, and F. Toschi. Intermittency and universality in fully developed inviscid and weakly compressible turbulent flows. *Physical Review Letters*, 100(23), 2008.

[63] A.G. Kritsuk, M.L. Norman, P. Padoan, and R. Wagner. The statistics of supersonic isothermal turbulence. *The Astrophysical Journal*, 665(1):416–431, 2007.

[64] W. Schmidt, C. Federrath, and R. Klessen. Is the Scaling of Supersonic Turbulence Universal? *Physical Review Letters*, 101(19), 2008.

[65] R.D.W. Bowersox. Extension of equilibrium turbulent heat flux models to high-speed shear flows. *Journal of Fluid Mechanics*, 633:61–70, 2009.

[66] I.W. Ekoto, R.D.W. Bowersox, T. Beutner, and L. Goss. Response of supersonic turbulent boundary layers to local and global mechanical distortions. *Journal of Fluid Mechanics*, 630:225–265, 2009.

[67] S. Boldyrev. Kolmogorov-burgers model for star-forming turbulence. *The Astrophysical Journal*, 569(2):841, 2002.

[68] Panickacheril J.J., D.A. Donzis, and K.R. Sreenivasan. Does dissipative anomaly hold for compressible turbulence? *Journal of Fluid Mechanics*, 920:A20, 2021.

[69] J.P. John, D.A. Donzis, and K.R. Sreenivasan. Solenoidal scaling laws for compressible mixing. *Physical Review Letters*, 123:224501, 2019.

[70] R. Samtaney, D.I. Pullin, and B. Kosović. Direct numerical simulation of decaying compressible turbulence and shocklet statistics. *Physics of Fluids*, 13(5):1415–1430, 2001.

[71] J. Wang, Y. Shi, L-P. Wang, Z. Xiao, X. T. He, and S. Chen. Scaling and statistics in three-dimensional compressible turbulence. *Physical Review Letters*, 108(21), 2012.

[72] J. Wang, T. Gotoh, and T. Watanabe. Scaling and intermittency in compressible isotropic turbulence. *Physical Review Fluids*, 2(5), 2017.

[73] J. Wang, T. Gotoh, and T. Watanabe. Spectra and statistics in compressible isotropic turbulence. *Physical Review Fluids*, 2(1), 2017.

[74] J. Wang, T. Gotoh, and T. Watanabe. Shocklet statistics in compressible isotropic turbulence. *Physical Review Fluids*, 2(2), 2017.

[75] S. Jagannathan. *Reynolds and mach number scaling in stationary compressible turbulence using massively parallel high resolution direct numerical simulations*. PhD thesis, 2014.

[76] D.A. Donzis. *Scaling of turbulence and turbulent mixing using Terascale numerical simulations*. PhD thesis, 2007.

[77] R.S. Rogallo. Numerical experiments in homogeneous turbulence. page NASA Tech. Memo. 81315, 1981.

[78] S.A. Orszag. Numerical methods for the simulation of turbulence. *The Physics of Fluids*, 12(12):II–250, 1969.

[79] S.A. Orszag and G.S. Patterson. Numerical simulation of 3-dimensional homogeneous isotropic turbulence. *Physical Review Letters*, 28(2):76–&, 1972.

[80] G.S. Patterson and S.A. Orszag. Spectral calculations of isotropic turbulence - effecient removal of aliasing interactions. *Physics of Fluids*, 14(11):2538–&, 1971.

[81] V. Eswaran and S.B. Pope. An examination of forcing in direct numerical simulations of turbulence. *Computers and Fluids*, 16(3):257–278, 1988.

[82] D.A. Donzis and P.K. Yeung. Resolution effects and scaling in numerical simulations of passive scalar mixing in turbulence. *Physica D*, 239(14):1278–1287, 2010.

[83] T. Aoyama, T. Ishihara, Y. Kaneda, M. Yokokawa, K. Itakura, and A. Un. Statistics of energy transfer in high-resolution direct numerical simulation of turbulence in a periodic box. *Journal of Physical Society of Japan*, 74:3202–3212, 2005.

[84] Y. Kaneda and T. Ishihara. High-resolution direct numerical simulation of turbulence. *Journal of Turbulence*, 7(20):1–17, 2006.

[85] T. Ishihara, K. Morishita, M. Yokokawa, A. Uno, and Y. Kaneda. Energy spectrum in high-resolution direct numerical simulations of turbulence. *Physical Review Fluids*, 1, 2016.

[86] C. Rosales and C. Meneveau. Linear forcing in numerical simulations of isotropic turbulence: Physical space implementations and convergence properties. *Physics of Fluids*, 17:095106, 2005.

[87] P.K. Yeung, X.M. Zhai, K.R. Sreenivasan, C. Grebogi, R. Shaw, and H.L. Swinney. Extreme events in computational turbulence. *Proceedings of the National Academy of Sciences*, 112(41), 2015.

[88] D.A. Donzis and S. Jagannathan. Fluctuations of thermodynamic variables in stationary compressible turbulence. *Journal of Fluid Mechanics*, 733:221–244, 2013.

[89] S. Jagannathan and D.A. Donzis. Reynolds and Mach number scaling in solenoidally-forced compressible turbulence using high-resolution direct numerical simulations. *Journal of Fluid Mechanics*, 789:669–707, 2016.

[90] J.G.M. Eggels, F. Unger, M.H. Weiss, J. Westerweel, R.J. Adrian, R. Friedrich, and F. T. M. Nieuwstadt. Fully developed turbulent pipe flow: a comparison between direct numerical simulation and experiment. *Journal of Fluid Mechanics*, 268:175–210, 1994.

[91] D.A. Donzis, P.K. Yeung, and K.R. Sreenivasan. Dissipation and enstrophy in isotropic turbulence: scaling and resolution effects in direct numerical simulations. *Physics of Fluids*, 20:045108, 2008.

[92] J.P. Monty and M.S. Chong. Turbulent channel flow: comparison of streamwise velocity data from experiments and direct numerical simulation. *Journal of Fluid Mechanics*, 633:461–474, 2009.

[93] D.A. Donzis and P.K. Yeung. Resolution effects and scaling in numerical simulations of passive scalar mixing in turbulence. *Physica D*, 239:1278–1287, 2010.

[94] S. Khurshid, D.A. Donzis, and K.R. Sreenivasan. Energy spectrum in the dissipation range. *Physical Review Fluids*, 3:082601, 2018.

[95] H. Tennekes and J.L. Lumley. *A First Course in Turbulence*. The MIT Press, 1972.

[96] J. A. Domaradzki and D. Carati. A comparison of spectral sharp and smooth filters in the analysis of nonlinear interactions and energy transfer in turbulence. *Physics of Fluids*, 19(8):085111, 2007.

[97] F. Waleffe. The nature of triad interactions in homogeneous turbulence. *Physics of Fluids A: Fluid Dynamics*, 4:350, 1992.

[98] L.P. Wang, S. Chen, J.G. Brasseur, and J.C. Wyngaard. Examination of hypotheses in the Kolmogorov refined turbulence theory through high-resolution simulations .1. Velocity field. *Journal of Fluid Mechanics.*, 309:113–156, 1996.

[99] L.P. Wang, S. Chen, and J.G. Brasseur. Examination of hypotheses in the Kolmogorov refined turbulence theory through high-resolution simulations. Part 2. Passive scalar field. *Journal of Fluid Mechanics*, 400:163–197, 1999.

[100] V. Eswaran and S. B. Pope. An examination of forcing in direct numerical simulations of turbulence. *Computers and Fluids*, 16:257–278, 1988.

[101] P.K. Yeung, D.A. Donzis, and K.R. Sreenivasan. High-Reynolds-number simulation of turbulent mixing. *Physics of Fluids*, 17:081703, 2005.

[102] D.A. Donzis and K.R. Sreenivasan. Short-term forecasts and scaling of intense events in turbulence. *Journal of Fluid Mechanics*, 647:13–26, 2010.

[103] W.J.T. Bos and R. Rubinstein. Dissipation in unsteady turbulence. *Physical Review Fluids*, 2:022601, 2017.

[104] A. Yoshizawa. Nonequilibrium effect of the turbulent-energy-production process on the inertial-range energy spectrum. *Physical Review E*, 49, 1994.

[105] K. Horiuti and T. Tamaki. Nonequilibrium energy spectrum in the subgrid-scale one-equation model in large-eddy simulation. *Physics of Fluids*, 25:125104, 2013.

[106] J.G. Brasseur. Comments on the kolmogorov hypotheses of isotropy in the small scales. *AIAA Paper*, (91-0230), 1991.

[107] J.G. Brasseur and C-H. Wei. Interscale dynamics and local isotropy in high reynolds number turbulence within triadic interactions. *Physics of Fluids*, 6:842, 1994.

[108] C.W. Van Atta and J.C. Wyngaard. On higher-order spectra of turbulence. *Journal of Fluid Mechanics*, 72:673–694, 1975.

[109] M. Nelkin and M. Tabor. Time correlations and random sweeping in isotropic turbulence. *Physics of Fluids A: Fluid Dynamics*, 2:81–83, 1990.

[110] A. A. Praskovsky, E. B. Gledzer, M. Y. Karyakin, and Y. Zhou. The sweeping decorrelation hypothesis and energy–inertial scale interaction in high reynolds number flows. *Journal of Fluid Mechanics*, 248, 1993.

[111] R. H. Kraichnan. Eulerian and Lagrangian renormalization in turbulence theory. *Journal of Fluid Mechanics*, 83:349–374, 1977.

[112] H. Tennekes and J.L. Lumley. *A first course in turbulence*. MIT press, 1972.

[113] J.L. Lumley. Some comments on turbulence. *Physics of Fluids A: Fluid Dynamics*, 4:203–211, 1992.

[114] W.J.T. Bos, L. Shao, and J.P. Bertoglio. Spectral imbalance and the normalized dissipation rate of turbulence. *Physics of Fluids*, 19:045101, 2007.

[115] J.I. Cardesa, A. Vela-Martín, S. Dong, and J. Jiménez. The temporal evolution of the energy flux across scales in homogeneous turbulence. *Physics of Fluids*, 27:111702, 2015.

[116] C. Meneveau and T.S. Lund. On the lagrangian nature of the turbulence energy cascade. *Physics of Fluids*, 6:2820–2825, 1994.

[117] Y Tsuji. Intermittency effect on energy spectrum in high-Reynolds number turbulence. *Physics of Fluids*, 16(5):L43–L46, 2004.

[118] S. Chen, G. Doolen, J.R. Herring, R.H. Kraichnan, S.A. Orszag, and Z.S. She. Far-dissipation range of turbulence. *Physical Review Letters*, 70(20):3051, 1993.

[119] J. Schumacher. Sub-kolmogorov-scale fluctuations in fluid turbulence. *European Physical Letters*, 80(5):54001, 2007.

[120] T. Ishihara, T. Gotoh, and Y. Kaneda. Study of high–reynolds number isotropic turbulence by direct numerical simulation. *Annual Review of Fluid Mechanics*, 41:165–180, 2009.

[121] R.H. Kraichnan. The structure of isotropic turbulence at very high reynolds numbers. *Journal of Fluid Mechanics*, 5(4):497–543, 1959.

[122] L. Sirovich, L. Smith, and V. Yakhot. Energy-spectrum of homogeneous and isotropic turbulence in far dissipation range. *Physical Review Letters*, 72(3):344–347, 1994.

[123] Z.-S. She and E. Jackson. On the universal form of energy spectra in fully developed turbulence. *Physics of Fluids*, 5:1526–1528, 1993.

[124] C. Foias, O. Manley, and L. Sirovich. Empirical and stokes eigenfunctions and the far-dissipative turbulent spectrum. *Physics of Fluids A*, 2(3):464–467, 1990.

[125] L.M. Smith and W.C. Reynolds. The dissipation-range spectrum and the velocity-derivative skewness in turbulent flows. *Physics of Fluids A: Fluid Dynamics*, 3(5):992–994, 1991.

[126] O.P. Manley. The dissipation range spectrum. *Physics of Fluids A: Fluid Dynamics*, 4(6):1320–1321, 1992.

[127] K.R. Sreenivasan. On the fine-scale intermittency of turbulence. *Journal of Fluid Mechanics*, 151:81–103, 1985.

[128] S. Chen, G. Doolen, J.R. Herring, R.H. Kraichnan, S.A. Orszag, and Z-S. She. Far-dissipation range of turbulence. *Physical Review Letters*, 70(20):3051–3054, 1993.

[129] T. Ishihara, Y. Kaneda, M. Yokokawa, K. Itakura, and A. Uno. Energy spectrum in the near dissipation range of high resolution direct numerical simulation of turbulence. *Journal of Physical Society of Japan*, 74(5):1464–1471, 2005.

[130] Z-S. She and E. Jackson. On the universal form of energy spectra in fully developed turbulence. *Physics of Fluids A*, 5(7):1526–1528, 1993.

[131] R.H. Kraichnan. The structure of isotropic turbulence at very high Reynolds numbers. *Journal of Fluid Mechanics*, 5:497–543, 1959.

[132] A. Bershadskii. Distributed chaos in the Hamiltonian dynamical systems and isotropic homogeneous turbulence. 2018.

[133] W. Dobler, N.E.L. Haugen, T.A. Yousef, and A. Brandenburg. Bottleneck effect in three-dimensional turbulence simulations. *Physical Review E*, 68(2):026304, 2003.

[134] R.H. Kraichnan. Intermittency in the very small scales of turbulence. *Physics of Fluids*, 10(9):2080–2082, 1967.

[135] G.K. Batchelor. *The theory of homogeneous turbulence*. Cambridge university press, 1953.

[136] A. N. Kolmogorov. A refinement of previous hypotheses concerning the local structure of turbulence in a viscous incompressible fluid at high reynolds number. *Journal Fluid Mechanics*, 13:82–85, 1962.

[137] Z-S. She and E. Leveque. Universal scaling laws in fully developed turbulence. *Physical Review Letters*, 72:336–339, 1994.

[138] R. Benzi, S. Ciliberto, R. Tripiccione, C. Baudet, F. Massaioli, and S. Succi. Extended self-similarity in turbulent flows. *Physical Review E*, 48:R29–R32, 1993.

[139] R. Benzi, S. Ciliberto, C. Baudet, and G.R. Chavarria. On the scaling of three-dimensional homogeneous and isotropic turbulence. *Physica D*, 80:385–398, 1995.

[140] K.P. Iyer, K.R. Sreenivasan, and P.K. Yeung. Reynolds number scaling of velocity increments in isotropic turbulence. *Physical Review E*, 95(2), 2017.

[141] J. Schumacher, J.D. Scheel, D. Krasnov, D.A. Donzis, V. Yakhot, and K.R. Sreenivasan. Small-scale universality in fluid turbulence. *Proceedings of the National Academy of Sciences*, 111(30):10961–10965, 2014.

[142] J.D. Gibbon and C.R. Doering. Intermittency and regularity issues in 3d navier-stokes turbulence. *Archive for Rational Mechanics and Analysis*, 177(1):115–150, 2005.

[143] P.K. Yeung, D.A. Donzis, and K.R. Sreenivasan. Dissipation, enstrophy and pressure statistics in turbulence simulations at high Reynolds numbers. *Journal of Fluid Mechanics*, 700:5–15, 2012.

[144] J. Schumacher, A. Pandey, V. Yakhot, and K.R. Sreenivasan. Transition to turbulence scaling in Rayleigh-Bénard convection. *Physical Review E*, 98(3), 2018.

[145] S.R. Yoffe and W.D. Mccomb. Onset criteria for freely decaying isotropic turbulence. *arXiv*, 2018.

[146] M.F. Linkmann and A. Morozov. Sudden relaminarization and lifetimes in forced isotropic turbulence. *Physical Review Letters*, 2015.

[147] H-Y. Shih, T-L. Hsieh, and N. Goldenfeld. Ecological collapse and the emergence of traveling waves at the onset of shear turbulence. *Nature Physics*, 12(November 2015):10–13, 2015.

[148] D. Barkley, B. Song, V. Mukund, G. Lemoult, M. Avila, and B. Hof. The rise of fully turbulent flow. *Nature*, 526(7574):550–553, 2015.

[149] D. Buaria, A. Pumir, E. Bodenschatz, and P.K. Yeung. Extreme velocity gradients in turbulent flows. *New Journal of Physics*, 21(4):043004, 2019.

[150] S. Chen, K.R. Sreenivasan, M. Nelkin, and N.Z. Cao. Refined similarity hypothesis for transverse structure functions in fluid turbulence. *Physical Review Letters*, 79:2253–2256, 1997.

[151] B. Dhruva, Y. Tsuji, and K.R. Sreenivasan. Transverse structure functions in high-reynolds-number turbulence. *Physical Review E*, 56(5):R4928–R4930, 1997.

[152] G. Stolovitzky, K.R. Sreenivasan, and A. Juneja. Scaling functions and scaling exponents in turbulence. *Physical Review E*, 48:R3217–R3220, 1993.

[153] G. Gotoh, D. Fukayama, and T. Nakano. Velocity field statistics in homogeneous steady turbulence obtained using a high-resolution direct numerical simulation. *Physics of Fluids*, 14:1065–1081, 2002.

[154] T. Watanabe and T. Gotoh. Inertial-range intermittency and accuracy of direct numerical simulation for turbulence and passive scalar turbulence. *Journal of Fluid Mechanics*, 590:117–146, 2007.

[155] M. Nelkin. Enstrophy and dissipation must have the same scaling exponents in the high Reynolds number limit of fluid turbulence. *Physics of Fluids*, 11:2202–2204, 1999.

[156] D.A. Donzis, K.R. Sreenivasan, and V. Yakhot. Emergence of turbulent behavior for passive scalars. In *APS Division of Fluid Dynamics Meeting Abstracts*, APS Meeting Abstracts, page B28.002, 2019.

[157] J. Friedrich, G. Margazoglou, L. Biferale, and R. Grauer. Multiscale velocity correlations in turbulence and Burgers turbulence: Fusion rules, Markov processes in scale, and multifractal predictions. *Physical Review E*, 98(2), 2018.

[158] D.A. Donzis and J.P. John. Universality and scaling in homogeneous compressible turbulence. *Physical Review Fluids*, 5:084609, 2020.

[159] D. Buaria and K.R. Sreenivasan. Dissipation range of the energy spectrum in high reynolds number turbulence. *Physical Review Fluids*, 5:092601, 2020.

[160] J.P. Laval, B. Dubrulle, and S. Nazarenko. Nonlocality and intermittency in three-dimensional turbulence. *Physics of Fluids*, 13(7):1995–2012, 2001.

[161] J. Jiménez. Intermittency and cascades. *Journal of Fluid Mechanics*, 409:99–120, 2000.